Titre: Title:	Mechanical Analysis of Doxorubicin Induced Cardiotoxicity on an Animal Model
Auteur: Author:	Eric Buzaglo
Date:	2019
Type:	Mémoire ou thèse / Dissertation or Thesis
Référence: Citation:	Buzaglo, E. (2019). Mechanical Analysis of Doxorubicin Induced Cardiotoxicity on an Animal Model [Mémoire de maîtrise, Polytechnique Montréal]. PolyPublie. https://publications.polymtl.ca/4002/

URL de PolyPublie: PolyPublie URL:	https://publications.polymtl.ca/4002/
Directeurs de recherche: Advisors:	Delphine Périé-Curnier
Programme: Program:	Génie biomédical

POLYTECHNIQUE MONTRÉAL

affiliée à l'Université de Montréal

Mechanical Analysis of Doxorubicin Induced Cardiotoxicity on an Animal Model

ERIC BUZAGLO

Institut de génie biomédical

Mémoire présenté en vue de l'obtention du diplôme de *maîtrise ès sciences appliquées*

Génie biomédical

Juin 2019

POLYTECHNIQUE MONTRÉAL

affiliée à l'Université de Montréal

Ce mémoire intitulé :

Mechanical Analysis of Doxorubicin Induced Cardiotoxicity on an Animal Model

présenté par **Eric BUZAGLO**

en vue de l'obtention du diplôme de *Maîtrise ès sciences appliquées*

a été dûment accepté par le jury d'examen constitué de :

L'Hocine YAHIA, président

Delphine PÉRIÉ-CURNIER, membre et directrice de recherche

Boris CHAYER, membre

DEDICATION

To the people who were involved with this research and for those who are directly affected by cardiotoxic anti-cancer treatments that may one day benefit.

ACKNOWLEDGEMENTS

I would like to first and foremost thank my research director Dr. Périe-Curnier for taking me under her wing for this extended study. By providing me the tools, background notions and resources, I was able to further my knowledge in the Biomedical Engineering sector, all while enriching my prior background in Mechanical Engineering. Since the very beginning, Dr. Périe-Curnier challenged me and allowed me to satiate my deep curiosity of the how and why things work in the biomedical world. A big thank you goes out as well to Boris Chayer, Lab Engineer at the CrCHUM, who patiently sat with us long hours to obtain data results for each sample we've tested. He also made us think more critically and helped us explore why certain graphs obtained out of order results. Another thank you is extended to Sophie Lerouge who allowed us to book the rheology room with very little trouble and giving us access to all her lab equipment. Lastly, I would like to thank Yassin Seddik and Benoit Waeckel for their involvement with this project during their stage to help accelerate what was a long list of work needed to complete my research. They've contributed immensely to the success of this experimentation and proved to be valuable when it came time to establishing testing protocols.

RÉSUMÉ

Objectif : La chimiothérapie a fait ses preuves au fils des années comme traitement principal permettant de détruire les cellules cancéreuses présentes dans plusieurs types de cancers. La doxorubicine a longtemps été utilisée comme un agent anti-cancérigène dans la chimiothérapie mais elle entraine des effets secondaires dans le corps tels que la suppression de plaquettes et de globules blancs, le développement de l'alopécie, ou encore la perte de myofibrille dans les parois du cœur. De plus, la doxorubicine peut amener des effets cardiaques comme un arrêt du cœur.

L'objectif de ce travail est de proposer des solutions pour détecter les effets cardiotoxiques de cet agent, au moyen de la spectrométrie Raman et de la rhéologie, en faisant des tests moléculaires et mécaniques sur des cœurs de porc.

Matériel et méthodes : Des échantillons de cœur de porc ont été récupérés d'une étude dans laquelle cinq miniporcs Yucatan femelles ont reçu une dose totale de 375mg/m^2 de doxorubicine administrée en cinq fois à trois semaines d'intervalles, formant le groupe expérimental appelé groupe 'DOXO'. Par ailleurs, deux miniporcs ont reçu une injection saline selon le même protocole, formant le groupe 'untreated'. À l'aide d'un rhéomètre, des tests de frequency sweep et de relaxation ont été effectués sur ces échantillons pour mesurer la contrainte de cisaillement (G), le module de perte (G'') et finalement le module de stockage (G'). En parallèle, des tests en spectroscopie Raman ont été effectués pour déterminer la composition moléculaire des échantillons.

Résultats: Nous avons obtenu un comportement linéaire pour une déformation de γ =1,6% lors des tests de strain sweep. Cette déformation a été appliquée pour les tests de frequency sweep et de

contrainte-relaxation. Le test de frequency sweep nous permet de conclure à une baisse globale des propriétés mécaniques des échantillons DOXO dans le septum par rapport au groupe « untreated » alors que nous avons constaté une augmentation dans les ventricules gauches et droits. Lors des tests de relaxation, nous avons trouvé une grande diminution dans les propriétés mécaniques des échantillons du groupe DOXO par rapport au groupe 'untreated'. Quant aux résultats de la spectrométrie Raman, nous avons obtenu une baisse générale du collagène et des lipides dans les échantillons DOXO, ce qui suggère une diminution dans la rigidité structurelle. Les résultats obtenus par rhéométrie ont été comparés aux résultats obtenus par spectroscopie Raman et nous avons observé une corrélation significative.

Conclusion: Les propriétés mécaniques et la composition chimique du tissu cardiaque ont été altérées par le traitement à la doxorubicine chez des mini-porcs Yucatan. Cette experimentation, associée à de futures études, permettra de définir de nouveaux biomarqueurs des traitements à la doxorubicine, et à long terme de trouver des solutions permettant de réduire l'effet cardiotoxique.

Mots clés: Cardiotoxicité, Doxorubicine, rhéométrie, Strain Sweep, Frequency Sweep, Test de contrainte-relaxation, Spectrométrie Raman

ABSTRACT

Purpose: Chemotherapy has been proven to be the best way to eliminate several types of cancer. However, derived from this form of treatment is its cardiotoxic damage and overall functioning of the human heart. Young patients receiving a high dosage are the most prone to develop this cardiotoxicity, which can occur either early or late after treatment. This study aims to specifically investigate the effects doxorubicin has on the overall mechanical and morphological properties in the heart.

Material & Methods: Five young female miniature swines received five 75mg/m^2 injections of doxorubicin every three weeks for a total cumulative dose of 375mg/m^2, constituting the experimental group called DOXO samples. Two miniature swines received a saline injection under the same protocol, constituting the untreated group. These samples were subjected thereafter to frequency sweep and stress-relaxation test in order to determine the shear modulus (G), loss modulus (G") and storage modulus (G') using a rheometer. In parallel, samples were also placed in a raman probe after being submerged in a saline solution. This was used for the Raman Spectrometry portion of the experimentation where the goal of this last one was to determine to molecular composition of each sample tested through the notions of detecting various Raman shift along the domain.

Results: Miniature swines receiving chemotherapy yielded a difference in the mechanical properties. The septum portion of the heart showed an overall diminishment in the storage and loss modulus whereas the left and right ventricle showed an overall strengthening of these parameters. The stress-relaxation test which is the most deterministic test studied showed a clearer drop in the mechanical properties of the DOXO samples. In the Raman Spectrometry study, results obtained

showed an overall decrease in the collagen and lipids content in the DOXO samples. This can be linked potentially to the overall degradation of the sample's structural rigidity. This is why there was a strong correlation between the mechanical testing conducted and the Raman Spectrometry test.

Conclusion: The mechanical properties and the chemical composition of the cardiac tissue altered but the doxorubicin treatment on the Yucatan miniature swine. The combination between this experimentation and future advancements will help characterize biomarkers for the doxorubicin agent, which can ultimately lead to finding solutions on how to reduce its manifestation on the central cardiac cavity.

Keywords: Cardiotoxicity, Doxorubicin, Miniature Swine, Rheometry, Strain Sweep, Frequency Sweep, Stress-Relaxation Test, Raman Spectrometry

TABLE OF CONTENTS

LIST OF TABLES

LIST OF FIGURES

LIST OF SYMBOLS AND ABBREVIATIONS

ACIA	Agence Canadienne d'inspection des aliments
ANT	Anterior
CEPSUM	Centre d'éducation physique et des sports de l'Université de Montréal
CIPA	Comité Institutionnel de Protection des Animaux
CMR	Cardiovascular Magnetic Resonance
CrCHUM	Centre de recherché Centre Hospitalier Université de Montréal
G	Shear Modulus
G'	Storage Modulus
G"	Loss Modulus
LV	Left Ventricle
MFD	Mean Fiber Direction
MRE	Magnetic Resonance Elastography
MRI	Magnetic Resonance Imaging
POST	Posterior
RV	Right Ventricle

LIST OF APPENDICES

CHAPTER 1 INTRODUCTION

The doxorubicin agent, a form of anthracycline, used for many years as an anti-cancer agent during chemotherapy, has reliably helped patients on their road to remission. However, this agent has also been linked to cause cardiotoxic affects in the heart such as the suppression of platelets and white blood cells, the development of alopecia, causing hair loss, and morphological effects such as the loss of myofibrils on the walls of the heart (Aissiou et al., 2016). More notably, doxorubicin can have permanent effects such as a degradation of the heart's function. The two most commonly used anthracyclines up until now has been doxorubicin and epirubicin (Kaklamani et al., 2003).

There has been attention drawn to patient's heart condition post chemotherapy and the long term impact anthracyclines has on the heart. Making use of echocardiography and MRI, studies were conducted to understand the long-term impacts the treatment poses on the heart though it has been difficult to draw conclusions on the effectiveness these imaging tools have on not only detecting the associated cardiotoxicity but characterizing it as well. This raises the need to further explore the fundamental understandings of the evolution of this cardiotoxicity, characterizing it by finding biomarkers, and to ultimately find methodologies to reduce its cardiotoxic effects, all in the intention to benefit the recipients receiving these treatments.

Though the digestive system presents anatomical differences between a swine's heart with that of a human, the miniature swine heart's structure, function and anatomy make this animal a good overall candidate for this research (Kohn et al., 2011). In addition, the miniature swine's heart

presents similarities in the form of heart damages and side effects to humans where the treatment regimen is similar to those used in a clinical setting (Herman and Ferrans, 1983). These reasons highlight why the miniature swine is of particular interest for the study of doxorubicin. Adopting the miniature swine as a model based on the previous mentions allows us to formulate the following scientific objective:

O1- Characterize the mechanical properties of the myocardium following doxorubicin chemotherapy on animal samples.

O2- Characterize the chemical properties of the myocardium following doxorubicin chemotherapy on animal samples.

O3- Characterize the doxorubicin cardiotoxicity from the combination of mechanical and chemical parameters of the myocardium.

The hypothesis of this research is that samples from animals exposed to doxorubicin will have diminished mechanical properties when withstanding the torsional and shear stresses applied on both sets of samples. The hypothesis will be refuted if the mechanical properties remain similar when comparing doxorubicin-induced samples versus non-treated samples.

In the second chapter, a critical literature review will be presented to help define the different notions allowing to deepen the reader's understanding behind the context of the research at hand. Following this, the third chapter will go over the experiments and protocol put in place to conduct the tests along with the results obtained. The fourth chapter will also go over the secondary form of experimentation on our samples which involve Raman Spectrometry. Lastly, the perspectives drawn from these studies will allow for further future advancements.

CHAPTER 2 LITERATURE REVIEW

2.1 Heart Anatomy

The heart's function is to circulate oxygenated and deoxygenated blood throughout the body including its extremities. It is composed of muscular fibers and is considered to be the primary motor organ of the human body. The functioning of the cardiac cycle is explained from the contraction of four of its main chambers which includes the left atrium (LA), the right atrium (RA), the left ventricle (LV) and the right ventricle (RV). These last two are subsets of the apex and can be located near the bottom as conveyed in (Figure 2.1). The interatrial septum is what separates the two atrium cavities while the interventricular septum is what separates the lower left and right ventricules. This separation causes the inability for both the atriums and the ventricles to not being able to communicate to one another. However, the right ventricle can communicate to the right atrium via the tricuspid valve. On the opposite side, the mitral valve is what helps connect the left ventricle from the mitral valve.

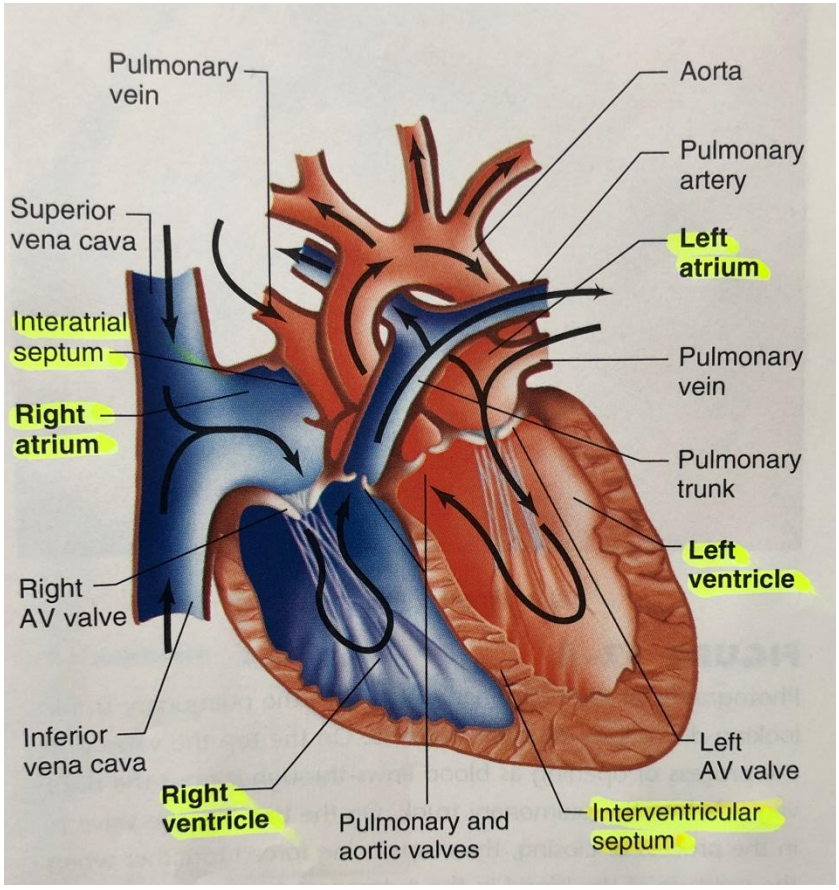

Figure 2.1- Anatomy of heart – modified from Human physiology – The Mechanisms of Body Function (Widmaier, 2014)

2.1.1 **Cardiac Cycle**

Three major components that culminate the cardiac system are the blood vessels, the blood vessels themselves and finally, the heart. In order to oxygenate the blood, at every contraction, blood is pumped towards the inside of the cavities and is then circulated towards all the remaining organs in the body. We refer ourselves to the schematic, which describes the transfer from deoxygenated to oxygenated blood (Figure 2.2). The two circuits of the cardiac function are the pulmonary circulation and the systemic circulation. Firstly, the pulmonary circulation consists of deoxygenated blood entering the right ventricle through the lungs where it is then sent to the left

atrium. When blood is oxygenated during the pulmonary circulation, the blood returns to the left atrium via the pulmonary veins, sent to the left ventricle where it is then distributed throughout the major organs with the help of the aortic valve. The blood is then sent through the systemic circulation from the left ventricle, going through all the tissues and organs found around the body where it is then deposited in the right atrium. In both circuits, the vessels carrying blood away from the heart are known as the arteries. The vessels where blood is incoming are better known as veins.

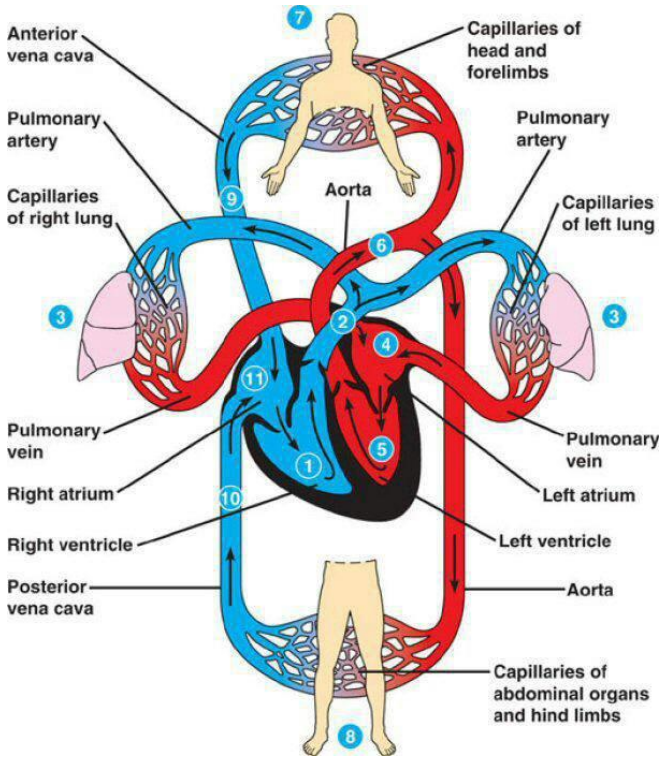

Figure 2.2 Blood Circulation – modified from https://www.pdhpe.net/the-body-in-motion/

The systole and diastole are the two main phases that represent the cardiac cycle. The systole phase takes place when the heart contracts to pump blood out by contracting itself. On opposite ends, the diastole relaxes the heart after its contraction and fills out the two atrium chambers with blood.

2.1.2 **Biology and Biochemistry of cardiac tissues**

The cardiac tissue that encapsulates the cavity is composed of three distinctive layers; each with their distinctive role and property. These thin sheets superposed one on top of the other allow for an easier systole and diastole phase to take place during the cardiac cycle. The primary layer which constitutes as the main layer of the cardiac tissues is called the myocardium, also known as the muscular tissue of the heart. This layer comprises the majority of the heart's weight and is sandwiched between the two inner and outer layer. Within this layer lay the cardiomyocyte cells whose role is to carry information to the nervous system allowing the nervous system to send a signal to trigger the heart's contraction or relaxation. The inner most layer is called the endocardium tissue which is a smooth membrane covering the inner chambers of the heart. The outer most layer is the epicardium layer which is considered to be the skeletal layer of the cardiac tissue.

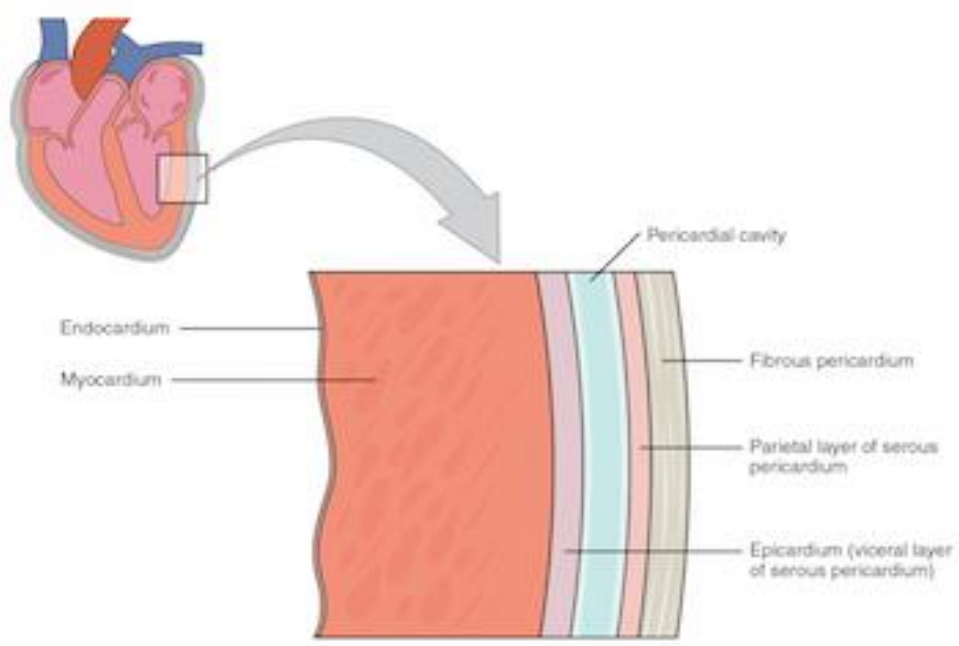

Figure 2.3 Layer Composition of the Heart Wall – modified from https://study.com/academy/lesson/endocardium-definition-function.html

The outer most layer also known as the extracellular matrix, collagen can be found and provides support to the tissues encapsulating the heart. This fiber, which is most frequently, allows the cardiac muscle to not only maintain its global shape but permits it to be either flexible or resistant during the cardiac cycle. Other important fibers include the elastine which allows for a greater elasticity of the myocardium space. This elasticity is important in order to prevent tears. Most studies covering the extracellular matrix of the myocardium's mechanical function base themselves on the different types of fibers found and play an important overall role to the extracellular matrix.

2.2 Forms of Cancer Treatments and its effects

2.2.1 Anthracycline based Chemotherapy

Anthracycline chemotherapy is still to this date an important form of treatment to eliminate cancer cells. This administered potent drug is a class of chemotherapeutic agent extracted from Streptomyces bacterium. The beneficial effects from anthracycline span from hematological malignancies to solid tumors (Moudgil et al., 2017). Anthracyclines interferes with the cancer cell's DNA metabolism and the production of its RNA once it is injected. By inducing the patient with oxygen-derived free radicals and superoxides through the injection of anthracycline, this causes damage to the cell's DNA by inhibiting a synthesis from further taking place causing them to die. There are four types of very similar anthracyclines; daunorubicin, doxorubicin, idarubicine and epirubicin. The first molecule explored in the early 1960s when anthracycline chemotherapy

was explored was the daunorubicin drug (Butler et al., 2009). This red potent liquid prevented cancer cells to split into two due to tangled DNA strands which help slow down or eliminate cancer cell growth. Since then, doxorubicin has emerged as being the most widely used anthracycline though there still advantage in using the 3 other anthracyclines in certain cases such as daunorubicin for the treatment of acute leukemias (Kaklamami et al., 2003). Doxorubicin's use in breast cancer started after the observation that it produced high response rates in metastatic disease. Metastatic disease is the medical term used for cancer that spreads from one original place in the body to another. Since this discovery, numerous tests to treat early-stage breast cancer have allowed doxorubicin to be a core component of chemotherapeutic regimens (Kaklamami et al., 2003).

Epirubicin, the 4'-epimer of doxorubicin (Figure 2.4) is also highly active in treating metastatic disease and was created because of its proven clinical testing to prevent a higher toxicity profile than that of doxorubicin. Epirubicin differentiates itself structurally from doxorubicin in the epimerization of the hydroxyl group in position 4 of the amino sugar moiety (Kaklamami et al., 2003). Both drugs are metabolized in the liver and eliminated through the bile (Zhang et al., 2014).

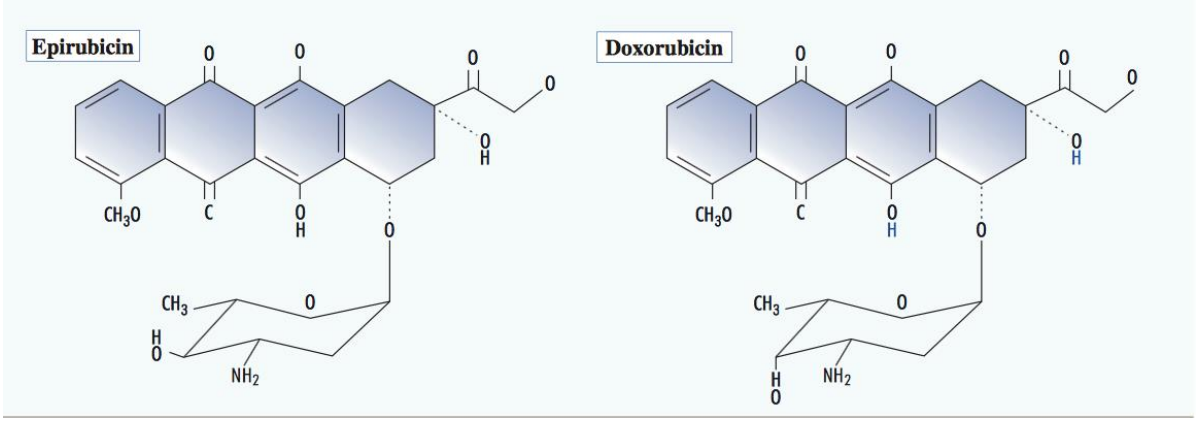

Figure 2.4 Anatomic structure comparing the main types of Anthracycline – modified from (Kaklamami et al., 2003).

2.2.2 **Cardiotoxic Effects of Anthracyclines**

Side effects of anthracycline are numerous such as the suppression of platelets and white blood cells in the bone marrow, diarrhea, but mostly alopecia, which causes human hair loss and other morphological effects such as the loss of myofibril on the outer shell of the heart. Most notably, the main and serious side effects of anthracycline during cancer chemotherapy is its cardiotoxic impact, which remains the main focus of this research.

Anthracycline administered into the human body in intravenous form can be subdivided into three stages of cardiotoxic effects. At the first stage, the effects are already evident after a single administration, which includes disturbances in cardiac rhythm and changes in blood pressure (Pecoraro et al., 2017). The second stage includes cardiac dilation and cardiomyopathy, a disease in the heart's muscle. Lastly, the third stage of cardiotoxic effects due to anthracycline is terminal due to a stop of the heart's function (Pecoraro et al., 2017). Doxorubicin-induced cardiotoxicity is mainly related to the accumulation of the repetitive doses required during a patient's treatment process. The dose administered varies from patient to patient but is usually between 30 and 70mg/m^2 with a maximum cumulative administration of 120 mg/m^2 (Schellens et al., 2005). The accumulation of these doses cannot exceed 500 mg/m^2 which implies a maximum treatment period of four weeks though recent studies indicate damages caused by anthracycline are noticed even after a single administration (Pecoraro et al., 2017).

2.2.3 **Cause of Cardiotoxicity**

The exact cause of anthracycline's cardiotoxic effects is not fully explored nor understood but it is assumed to be due to a multitude of reasons. Several studies indicate that doxorubicin induced cardiomyopathy is characterized by abnormal calcium homeostatis (Zhang et al., 2014). Doxorubicin administration is able to induce calcium dysregulation and Connexin43 (Cx43) in a rat's cardiomyoblast cell line noticed immediately after administration (Pecoraro et al., 2015). The aim of this study was to investigate the effects of DOXO administration on Cx43 expression and localization in a short-term model where they performed an echocardiography on mice.

2.2.4 **Previous Studies to Reduce Cardiotoxicity**

In order to reduce the cardiotoxic effects, researchers have analyzed many options over the course of the past decades. A published study by Geisberg et al. highlights a few strategies considered to help reduce or eliminate anthracycline's cardiotoxicity (Geisberg et al., 2010). The first includes limiting the cumulative exposure of anthracyclines. This would entail encapsulating anthracyclines in liposomal microparticles or modifying the rate of discussion (Geisberg et al., 2010). Encapsulating the drug seems to have been a preference in the study because of "vascular permeability changes in malignant tissue." Other strategies included changing the rate of anthracycline's administration, making changes to the formulation or also exploring alternative drugs that present less of cardiotoxic effect. In another study covered by Conway et al. he proposed similar tactics to minimize the cardiotoxic impact. There is alternative medication called dexrazoxane, which mimics the behavior of anthracycline. However, dexrazoxane has a negative

impact on the bone marrow's function due to the increase of myelosupression (Seymour., et al 1999). Next, avoiding the administration all together is something to be considered though the original purpose of anthracycline is to help kill the DNA in the cancer cells. Another study conducted by Dalen et al. proposes other agents as a substitute such as iron chelator, dexrazoxane as a means to reduce anthracycline-induced free radical formation (Dalen et al., 2005). While trying to prevent the cardiotoxic effect, Dalen et al. mentions potential adverse effects including limits to the tumor response (Dalen et al., 2005). However, the study concludes a more favorable outcome this drug has on the cardiotoxic impact.

All these techniques presented in all three articles can potentially help reduce or eliminate anthraycline's cardiotoxic effects. Unfortunately, the combined studies up until now still do not provide a sufficient amount of biomarkers that would ultimately help draw concrete solutions on the cardiotoxity levels of the doxorubicin agent. This is where the added value of this research report comes in so that drawing conclusions from the characterization of doxorubicin's cardiotoxicity based on the mechanical test results can help determine methods such as effective injection concentrations of doxorubicin, clinical diagnostics, therapeutic interventions or material design for tissue engineering.

2.3 **Animal studies of Anthracyclines Cardiotoxic Effects**

The study regarding the cardiotoxic effects of doxorubicin originated with Mettler *et al*. where he made use of a rat model. The evaluation and the feasibility of the rat as a pertinent model was demonstrated in this study (Mettler et al., 1977). This study found that the overall mass of the rats treated with doxorubicin had dropped compared to the untreated models (Robert et al., 2007). Since then, newer adapted protocols, which includes variations in the anthracycline dosages and

concentration, were introduced. Another study using non-rodent animals such as guinea pigs, rabbits, dogs and non-human primates received seven dosages (1mg/kg) of doxorubicin during the span of 7 weeks. The subjects were unable to gain any weight during the experimentation in addition to suffering from respiratory problems linked to the interrupted cardiac cycle (Vargas et al., 2015).

Another study conducted by Herman et al. in the early 80s provided weekly dosages of 1mg/kg over the course of four months to dogs (Swindle et al., 2012). After four months of close monitoring, the results showed a loss of myofibril protein in the doxorubicin treated subjects. Like the previous studies, the dogs were subjected to weight loss over the course of the study (Swindle et al., 2012).

Although many animal models have been used to study doxorubicin toxicity, several restrictions limit their use. This is why Manno *et al*. chose a non-rodent animal, specifically the guinea pig as a mean to further study anthracycline's impact on the myocardium. In total, three groups of three female and male miniature swines received 1.5mg/kg at intervals of three weeks over seven cycles. A weight loss was observed in the female model after only four cycles while there were suppression effects of doxorubicin on the bone marrow which caused hematological suppression on all 18 subjects. Such effects caused a decline in the red blood cells. The study concludes by stating that due to the close resemblance of the minipig to the human heart, this model should be the non-rodent species of choice for all future testing involving the study of doxorubicin (Manno et al., 2015).

In 2013, Dr. Curnier experimented with Doxorubicin induced models and referred the study of myocardial damage using endomyocardial biopsy of the right ventricle to be the "gold standard"

(Mohamed et al., 2013). It provides reliability however poses disadvantages such as it being an invasive procedure which can cause risks so necessary training is needed in order to study the symptoms of doxorubicin using this approach. Concerning the left ventricle, 2D and 3D echocardiography has proven through this study to properly estimate the ejection fraction and information such as area and volume measurements. The results obtained showed to have similar results to that of cardiovascular MRI (Mohamed et al., 2013).

Up until now, many studies conducted on the myocardium model involved histological analysis, MRI testing and imaging protocol such as cardiovascular MR (CMR) but very little development has emerged on the actual mechanical properties of the samples. The study, which compares the mechanical properties of the untreated and treated samples, will allow the characterization of structural damages induced on the heart from a mechanical standpoint. A device formally used to study tissue properties is the rheometer and will be discussed in the following literature review, which covers the science of rheology.

2.4 Characterization of tissues mechanical behavior using Rheological Testing

Rheology is a technique to measure and describe the overall behavior and deformation of any form of solid material. A popular equipment that measures all forms of deformations such as the shear stress of a material is the rheometer. The rheometer measures with high precision information such as the rotation and step strain using a sample-adaptive controller, the gap measurement and thickness of samples and the normal force of a material using high-precision air bearings. There are two types of rheometer. The first is a rheometer that controls the applied shear stress or shear strain better known as the shear rheometer. The second is called an extensional rheometer, which,

as the name describes, applies an extensional stress, or extensional strain on samples being studied (Pipe, Majmudar and McKinley et al., 2008).

An important measurement used for this experimentation is the shear stress which can be defined as:

$$\tau = F / A$$

where F is the shear force (in N, newton) and A is the shear area A (in m^2). The unit for shear stress is 1 N/m^2 = 1 Pa (Pascal). A rheometer records the shear force via the torque at each measuring point.

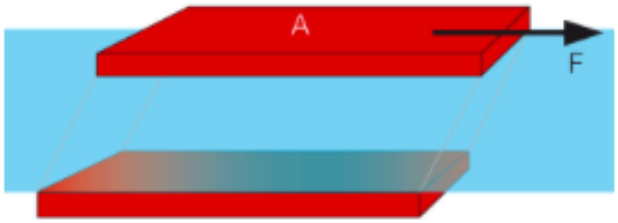

Figure 2.5 Two-plates model used to define the shear stress using the parameters shear force F and shear area A of the upper, movable plate – modified from https://wiki.anton-paar.com/en/basics-of-rheology/

The two-plate model is used to define the rheological parameters to better understand matter's behavior. For example, shear is applied to a sample sandwiched between two plates. The lower plate (base) is mounted on a very rigid support and the upper plate can be moved parallel to the lower plate which in the rheometer's case is the spindle as seen in Figure 2.6.

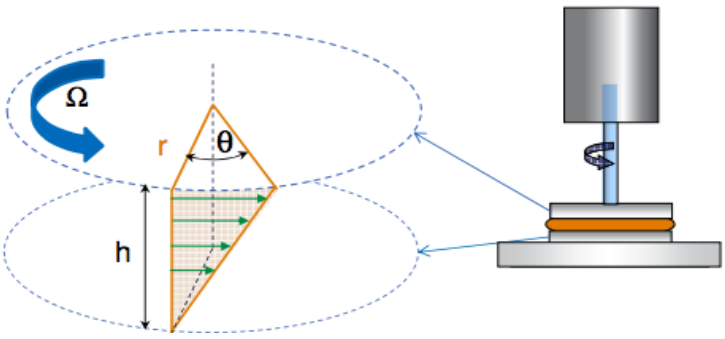

Figure 2.6 Torsion Flow in Parallel Plates

The shear stress can also be defined as the relationship between the spindle's radius and the torque seen in Figure 2.6. $$\tau = \frac{2}{\pi r^3} \text{ x } M$$

where τ = shear stress

r = plate radius

M = torque in μN . m

The shear strain is defined as the relationship between the plate's spacing, angular motor deflection and the plate radius. $$\Upsilon = \frac{r}{h} \text{ x } \theta$$

where Υ = shear strain

r = plate radius

h =distance between 2 plates

θ = angular motor deflection in radians

It is important when it comes to selecting the spindle dimension to choose one that will correspond not only to the specimen dimension but to its viscosity as well. A low viscous substance such as milk should be measured with a spindle diameter equal to 60mm, a medium viscous substance such as honey should be measured with a spindle diameter equal to 40mm and a highly viscous substance such caramel or tissue culture should be measured with a spindle diameter of either 20mm or 25mm (Kalyanamaran et al., 2012).

Figure 2.7 Selection of Spindle based on Sample Diameter

The greater the spindle's circumference, the better suited it is to analyze smaller changes in sample's deformation and is more optimized for increased sensitivity. In addition, the smaller the shear stress that is applied on the substance located in between the plates. This holds true by analyzing the mathematical equation defining the shear stress: $\boldsymbol{\tau = \frac{2}{\pi r^3} \text{ x } M}$

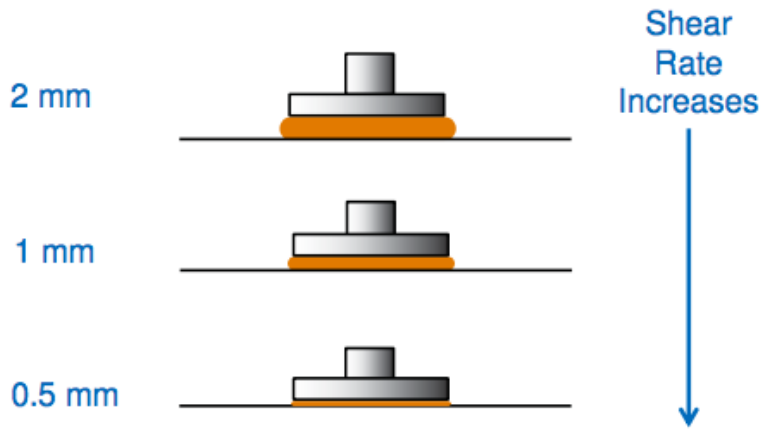

Figure 2.8 Plate Diameter Relationship to the Shear Stress

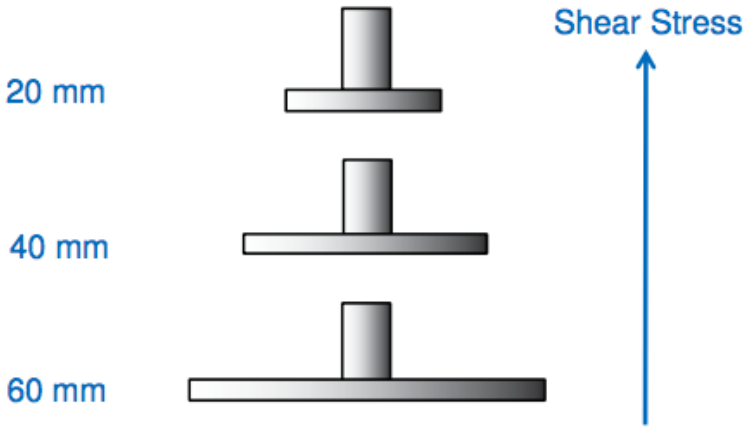

Figure 2.9 Plate Gaps Relative to the Shear Rate

Another important component of calculating substance properties is by measuring the thickness of the material being placed in between the plates. As the gap height between the plate decreases, the overall shear rate applied to the material increases.

The shear rate can be defined as the following: $\dot{\gamma} = \Omega \times \frac{r}{h}$

where $\dot{\gamma} = \text{shear rate}$

Ω = Motor angular velocity in rad/sec

r = spindle radius

h = distance between 2 plates

The specific rheometer used for the experimentation at the CrCHUM, Centre de recherché Centre Hospitalier Université de Montréal, was the MCR 301 fabricated by Antor-Paar, which can be found in Figure 2.10. The advantage of a two-plate rheometer is the ability to perform long stress-relaxation tests for a multitude of substance shape size and viscosity.

Figure 2.10 Components of the Antor Paar MCR 301 Rheometer

In a rheometer, the loading applied on a material and the stress is derived from the torque. The formula for stress is

where σ = Stress (Pa or Dyne/cm^2)
M = torque in N·m or gm·cm
K_σ = Stress Constant

and the stress constant, K_σ , is a geometry dependent factor.

Aside from characterizing biomarkers using mechanical testing with the aid of the rheometer, the goal of the experimentation is to link these results with those of the results obtained in Raman spectrometry.

2.5 **Raman Spectrometry**

Spectrometry is a science technique used in chemistry to help identify molecules based on the observed vibrational, rotational and other low frequency modes in a given system. This technique uses a laser light source at frequency ω_0 to irradiate a sample in order to generate Raman scattered light. The Raman spectrum allows then to identify the fingerprint of the sample's molecules to identify substances including polymorphs and inorganic material. Not only does it help identify the molecules but it also helps evaluate local crystallinity, orientation and stress. When foreign material is discovered on the surface or within a substance or part, a spectrum of this particle can be taken for identification. Raman Spectrometry can analyze this particle even if it is smaller than 1 micron.

The Raman device used for this study contained fiber optic cables, Emvision, LLC, connected to a NIR spectrum-stabilized laser (Jermyn et al., 2015). The specific device was an "in -house" system and was conducted at the CrCHUM and was composed of five main components typically found on all Raman Spectrometry devices: an entrance slot which caps a light wave, an entrance collimator, which synthesizes the light wave, an area where light diffraction occurs, a secondary collimator which serves as an exit for the diffracted light and finally a detector (St - Arnaud., 2017). The myocardium tissues were preserved in a formalin solution for over a year and then conserved in a saline solution throughout the gathering period of raman wavelengths from the measurements.

Raman Spectrometry differs from other sample testing being conducted for this experimentation such that it involves a non-contact and non-destructive analysis of samples when being tested. In addition, Raman spectrometry benefits from not needing sample preparation. It can be prepared in many states such as gas, liquid, solid and even crystal (Kumamoto and Fujita, 2003). Lastly, samples only need an exposure of 10ms to 1sec to get a Raman spectrum crystal (Kumamoto and Fujita, 2003).

Scattering of incident lights when introduced to a molecule, as shown in Figure 2.11, works either elastically or inelastically. When light is scattered by matter, almost every form is done elastically, and is called Rayleigh scattering. This form is done through no change in energy. The smaller percentage is considered to be the inelastic process, for which different energy causes different incident light. The observation was first conducted experimentally by Chandrasekhara Venkata Raman in 1928 and is better known to this day to be called the Raman effect.

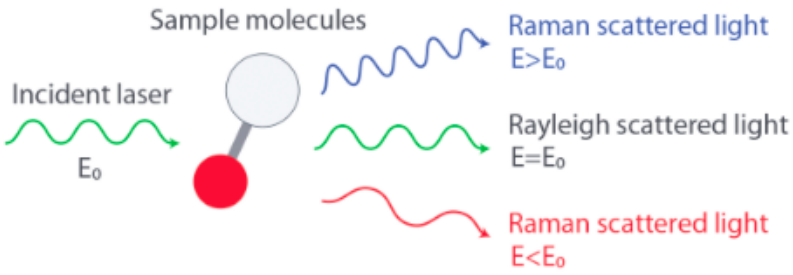

Figure 2.11 Scattering of Light by Molecules – modified from https://www.nanophoton.net/raman/raman-spectroscopy.html

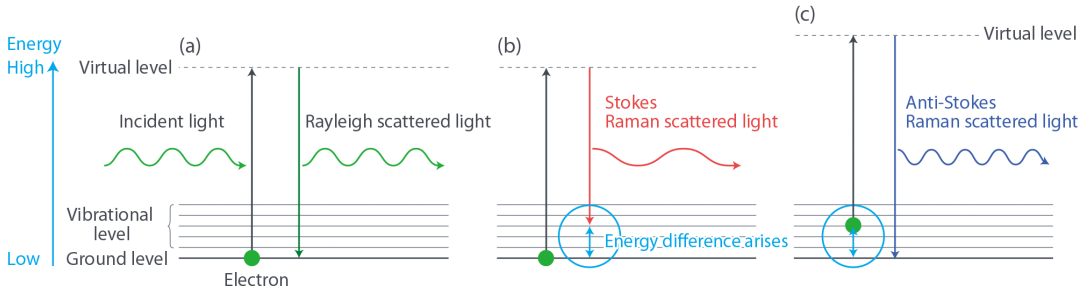

Figure 2.12 Diagram of the Rayleigh and Raman Scattering Processes – modified from https://www.nanophoton.net/raman/raman-spectroscopy.html

When a principal incident light comes into contact and interacts with a sample molecule, it distorts the cloud and creates a virtual space, as seen in section (a) of Figure 2.12. This state is not stable and causes the photon to re-radiate as scattered light almost immediately. Rayleigh describes the process where an electron in the ground level gets excited and falls to the original ground level. It does not involve any energy change so Rayleigh scattered light has the same energy as incident light meaning both lights have the same wavelength.

Raman scattering can be classified as two types, Stokes Raman scattering and anti-Stokes Raman scattering. Stokes Raman scattering is a process in which an electron is excited from the ground level and falls to a vibrational level. It involves energy absorption by the molecule, and thus, Stokes Raman scattered light has less energy (longer wavelength) than incident light.

Dissimilarly, the process of anti-Stokes Raman scattering involves an electron, which gets excited from the vibrational level to the ground level. This means an overall energy transfer to the scattered photon and causes the anti-Stokes Raman scattered light to gain more energy (shorter wavelength) than that of the incident light.

Based on Figure 2.13, which demonstrates the spectrum of ethanol, the Raman peak is found at 547.14nm obtained by a 532 nm excitation wavelength.

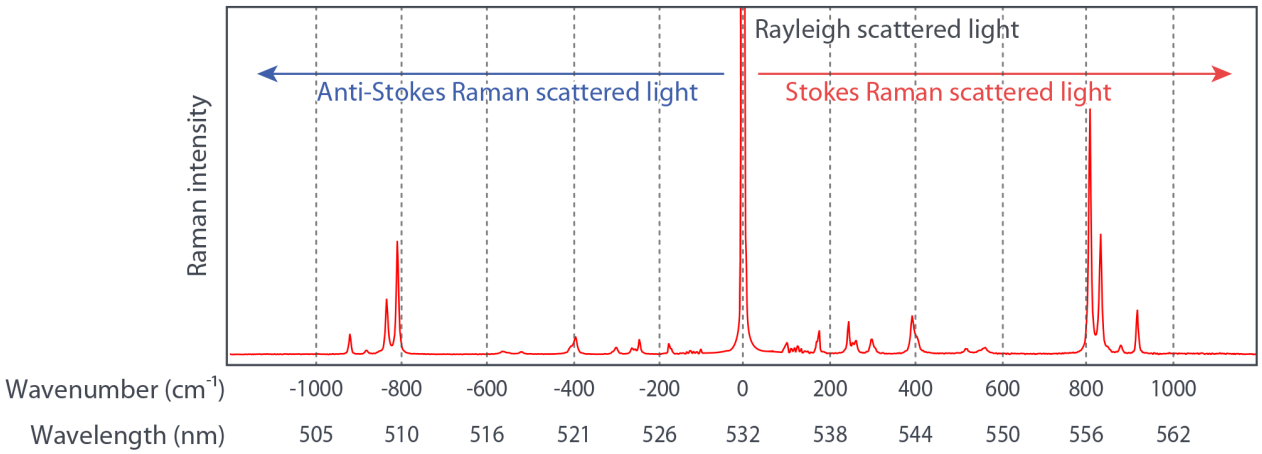

Figure 2.13 Raman spectrum of Ethanol

By calculation, the Raman shift can be obtained by applying the following mathematical formula:

$$\text{Raman shift} = \left(\frac{1}{532\,nm} - \frac{1}{547.14\,nm}\right)$$
$$= 520\,cm^{-1}$$

Not only is the location of the peak important, the shape of the peak is important as well. The shape helps determine the level crystallinity. The residual stress can also be determined by the direction and frequency of every Raman peak.

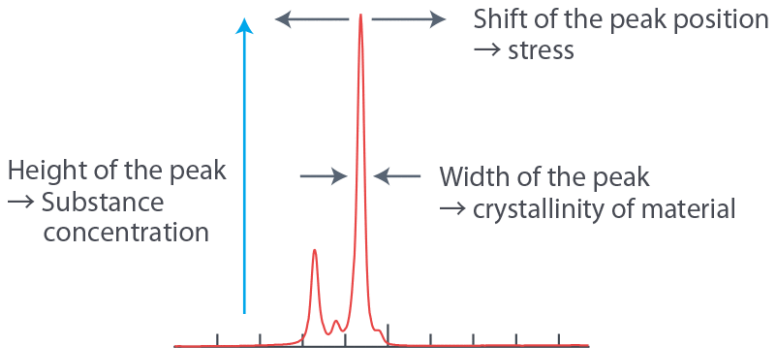

Figure 2.14 Determining the level of crystallinity by analyzing the Raman peak.

2.6 **Animal Studies Conducted Prior to Experimentation**

The samples used in this study originated from a previous animal study in which Yucatan miniature swine were treated with doxorubicin for 4 months and followed by cardiovascular Magnetic Resonance Imaging (CMR) in order to detect early cardiotoxicity. The protocol for the preparation and experimentation of their samples as well as ours was approved by the Comité d'éthique de protection animal at the CrCHUM.

The Sinclair Bio-Resources department located in Misouri provided seven miniature swine for the purpose of the experimentation. A silicone catheter was implanted in these infant animals via the left superior vena cava following the acclimation. All injections were administered through these vascular access ports. Five of the seven Yucatans were randomly selected to receive the doxorubicin injection while the remainder were administered with a saline solution. Once all animals were evaluated by three echocardiography and CMR, they were sacrificed. The major organs such as the liver, kidney, diaphragm, lung were preserved in liquid nitrogen before cytotoxic took effect due to the drug. Most notably, the heart was preserved for specific cardiotoxicity tests conducted by means of MRI, rheometry and Raman Spectrometry. The treatment and imaging protocols followed the guidance of Hermans and Ferrans's study (Herman and Ferrans et al., 1983). The time elapsed for the totality of the experimentation including echocardiography evaluation and sacrificing the animals was five months.

CHAPTER 3 RHEOMETRY OF THE MYOCARDIUM

3.1 Preparation of the Samples

The samples were dissected and preserved frozen at -80°C since the previous study described in the literature review. The samples were found in various shapes (Figure 3.1) and had to be thawed in order to prepare circular shapes of 20mm diameter and 2.5mm ±0.5mm thickness.

Figure 3.1 Parts before the requisition of samples used for experimentation

The resulting pieces illustrated in figure 3.2 were dissected using 3D printed equipment. The preparation is described in detail in the protocol below.

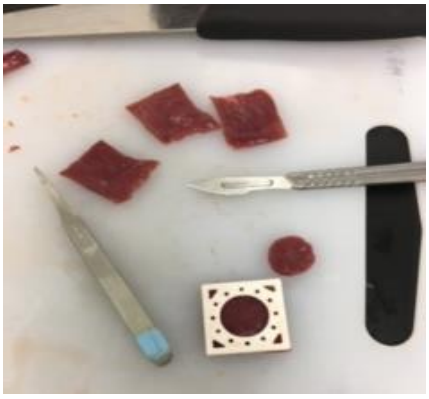

Figure 3.2 Samples being prepared before being placed in the Rheometer

3.1.1 **Tyrode's Solution**

The tyrode solution, invented by Maurice Tyrode, is an isotonic solution, meaning sharing the same osmotic pressure with interstitial fluid, used in physiological experiments such as tissue culture derived from Ringer-Locke's solution. Its primary content is sodium (NaCl) but differs from the Ringer-Locke's solution in that it contains magnesium. Since the tyrode solution is oxygenated, it helps preserve the physiological and mechanical properties of tissues irrigated in blood. Submerging once shaped in a circular disc will allow the samples to remain hydrated and prevent them from drying out before being placed on the rheometer's spindle. In order to realize the tyrode solution, 3 sub-solutions were prepared (Table 3.1) which, after their mixture with the proper proportions (Table 3.2), will allow us to get a fresh tyrode solution.

Figure 3.3 Preparation of the three sub-solutions at the CEPSUM

The sub-solutions are as follows:

Table 3.1 Three sub-solutions needed to compose the Tyrode Solution

Sub - Solution 1 :	Sub - solution 2 :	Sub - solution 3 :
141,425g of NaCL (10x)	5.293g of $CaCl_2$ + $2H_20$ (10x) 0.952g de$MgCl_2$ (10x)	Glucose for Tyrode (x10)
7,456g of KCl (10x)	0,584g of EDTA (10x)	Dextrose 19,800g (10x)
40,325g of $NaHCO_3$ (10x)		
0,808g of NaH_2PO_4 (10x)		

Additionally, the pH should be near neutral while taking into consideration that the pH levels are influenced by oxygenation. The resulting pH, measured by litmus paper was approximately 7.4 when preparing the tyrode solution. The slices were placed in the solution for ~ 20 minutes at room temperature to reduce shock before proceding in tissue culture validated by article (Qiao et al., 2019). To make a 1L of solution, we followed Sandstrom's recipe procedure below:

Table 3.2 Ratio needed for the mixture of the three sub-solutions

	50mL Solution	
1)	Mix:	100 mL of **Sub-solution 1** (10 X)
		800 mL of dd H_2O
2)	Gas with 5% CO_2 for approx. 30 min to adjust pH	
3)	Add:	100 mL **Sub-solution 2** (10X)
4)	Add:	100 mL **Sub-solution 3** 55 mM (10x)

3.1.2 **Cutting the Samples**

In order to get results as consistent and comparable as possible, the samples needed to be cut into circular shapes. To that end, we designed a slicer as a mean to place the part while pressing along the wall to perform evenly sliced samples. The holder for the peripheral cut was used afterwards to get a perfectly shaped circular disc. The CAD models of Figure 3.4 and Figure 3.5 were 3D printed.

Figure 3.5 Holder for Peripheral Cut

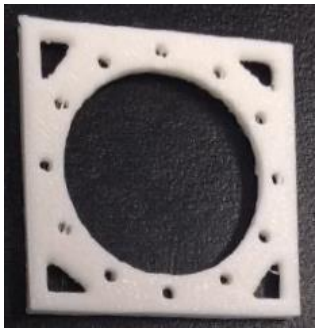

Figure 3.4 Slicer

In order to cut 5cm x 7cm samples (approximately 1/3 of each piece of miniature swine sample), we submerged a sharp knife in a beaker filled with heated water in order to penetrate the piece frozen at -80°C.

Samples were prepared two years after being sacrificied but were preserved in the freezer at -80°C. The procedure of harvesting the parts right after being sacrificed was followed and samples were prepared as for other future tests being conducted using the myocardium as the studied model. In an article written by Sirry et al., infarcted hearts were preserved as of the very first day post euthanasia (Sirry et al., 2016). Studies over the years including that of Stenman et al. studied the long term effects of tissues stored in the freeze at -80°C. The study concluded that there were no adverse effect on the tissues' histomorphology or RNA quality (Stenman et al., 2013).

Given that RNA is most susceptible in degradation when compared to other parts comprised in the composition of tissues and that of 153 samples studied over different period of time, no correlation with storage time was observed on the RNA quality (Stenman et al., 2013). The little to no effect on the RNA quality is emblematic to other compartments found in tissues. Though some of our samples showed slight signs of fracture, we did not fear alterations in the tissues' histomorphological and mechanical properties. However, the paper did put a preference towards very low storage temperature in liquid nitrogen as the method of choice for long-term storage but that either method worked.

Each piece of heart was dissected in as many samples that we could obtain while remaining consistent with the diameter set out to be 20mm with an overall thickness varying from 2-3mm. For this particular research, we opted to study three myocardial regions of the heart; the left ventricle (LV), the right ventricle (RV) and the septum going running from the base of the heart to the apex. Once the cardiac pieces were cut, we preserved the cut pieces in cubes of approximately (3cm x 3cm x 3cm) at -20°C.

The slicer allows a thickness of 2,5mm ± 0,5mm and the device to host the pieces allowed for a consistent diameter cut of 20mm. The initial proposal was to cut the pieces at 25mm to match the same diameter of the spindle located on the rheometer. However, after further analyzing the available pieces, it would have been difficult to maintain a 25mm diameter when some pieces were already smaller than expected.

Samples retrieved for the experimentation can be found listed in Table 3.3. It is important to know from which part each sample was retrieved in order to determine if some of the results

obtained can be derived from the physiological properties of the miniature swine as well as if there is a common denominator for the samples found from the same part but at a different compartment of the heart. The goal is to also determine the effects a sample's thickness has on the overall property of the myocardium tissue.

Table 3.3 Samples retrieved from Yucatan parts

Sample Thickness				Comments
Healthy		Doxo		
Code	Thickness (mm)	Code	Thickness (mm)	
40-13 LV Post	3,5mm	98 LV Ant 1	3mm	
40-13 LV Ant	3,1mm	98 LV Ant 2	2,8mm	
40-14 Septum	2,8mm	98 LV Post	2,3mm	
40-14 RV Post	2,9mm	96 Septum 1	2,5mm	
40-14 RV Post 2	2,9mm	96 Septum 2	2,3mm	
		96 Septum 3	2,3mm	
		96 LV Ant 1	2,8mm	
		96 LV Ant 2	2,825mm	
		96 LV Ant 3	2,3mm	
		96 LV Post 1	2mm	
		96 LV Post 2	2,5mm	Sample fractured through middle
		24 LV Ant 1	2,7mm	
		24 LV Ant 2	2,9mm	
		24 LV Post 1	1,532mm	
		24 LV Post 2	2,04mm	
		98 Septum 1	2,5mm	Sample fractured in 2 different areas
		96 RV Post 1	1,95mm	
		96 RV Post 2	1,8mm	Sample fracture and refrozen
		009 LV Post 1	2,8mm	
		009 LV Post 2	2,1mm	

The three areas of interest are the posterior left ventricle (LV POST), the anterior left ventricle (LV ANT) and the right ventricle (RV) and the septum. The left ventricle samples were more frequently used since it comprised a larger portion of the heart allowing to retrieve more

samples. Freezing, in general, causes visible or non-visible damage using virtually any practical method. The main changes caused in samples through freezing or unfreezing are dehydration and shrinkage, some form of chemical property alteration, a change in the overall structural integrity of a sample, and/or a grave breakdown better known as the “thaw-rigor” process (B.J Luvet et al., 1964). In total, 24 samples were used, both treated and untreated. Some samples showed sign of fracture in various areas due to the extensive period of being left frozen at -80°C but were still candidates as it had negligible effects on the overall structural integrity of the samples.

3.2 Mechanical Testing Protocol

The mechanical testing protocol was composed of a strain sweep test which helped determine the optimal deformation (ϒ), a frequency sweep to determine the sample’s storage, loss modulus and complex viscosity as a function of the applied frequency and a stress-relaxation test to help calculate the relaxation modulus of the samples. Finally, a redo of the frequency sweep was conducted to determine if the sample’s storage modulus altered during the stress-relaxation test. All these tests fall under the general rheological test called oscillation experiments.

3.2.1 Strain Sweep test

The goal for the strain sweep test using the rheometer is to determine the level of optimal deformation (ϒ) to apply during the frequency sweep test to insure that the response to the shear modulus is linear throughout the frequency domain of 0,1Hz to 100Hz. We first made the assumption of a homogenous heart. To perform this stage of our tests, we made use of a pig’s heart bought at the butcher to avoid the waste of the experimentation’s actual samples. We followed the

same procedure as if we would have used the samples by placing the pieces purchased at the butcher in the CEPSUM (Centre d'éducation physique et des sports de l'université de Montréal) freezer at -80°C.

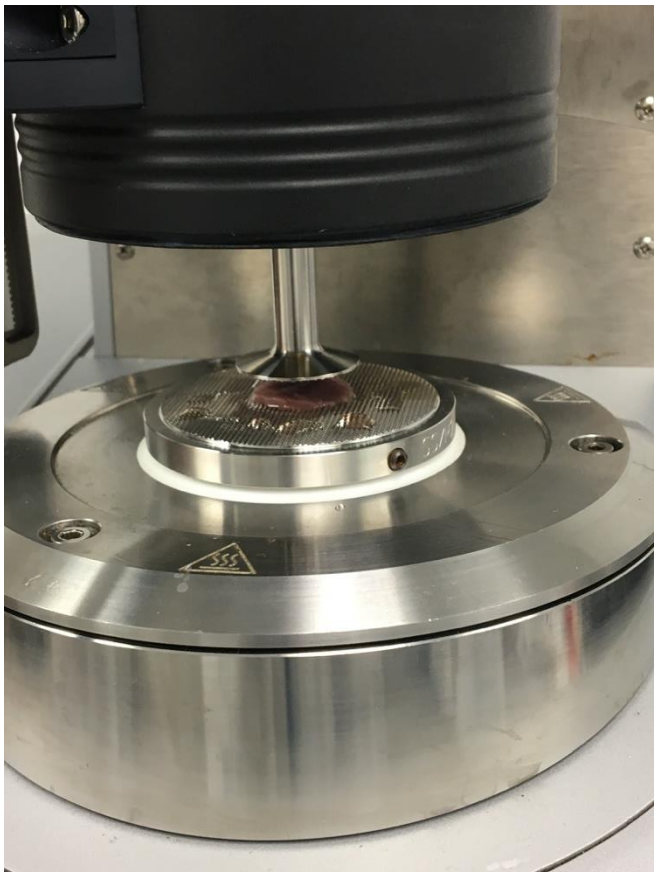

Figure 3.6 Sample being placed under the rheometer's spindle.

The samples used for the strain sweep were subjected to strain sweep tests varying from 1Hz, 10Hz, 25Hz, 50Hz and 100Hz on a deformation domain from 0.01% to 2%. This first step was repeated three times to insure consistent results.

3.2.2 **Frequency Sweep test**

The goal of the *frequency sweep* test was to validate the protocol by submerging the samples under the same conditions as if the real tests were being conducted. Once the protocol was validated with samples prepared from the butcher, the same procedure was used for the experimental samples. Again, we made the hypothesis of a homogenous heart.

Three prepared cylindrical samples on the myocardium part of the heart were submitted to 6 cycles of preconditioning at 0.1% beginning at 0.1Hz. The deformation value (Υ=1.6%) previously found in the strain sweep was used to perform the remainder of the frequency sweep test. The frequency range was conducted from 0.1Hz to 100Hz. The frequency up until 100Hz was imposed based on ω = 16 rad.s^{-1} and it being derived from $\omega = 2\pi f$. Refer to the graph A11 in Appendix to further understand this frequency range.

The preliminary *frequency sweep* tests on the butcher samples allowed us to determine that 20 measuring points was sufficient to achieve clear curbs all while limiting the acquisition time. All tests were performed at core body temperatures (37°C). The samples were subjected to 10 cycles of preconditioning at 0.1% with a deformation Υ=1.6%.

During the preliminary experiments, the specimen dried out quite rapidly. We originally made use of tyrode solution droplets, however, its isotonic properties caused the droplets to spread itself thin, reducing its permeability. This led us to making use of a low-viscous canola oil droplet applied on the periphery of the sample, inspired by (Nicolle, 2010) where we were able to preserve a hydrated sample all the way until the end of each test.

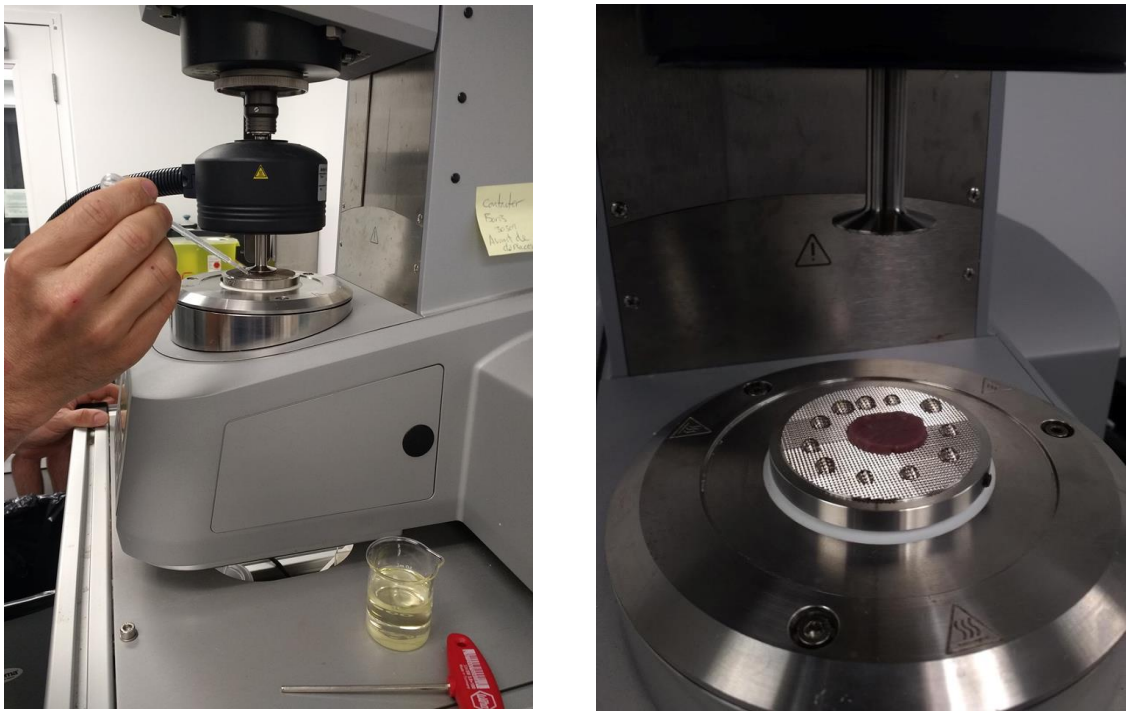

Figure 3.7 Droplets of Canola Oil Applied Around the Specimen

In addition, the viscosity of the canola oil was low enough relative to the sample that the tests were conducted in a negligible manner.

From the frequency sweep, the complex viscosity can be determined using the following formula:

Complex Viscosity = viscosity – i ˣ elasticity

where i is the complex identity [42]. The overall shear modulus can be found using the following formula:

$$G^* = G' + iG''$$

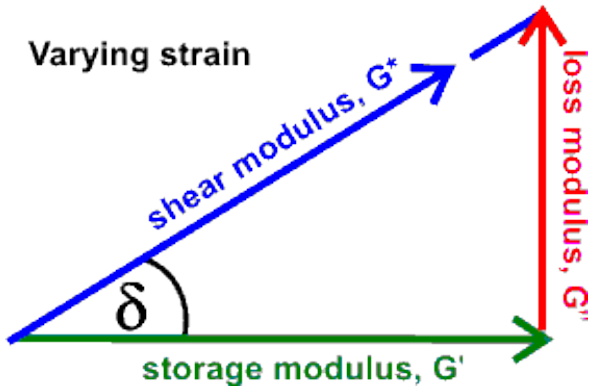

Figure 3.8 Pythagorian relationship between shear modulus, storage modulus and loss modulus

3.2.3 **Stress-Relaxation test**

The stress-relaxation test is used to determine a sample's viscoelasticity (stress over shear rate) and modulus (stress over strain) properties when subjected to a prolonged constant strain at a constant temperature. The viscoelasticity is a property of a material that exhibits both viscous and elastic character. The stress-relaxation test helps find the stress-relaxation modulus, G, also known as the shear modulus, which is the observed decrease in stress with respect to the strain generated in the structure. Measurements of G, G' and G'' with respect to time, temperature, frequency and stress/strain are important in order to characterize a material's viscoelasticity. The rate of stress of a sample to deform at a constant temperature is known as the shear rate. It is the slope created by the relaxation modulus vs. time. The reason that the stress relaxation test was chosen in this study was because the contact surface between the sample and the spindle remained constant for the entire test with a pre-set strain. Consequently, the stress is always proportional to the measured force (Cespi et al., 2007). This statement holds true only when samples are very similar in shape and size.

We reused each sample from the *frequency sweep* and conducted a stress relaxation test immediately after without accessing the samples in the rheometer's compartment. Three level of deformation were originally tested: 0.2%, 0.5% and 1% with a time of relaxation of 350 to 500 seconds in between each of four ramps tested. Ultimately, after obtaining unsatisfactory graphs with these three deformation percentages, through consulting the report of (Nicolle, 2010), the deformation value for the stress relaxation test had to be equivalent to that of the frequency sweep test (Υ=1.6%). The stress relaxation stage was repeated three times to insure consistency in the results. In total, 24 samples both treated and untreated were tested. The samples' codes were repetition based on the preceding test conducted by Dr. Périe-Curnier and her team in Australia back in 2014.

3.2.4 **Redo Frequency Sweep test**

Once the stress relaxation test was completed, we redid the frequency sweep test to make note of any variations caused by the relaxation test on the sample's storage modulus. The test itself consisted of the same procedure found in section 3.2.2.

3.3 Mechanical Testing Results

3.3.1 Strain Sweep results

The graph relating the shear stress as a function of the strain percentage in Figure 3.9 illustrates the curves obtained for the ten samples tested during the strain sweep. Firstly, there were no values for the deformation that were recorded below 0.8% due to the sensitivity of the machine. The second observation was that all the curves from 1Hz to 100Hz follow the same tendencies other than the curb at 50Hz which can be negated as an out of order deviation. Another observation was that in the lower strains, there were less data recorded compared to the higher strains. This greatly limited the domain of deformation values, beginning only at 1.4%. This also greatly limited the domain of values for the deformation for which we were seeking a period of linearity common to the entire curve. The frequency sweep was subdivided into two categories: the first set of frequency varying from 1Hz to 100Hz for samples submerged in the tyrode solution denoted by the letter "T." The 2nd category were samples placed directly under the spindle after slicing. The goal for this was to determine how the composition of the solution would affect the shear properties of the results.

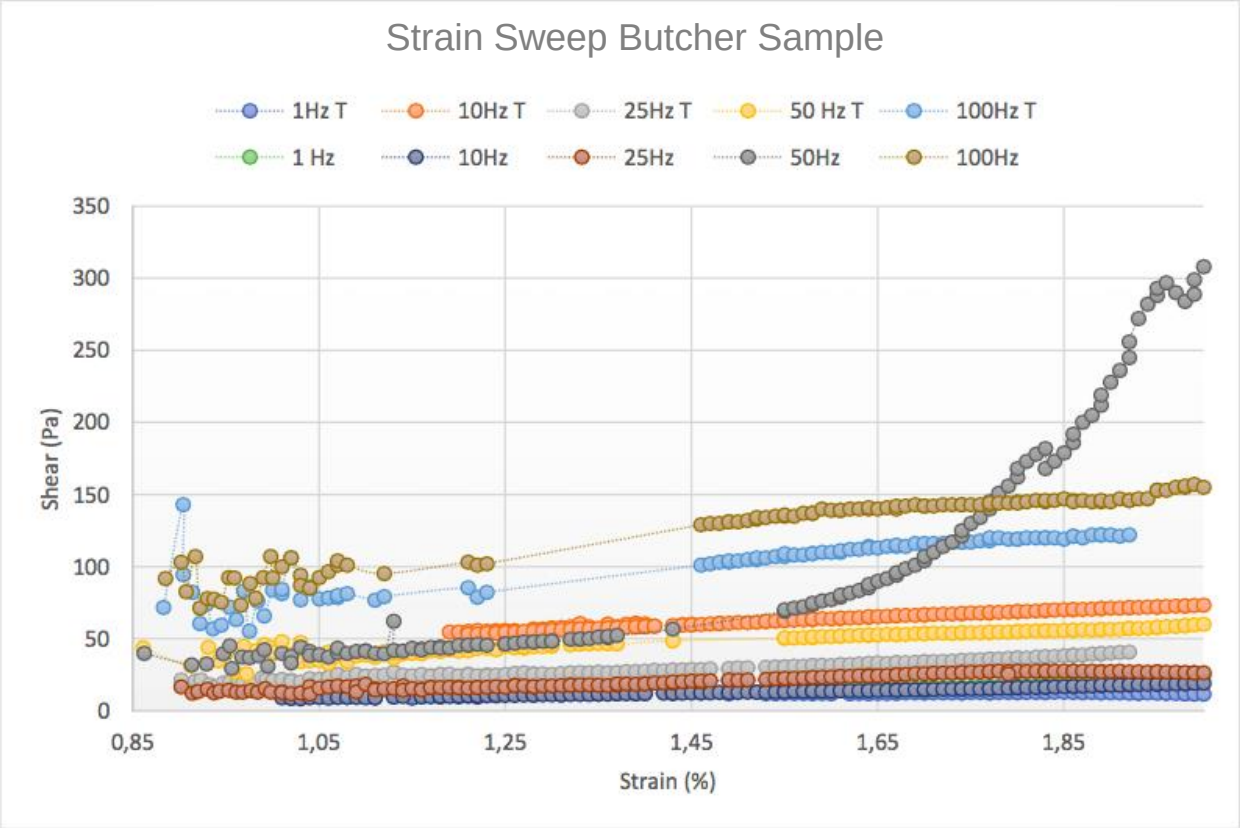

Figure 3.9 Results of the Strain Sweep from 1Hz to 100Hz for butcher samples

The strain sweep test allowed us to retain two sets of deformation that were used to conduct the frequency sweep. The first set of values varied from [1.7-1.9] % (Figure 3.10) and the second set being [1.5-1.7] % (Figure 3.11) as the goal of the R regression was to get closest to the value of 1,00.

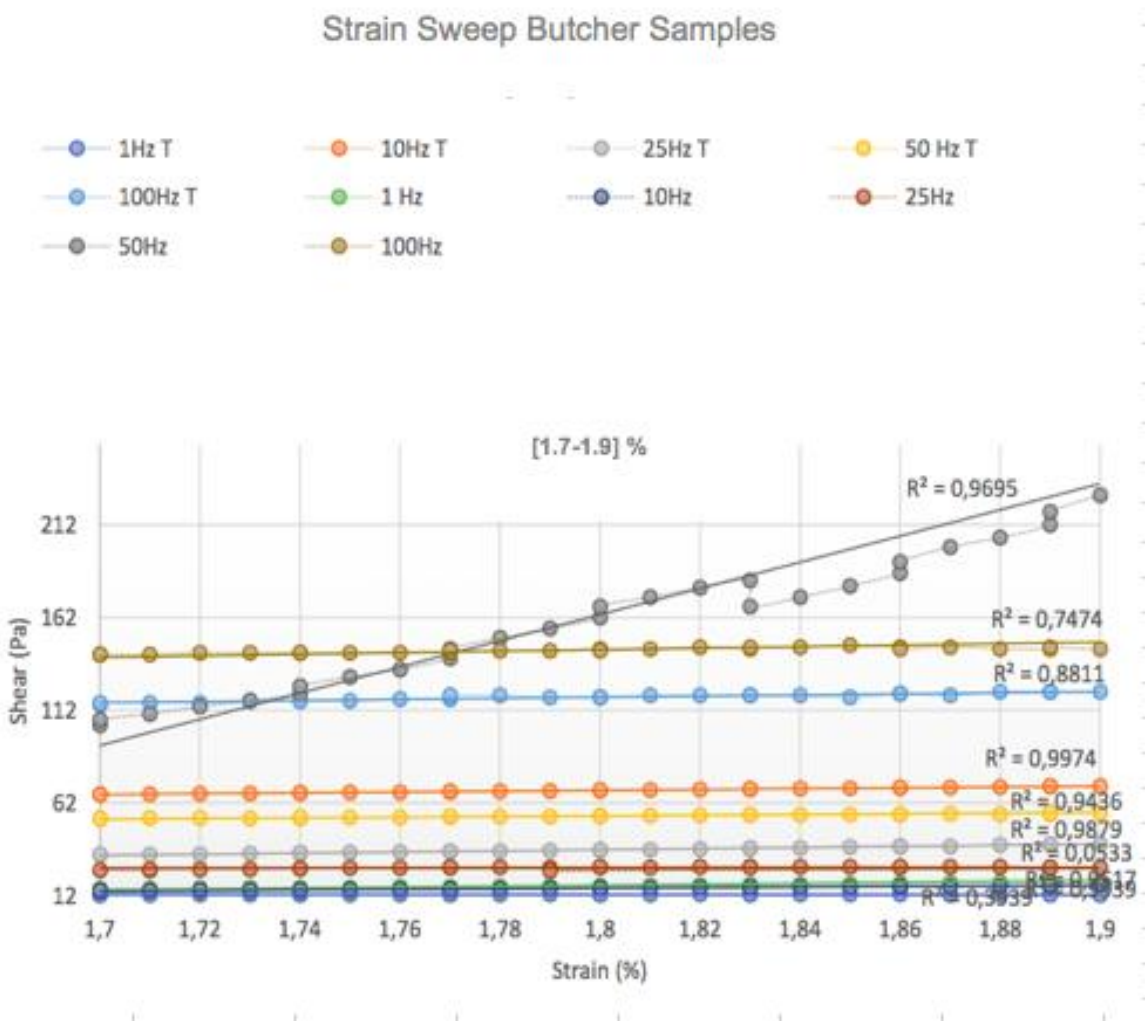

Figure 3.10 Linearity test finding R2 for the Strain Sweep [1.7-1.9] %

We still observe through Figure 3.11 as we do in Figure 3.10 another out of order regression this time for the frequency equal to 1Hz. If it is excluded from the data results, we obtain a regression coefficient of average value equal to 0.954 in Figure 3.10 whereas an average regression value of 0.9722 was observed in Figure 3.11, which is more of an acceptable value.

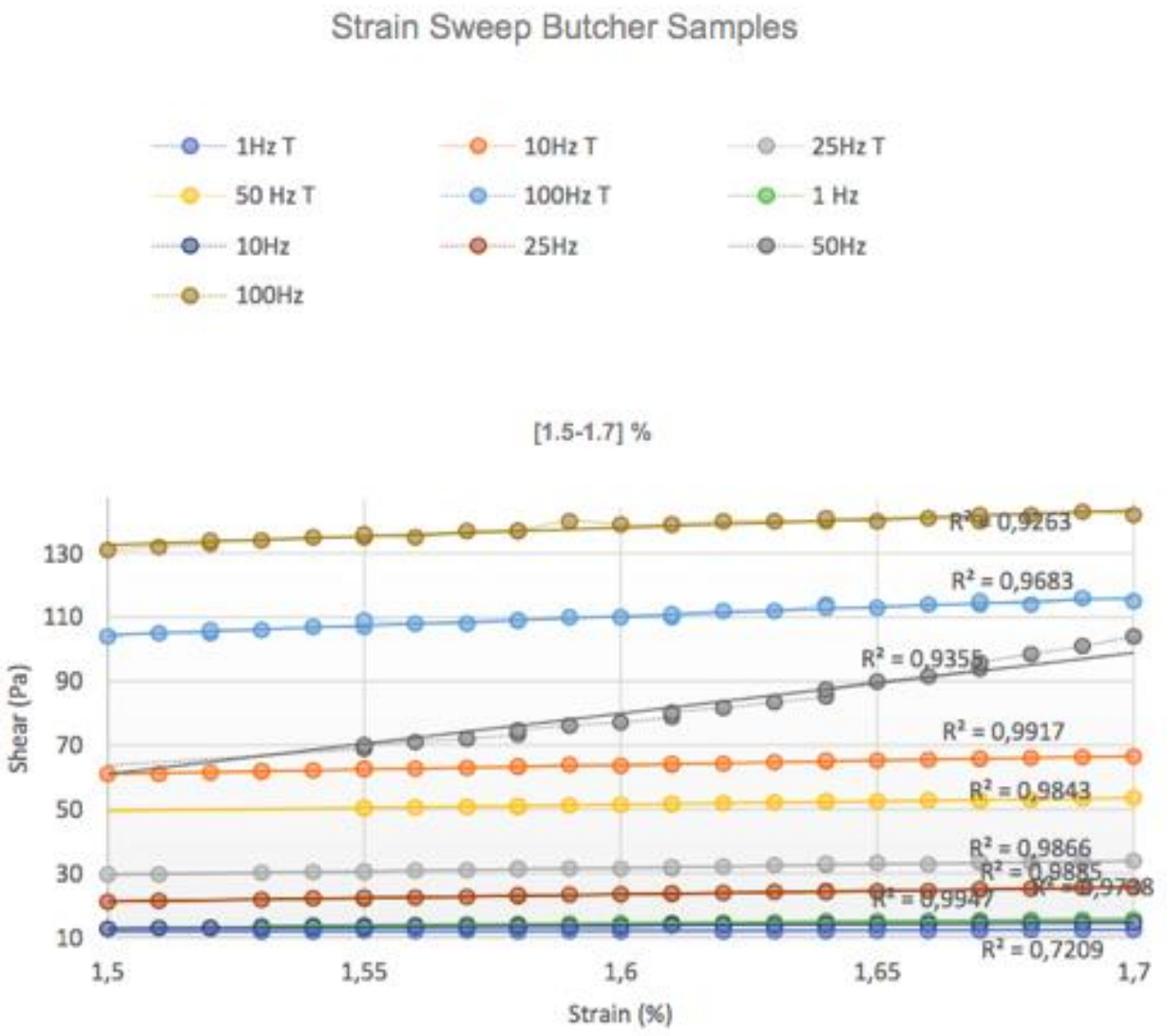

Figure 3.11 Linearity test finding R2 for the Strain Sweep [1.5-1.7%]

To conclude, though the second set of linearity conducted achieved similar regression coefficient averages than that of the interval [1.7 to 1.9]%, by force of an iterative approach, the deformation value of γ =1.6% was retained for the following frequency sweep. This deformation percentage is important as it will serve as the benchmark deformation value throughout the experimentation with the miniature swine samples.

3.3.2 Frequency Sweep Results

3.3.2.1 Frequency Sweep of Butcher Samples

After the five samples underwent six cycles of test, we generated graph 3.12, 3.13 and 3.14 at a deformation of 1.6% which displays the butcher samples' storage modulus, loss modulus and complex viscosity. We limited the study to collect all data points for all modulus' until 100Hz.

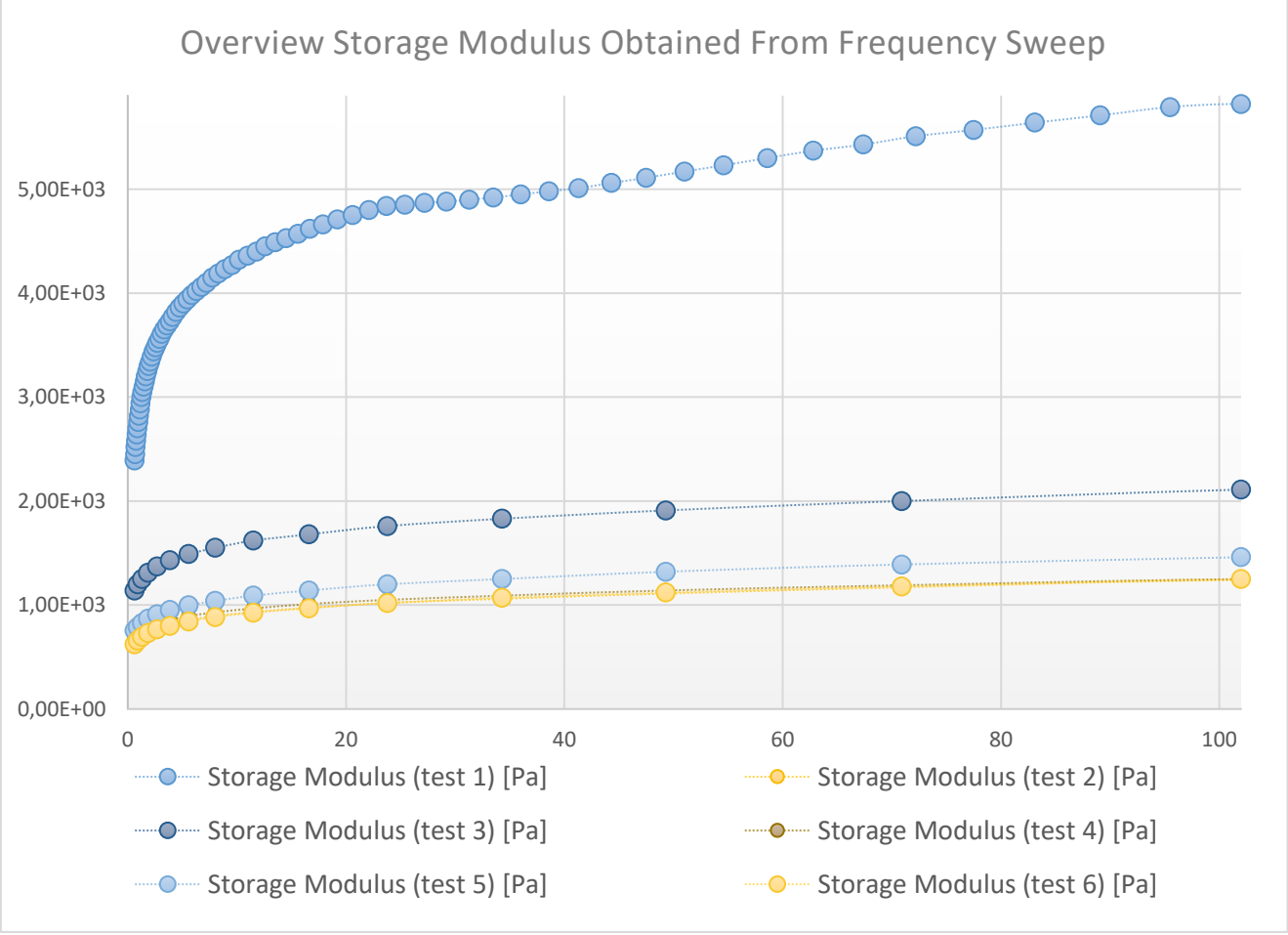

Figure 3.12 Storage Modulus Test Results Butcher Samples

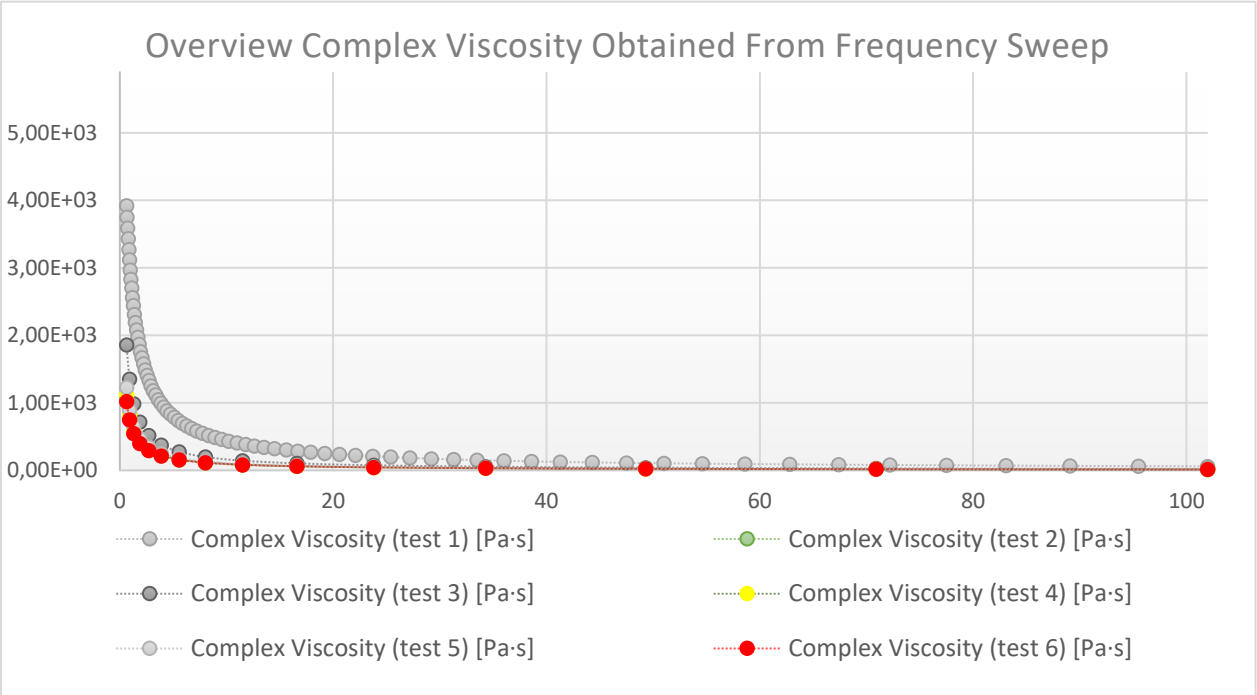

Figure 3.14 Complex Viscosity Frequency Sweep Test on Butcher Samples

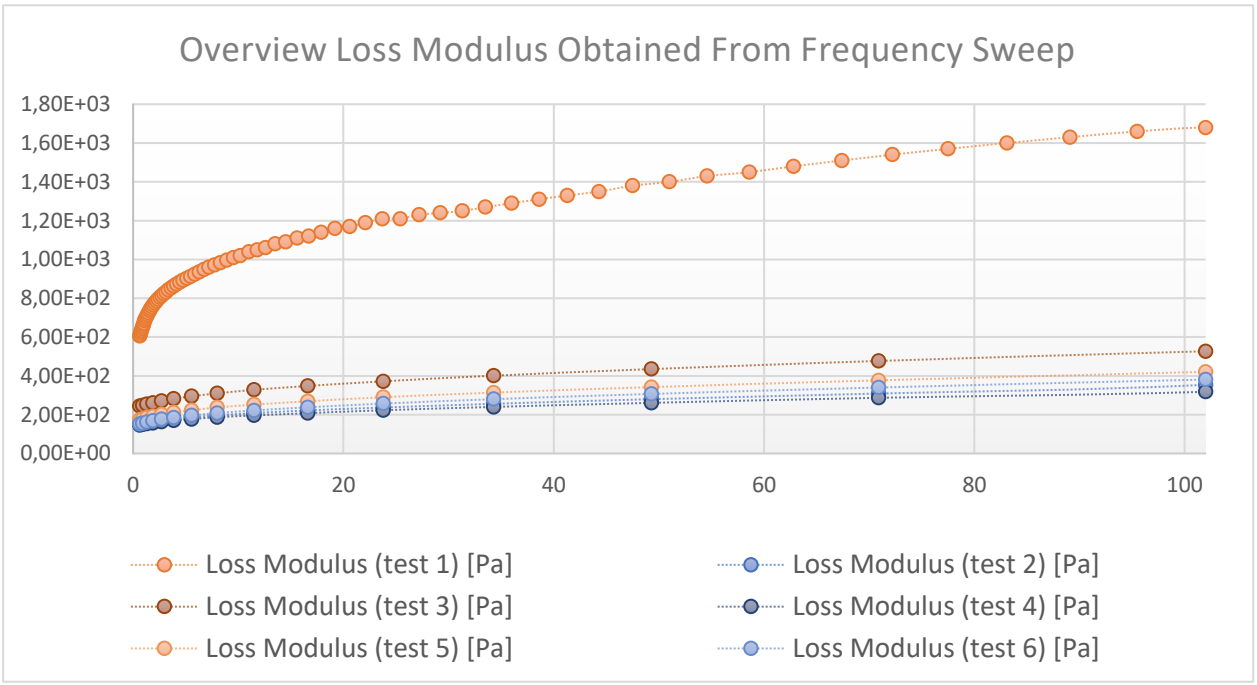

Figure 3.13 Loss Modulus Frequency Sweep Test on Butcher Samples

We achieved a frequency up to 100Hz during these test described in Figure 3.12, 3.13 and 3.14. Based on the data values obtained, we were able to trace the average and standard deviation value of G', G'' and of the complex viscosity for the five additional butcher sample tests. The storage modulus, G', in viscoelastic materials is a measure of the elastic response of a material which means that it measures the material's ability to store energy (Kalyanamaran et al., 2012). The higher the storage modulus, the more the material will be considered « solid » and will thus have a lower capacity to deform. The loss module, G'', also known as the viscous modulus is the ability for a material to dissipate energy such as heat (Kalyanamaran et al., 2012). The complex viscosity, η, describes the resistance for matter to flow. It is the relationship between the shear viscosity as a function of the material's shear rate (Kalyanamaran et al., 2012).

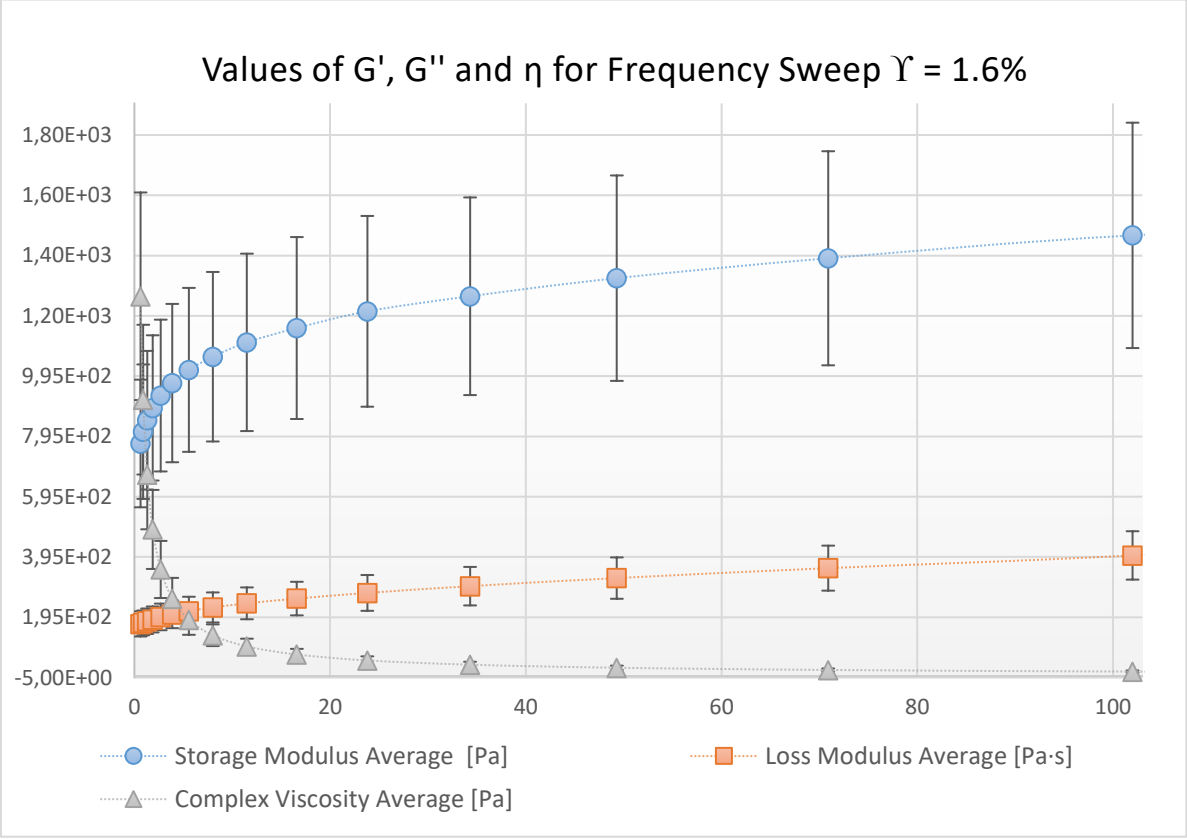

Figure 3.15 Visual Relationship between Complex Viscosity, G' and G''

The average and standard deviation combined for all three parameters interested in the study of the butcher samples can be found in Figure 3.15. The graph was derived from the individual graphs obtained for the storage modulus, loss modulus and complex viscosity.

Based on the tendencies of Figure 3.16, even though the results for the untreated hearts obtained are of a factor 1.4 times the amount of the butcher samples, the graph tendencies remain nearly similar. The average storage modulus for the untreated test samples tend to converge between 3.50E+03 and 4.00E+03 whereas the average storage modulus for the butcher samples had a tendency for a steady increase (slope ≈ 16) after 40 seconds. The average value of the data points found in the untreated samples curve was of $3.46*10^3$ and the average value for the data points found in the butcher samples was $4.9*10^3$. This allowed us to closely compare the samples from the butcher to the untreated samples due to the lack of samples retrieved.

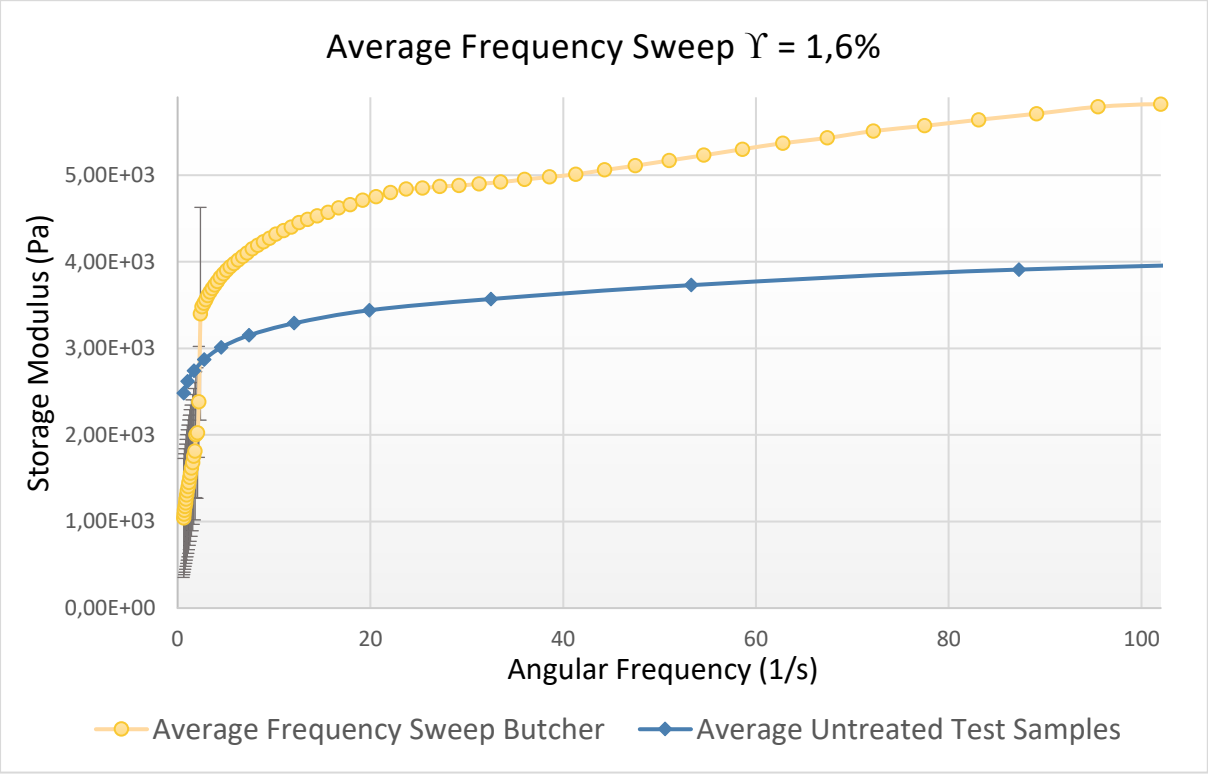

Figure 3.16 Storage Modulus Comparing Butcher to Untreated Samples

3.3.2.2 Frequency Sweep for Untreated and DOXO samples

i) Left Ventricle

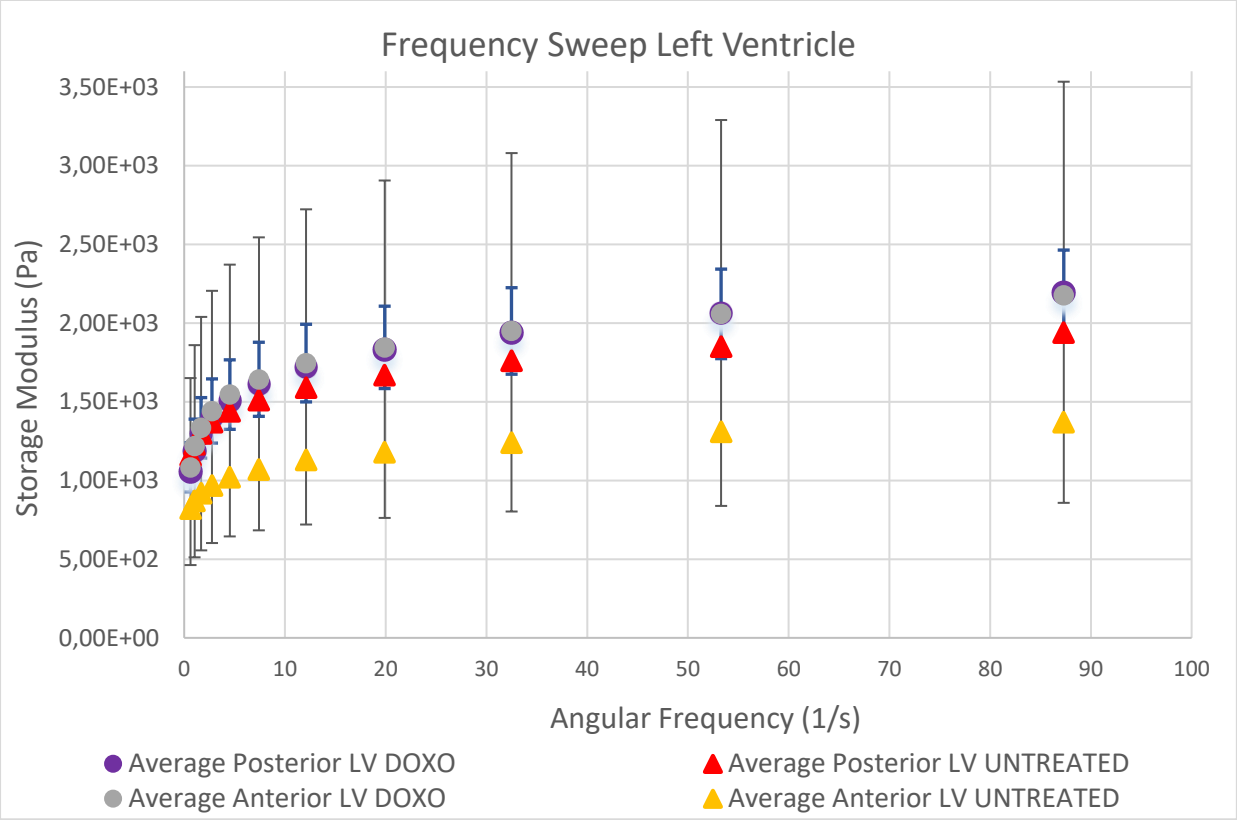

Figure 3.17 Average Storage Modulus results for the Left Ventricle Samples

The samples used can be consulted in Table 3.3. Based on Figure 3.17, we observed a higher storage modulus on average for DOXO samples denoted by the circular data point than we did for untreated samples. However, regardless of if the sample was treated or untreated with doxorubicin, both displayed similar storage modulus tendencies studied during the frequency sweep. The last item to observe from Figure 3.17 is that the posterior samples obtained a higher standard deviation (longer vertical error bar) than the anterior samples. There was an insufficient amount of samples

to calculate the standard deviation for the untreated samples, which explain why the triangular data points did no display vertical error bar marking its sample's standard deviation. To view the results for each sample code from Table 3.3 covering the left ventricle, the graph can be consulted in Appendix A, Figure A1 & A2.

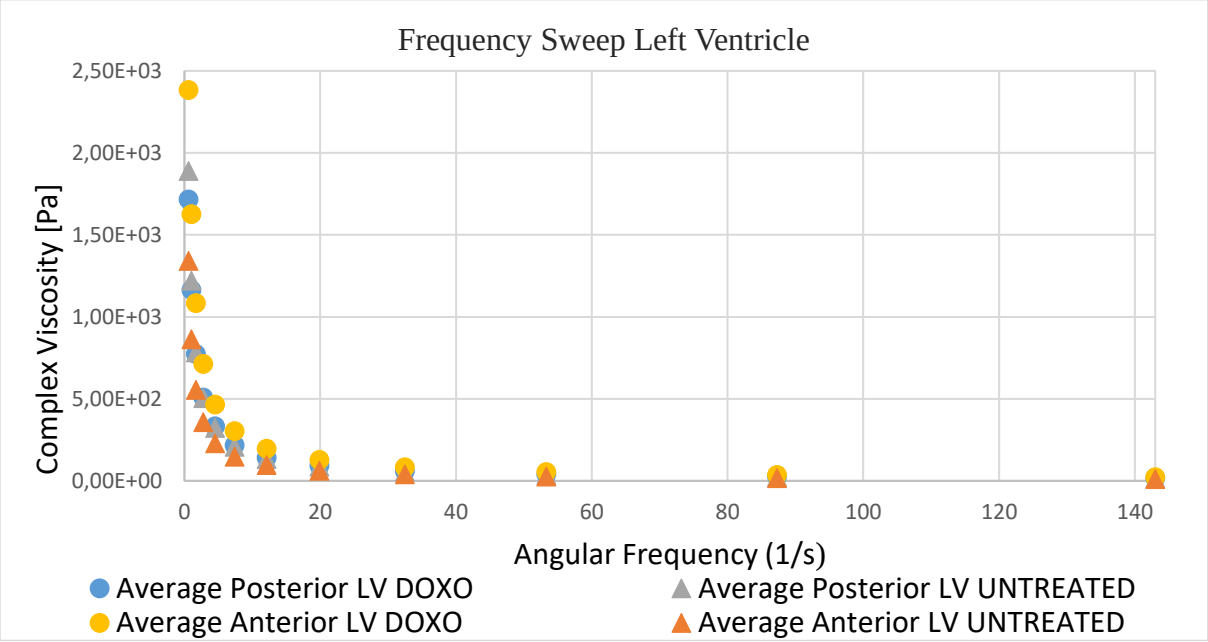

Figure 3.18 Average Complex Viscosity for Left Ventricle Samples

The results for the complex viscosity found in Figure 3.18 draw inconclusive results. The only pertinent information to note is of the similar complex viscosity found in both the untreated and DOXO samples which seems to be unaltered.

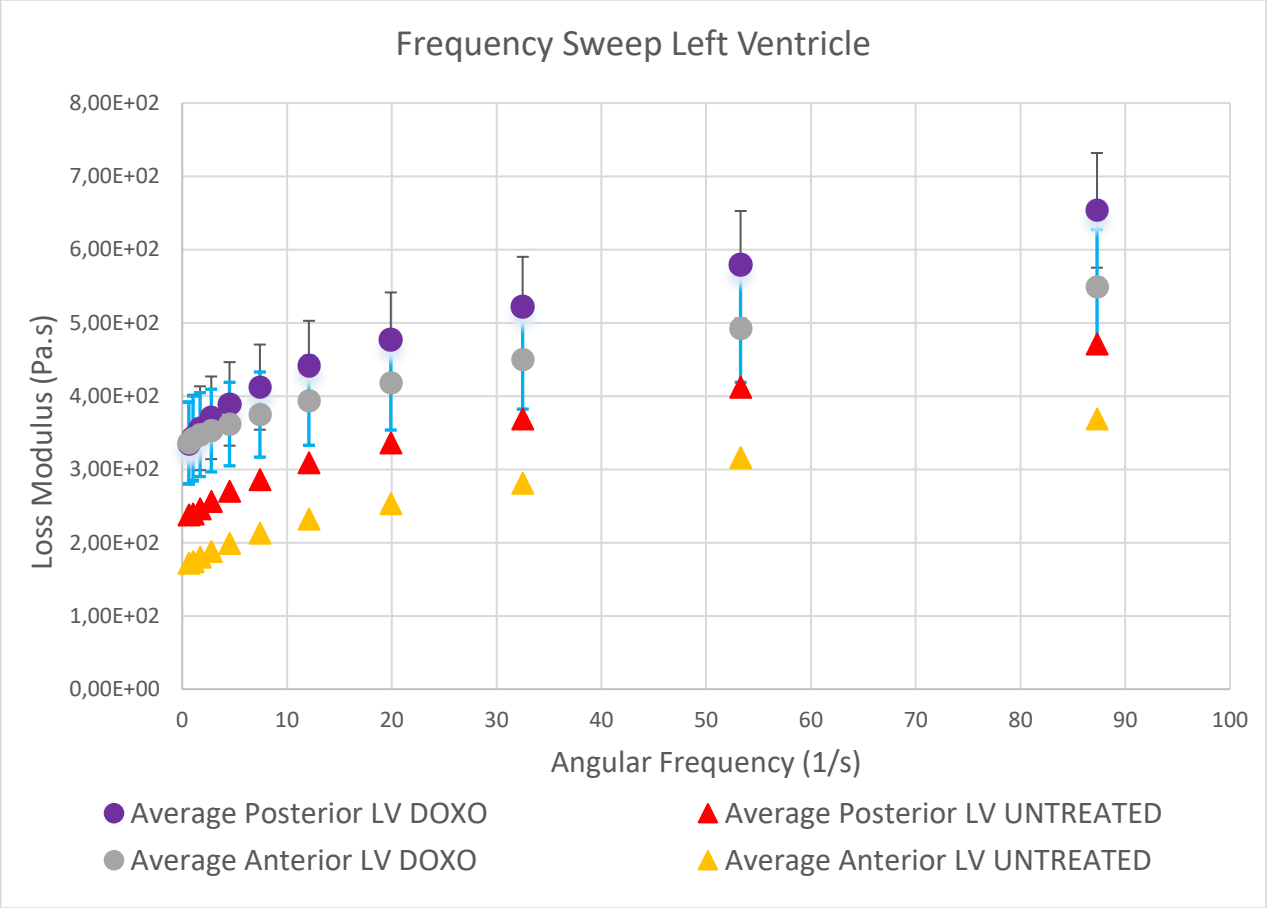

Figure 3.19 Average loss modulus for Left Ventricle Samples

The last measurement of interest is the loss modulus found in Figure 3.19. When combining all samples studied for the posterior and anterior left ventricles, we notice an increase in the loss modulus for the DOXO samples compared to the untreated samples. This result for the left ventricle is in line with the results obtained for the storage modulus.

ii) Septum

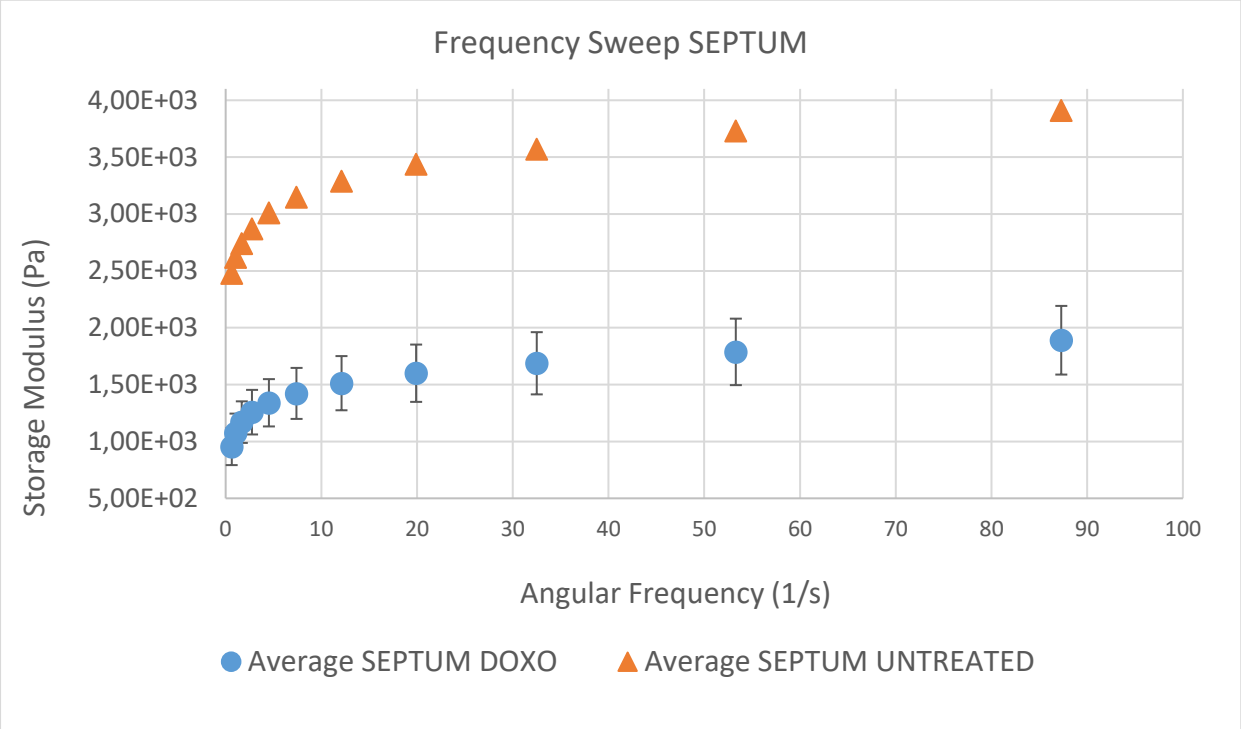

Figure 3.20 Average Storage Modulus Frequency Sweep Septum

Contrary to the left ventricle, the testing for the samples covering the septum show a diminishment of the storage modulus and loss modulus in those carrying the doxorubicin injection. The untreated samples exhibited an average storage modulus of $3.165*10^3$ Pa whereas the DOXO samples averaged $2.095*10^3$ Pa. This represents a 33% drop in the DOXO sample's viscoelastic ability to absorb energy. These results are retrieved from the tables found in Appendix B. Given the insufficient data can thus conclude that the doxorubicin agent has a greater negative impact in the septum in the mechanical properties than in the left ventricle. To view the results obtained for each sample code, a graph displaying the following for the septum samples in Appendix A, Figure A8.

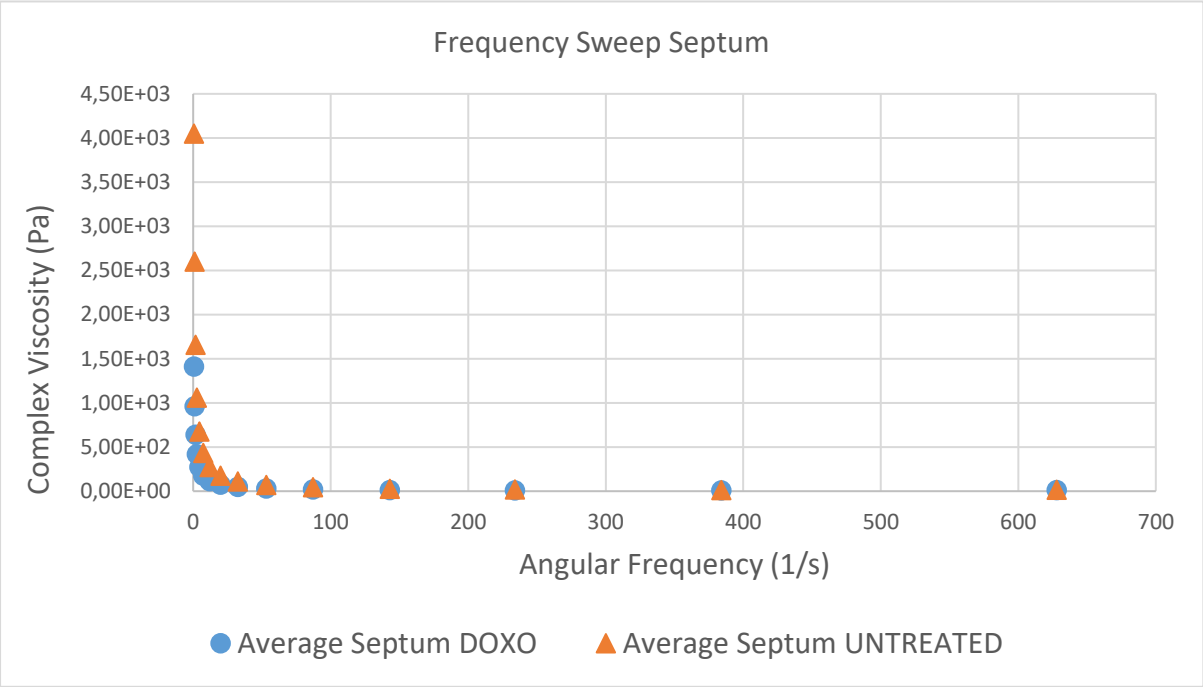

Figure 3.21 Average Complex Viscosity Frequency Sweep Septum

Similarly to the Complex Viscosity of the left ventricle, Figure 3.21 shows inconclusive results but both induced and non-induced samples had nearly identical complex viscosities. They were comparable in that they both outputted a rational function allure where samples converged to a complex viscosity almost immediately after we started collecting data points. This curve occurred not only for the septum but for the left and right ventricles as well.

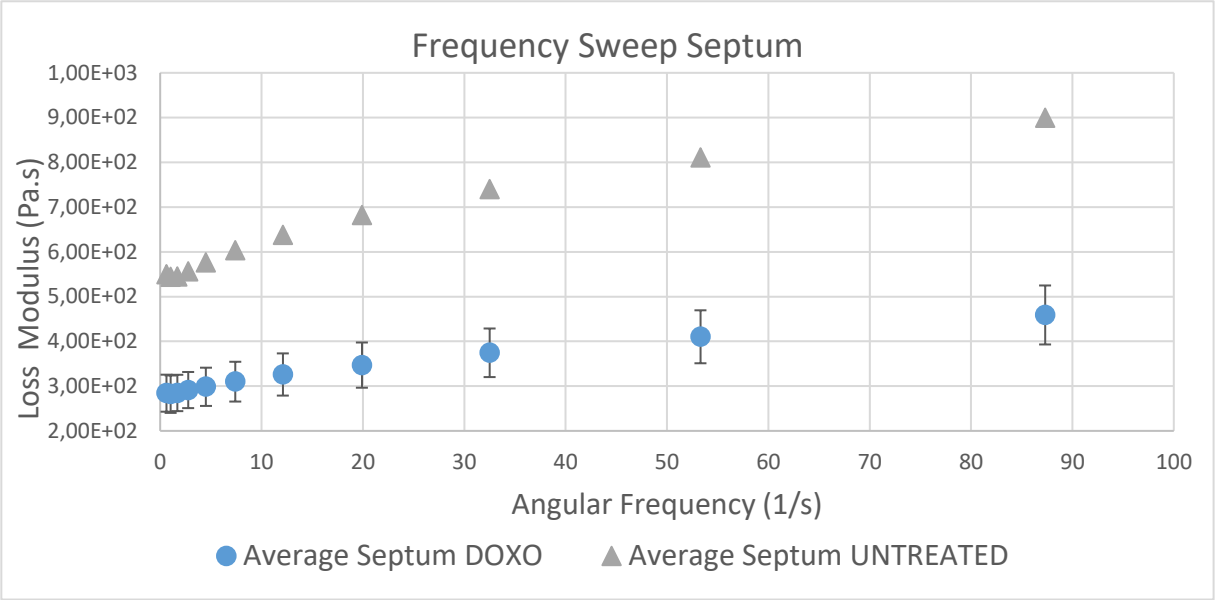

Figure 3.22 Average Loss Modulus Frequency Sweep Septum

As expected for the septum, Figure 3.22 shows a decrease in the average loss modulus of its samples similarly to the average storage modulus. This is expected because both the storage and loss modulus demonstrate a sample's viscous and elastic properties. They are also related based on its summation equating sample's shear modulus. Figure 3.22 correlates with our initial data synthesis where Septum sample's exhibit a drop in its moduli's when treated with doxorubicin.

iii) Right Ventricle

In this particular curve, Figure 3.23, both samples of the right ventricle treated with doxorubicin had near exact data values. This is why the sample's standard deviation is almost negligible in Figure 3.18. Even though they originate from the same miniature swine, other results showed variations even when the samples were sliced from the same part.

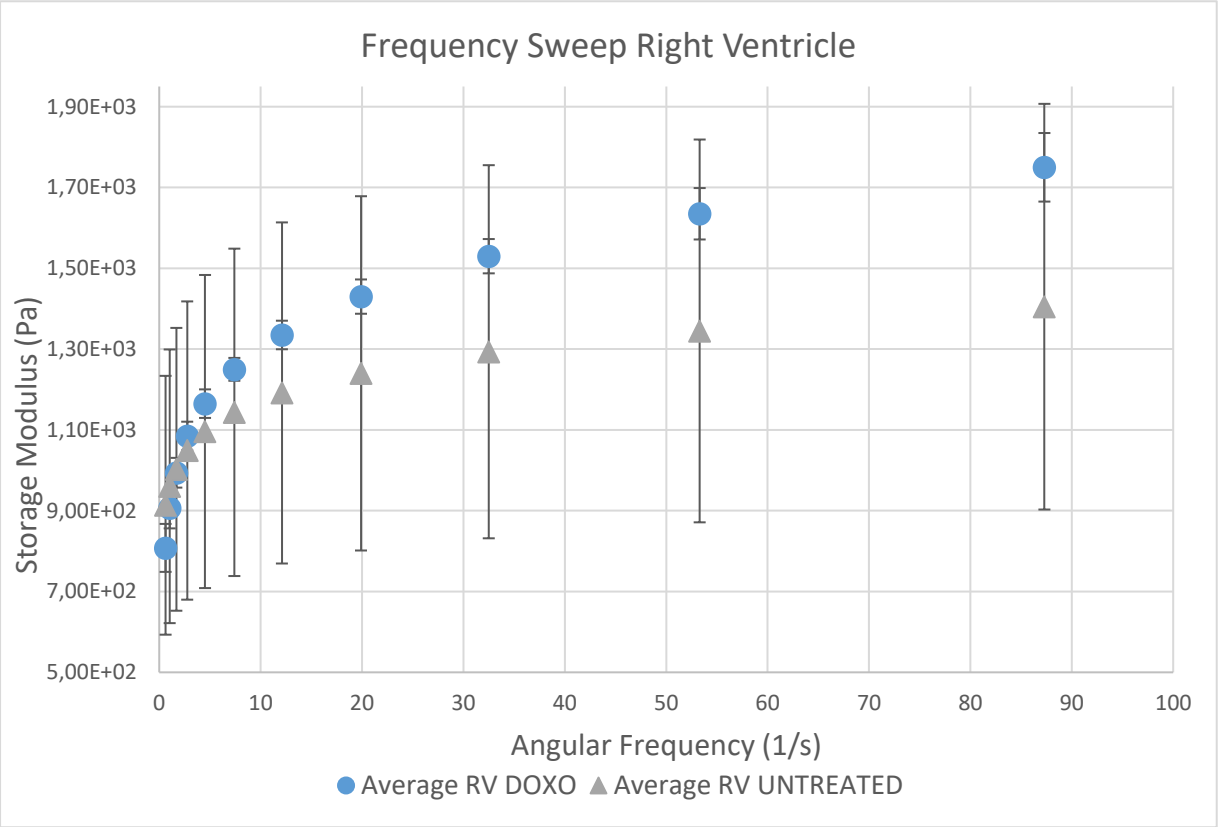

Figure 3.23 Frequency Sweep results for right ventricle

The results obtained for the right ventricle samples' frequency sweep show an overall increase in its storage modulus compared to the untreated samples. However, given the insufficient amount of data collected, we proceeded in making an inconclusive statement based on the lack of data

obtained. This can be due to the right ventricle samples being overly fractured to use for experimentation. The graph displaying all sample codes' data can be consulted in Appendix A, Figure A3.

3.3.3 Stress Relaxation test results

i) Posterior and Anterior Left Ventricle

Elements to retain looking at Figure 3.24 are that the test effectuated on untreated samples will

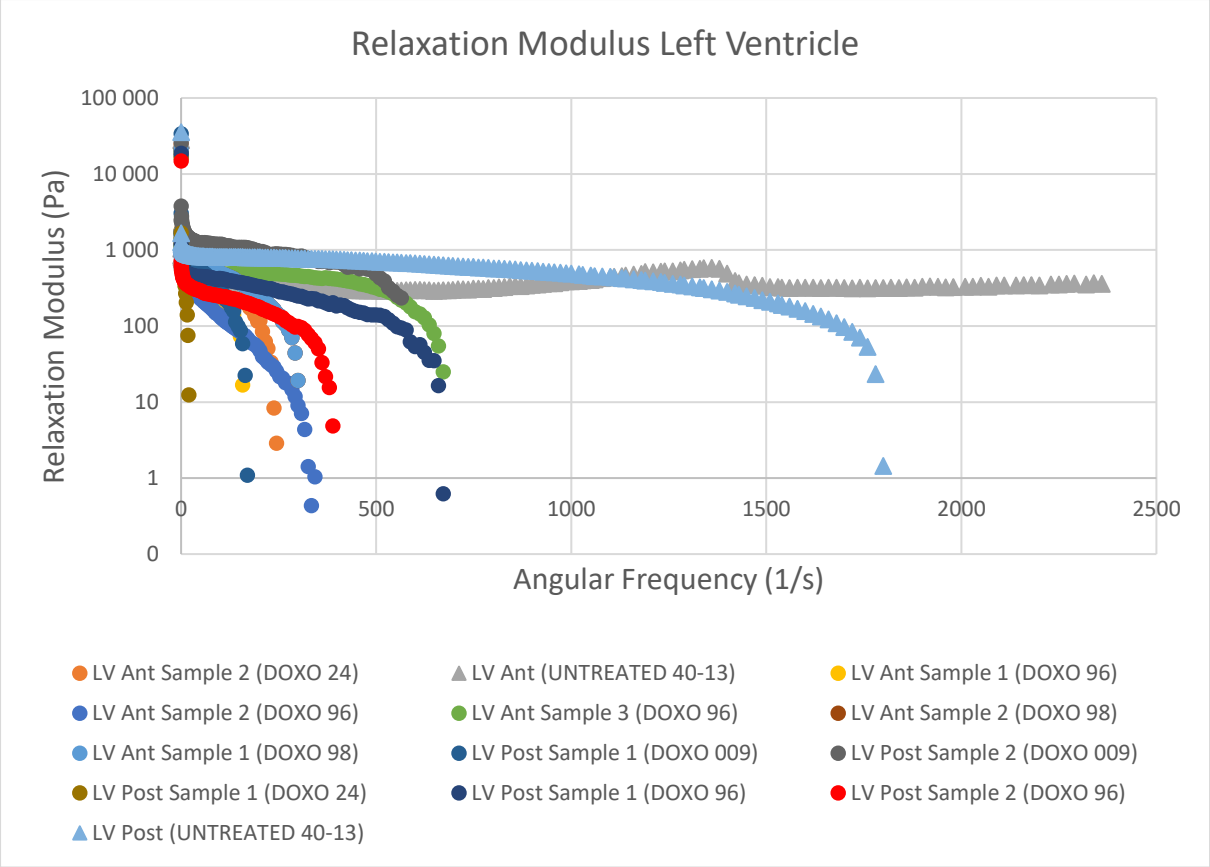

Figure 3.24 Relaxation Test Posterior Left Ventricle

drop at a rate 3x longer than the samples induced with doxorubicin. Sample 40-13's relaxation modulus dropped at 1800s (30 minutes) versus an average of 500s for the untreated samples (009, 24, 96 & 98). This graph shows a clear demonstration on the diminished impact doxorubicin

induced samples have on the mechanical properties. It is important to understand that the force applied goes to zero after the drop but the sample's deformation is still present.

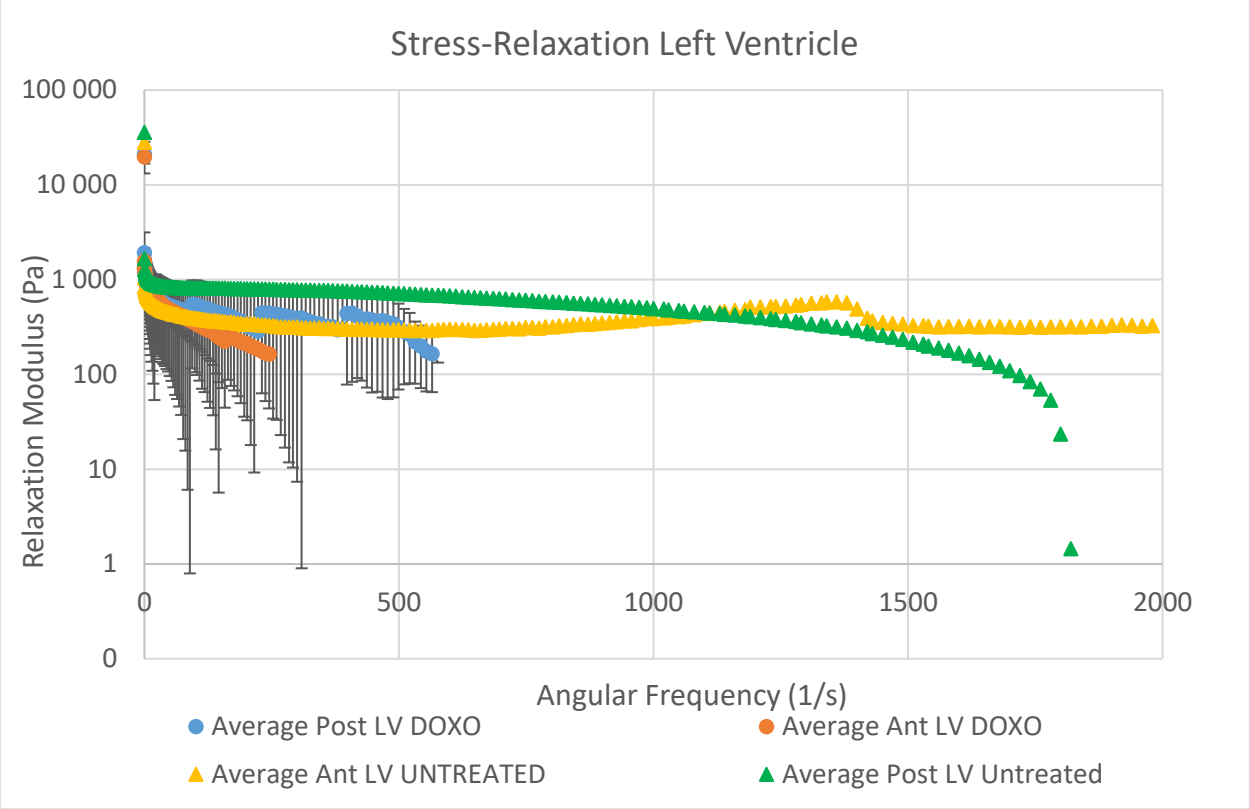

Figure 3.25 Average Relaxation Test Left Ventricle

In the Figure 3.25, the data points for each sample was combined into an average where the graph shows more closely the average drop in relaxation within the first 600s for the DOXO samples whereas both the anterior and posterior untreated samples dropped considerably later. The green and yellow curve representing the untreated samples show its ability to withstand a decrease in its relaxation modulus also known as its shear modulus. We stopped the relaxation testing on left ventricle sample after 2000 seconds (equivalent to 200 data points) because the curve tendency

was such that the force applied would not drop to zero and it reached to what seemed like its equilibrium state.

ii) Septum

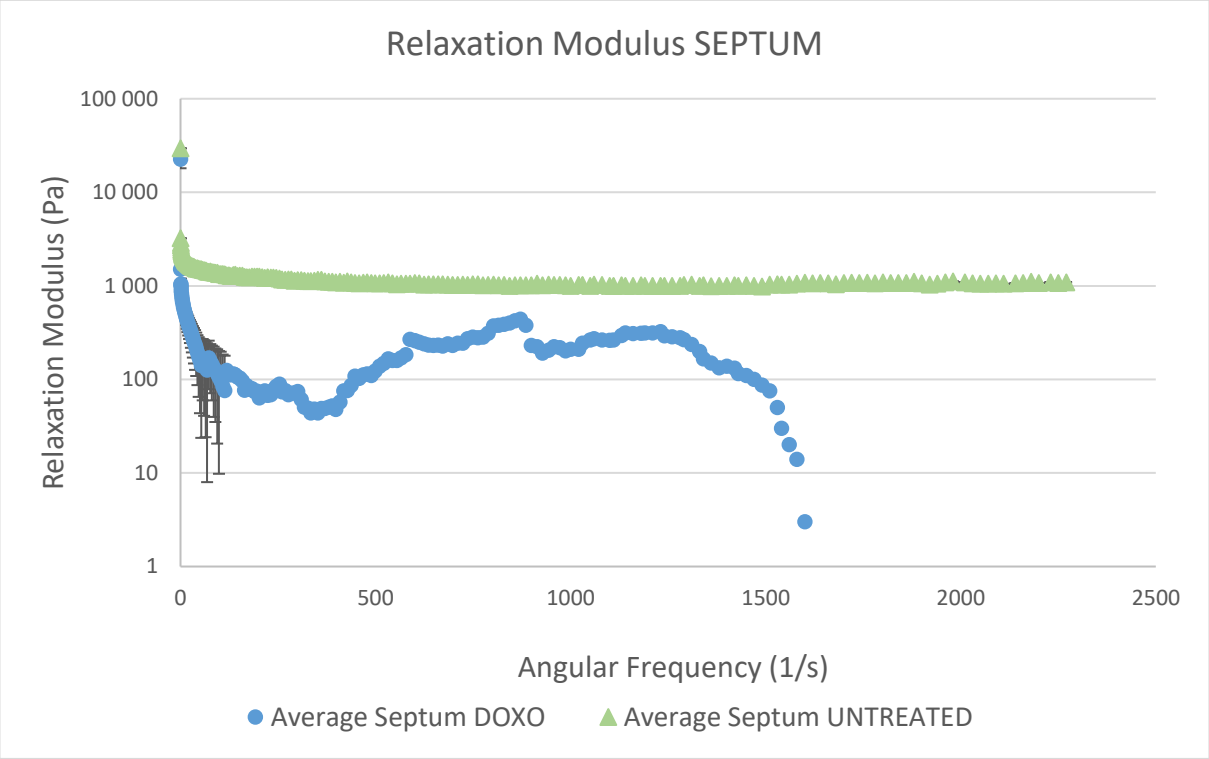

Figure 3.26 Average Relaxation Test Septum

The results of the septum samples show similar tendencies to those of the left ventricle samples where a radical drop in the samples are due to the injection of doxorubicin in the samples. This drop is more significant than the left ventricle samples. The standard deviations are more prominent within the first 100 seconds because it included sample-96 which ended up dropping in its shear modulus 113 seconds after test began. A reason we can justify why DOXO (sample 98) experienced a longer time to drop compared to other DOXO samples in the left, right ventricles as well as the septum is because sample 98 contained two major fractures as seen in Figure 3.27.

Figure 3.27 Fractured Septum Sample 98

Indeed, even if the septum samples maintain a constant relaxation modulus of approximately 10000 Pa, we observe a steep drop for the treated samples, which happens within the first 2 minutes. The average DOXO sample dropped around 230 seconds though in Figure 3.26, it dropped on average later on due to one particular sample (DOXO 98). This sample can be considered to be out of order and the standard deviation after 230 seconds is inexistent since this is the only sample carrying on with time.

The stress-relaxation test remains consistent for all sectors of the heart and allows us to thus omit the hypothesis that, compared to the left ventricle, the molecule of doxorubicin brings in higher degradation effects to the tissue at the septum level.

3.3.4 **Frequency retest results**

The samples pre and post test are subjected to the same initial forces. The preconditioning of the samples followed the same testing parameters except the post test samples exhibited a residual stress relative to the 'pre-test' samples.

i) Posterior and Anterior Left Ventricle

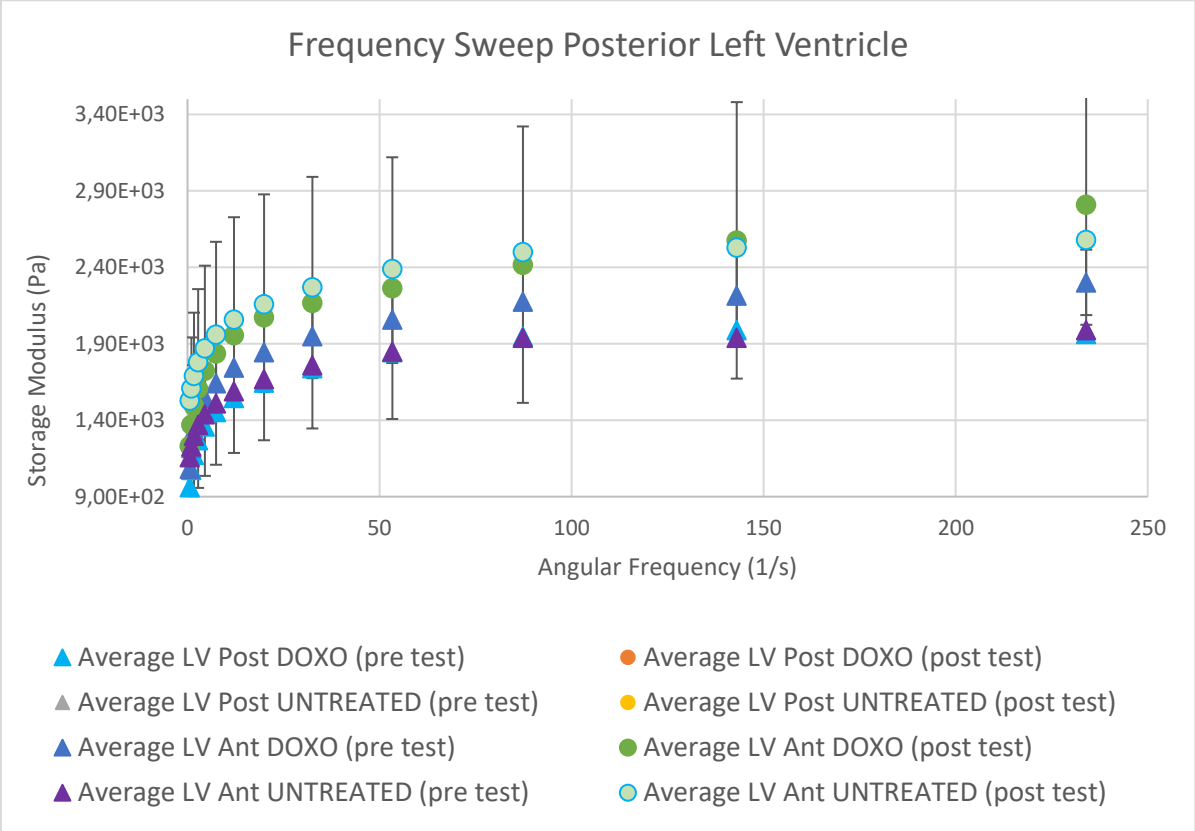

Figure 3.28 Frequency Sweep redone post relaxation test on left ventricle samples

The results following the stress-relaxation test are as follows in Figure 3.28 and the results obtained in each sample code can be consulted in the appendix figure A10. The curve for the left

ventricle represents similar overall tendencies for both the posterior and anterior samples. The curves show comparable frequency sweep results for the same part of the heart cavity but for samples differed by a treated and an untreated state. Samples found in the legend that cannot be conveyed in the graph is simply because those samples are superposed with the ones displayed in front of it. Based on the graph above, we observed a higher storage modulus than those effectuated by the pre-test samples. In Figure 3.28, the samples post-test, when a deformation was being applied, had an increase of force that ended up stabilizing itself as we increased the angular frequency. The samples post-test contains a residual stress that pre-test samples do not have. This allows us to characterize myocardium tissues based on the differences denoted in the curves above.

Is the variation in the storage modulus during the post frequency sweep due to the residual stress caused by the initial frequency sweep or due to the rotations caused during the stress-relaxation test? This still needs to be explored. However, we can say that the deformation percentage (Υ=1.6%) was used equally for both tests conducted.

The same analysis from the posterior samples applies to the anterior samples which exhibited the same overall increase in both the storage and loss modulus. By deduction, an overall increase in the shear modulus can be said by the following formula presented in the theory chapter.

$$G^* = G' + iG'$$

ii) Septum

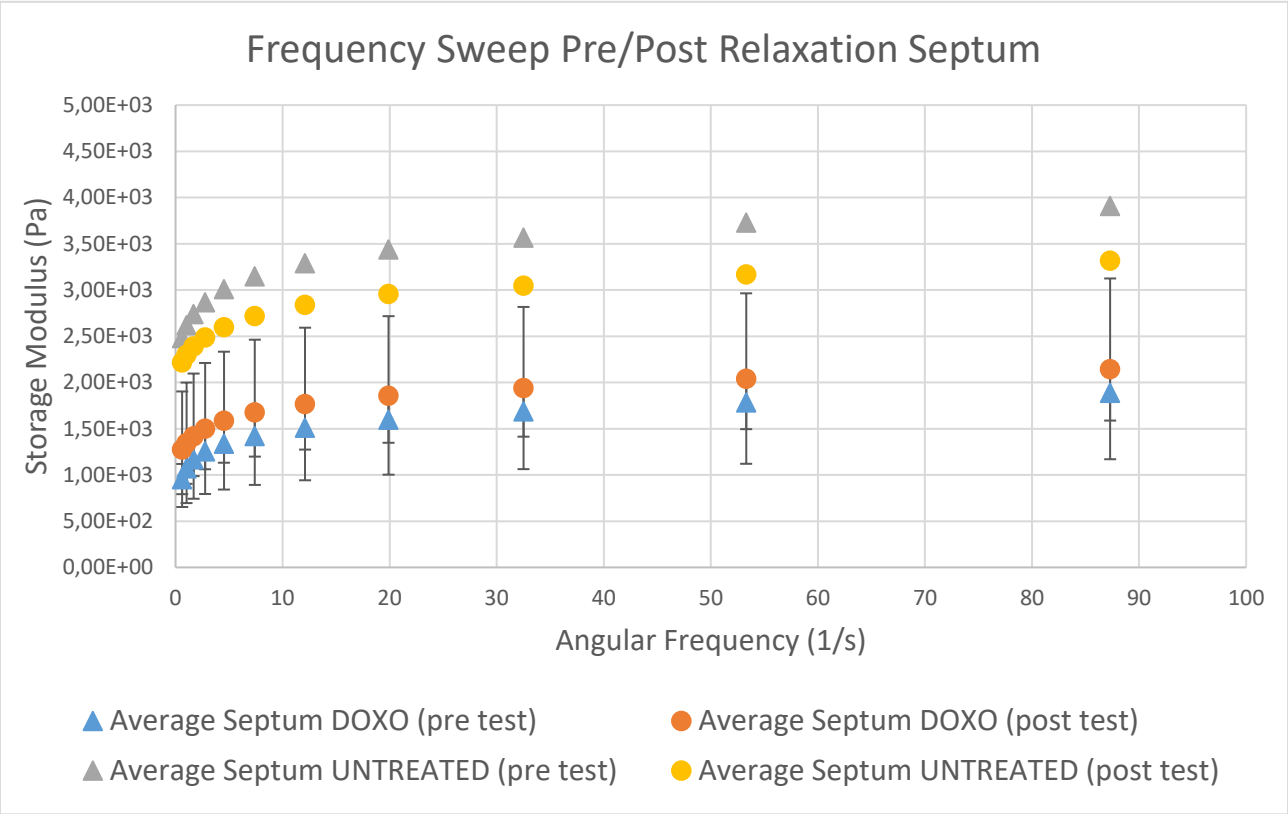

Figure 3.29 Frequency Sweep redone on septum samples post relaxation test

The untreated samples experienced a decrease in its overall storage modulus post stress-relaxation test as opposed to the DOXO samples in which its storage modulus increased after the stress-relaxation test. The graphical tendencies remained the same as the angular frequency increased. The goal was to distinguish the pre and post test results by having the post test samples with circular data points whereas the pre-test samples used triangular data points. The results obtained for each Septum sample's storage and loss module can be found in the appendix Figure A9 as well as Table B2.

In contrast to the posterior and anterior samples, the septum sample results showed varying results. Sample #1 & #2 of code 96 along with the untreated sample (40-014) showed a

diminishment in the storage modulus post relaxation test. The same goes for the loss modulus where sample #1 & #2 as well as the untreated sample (40-014) showed a diminishment of this modulus post relaxation.

iii) Right Ventricle

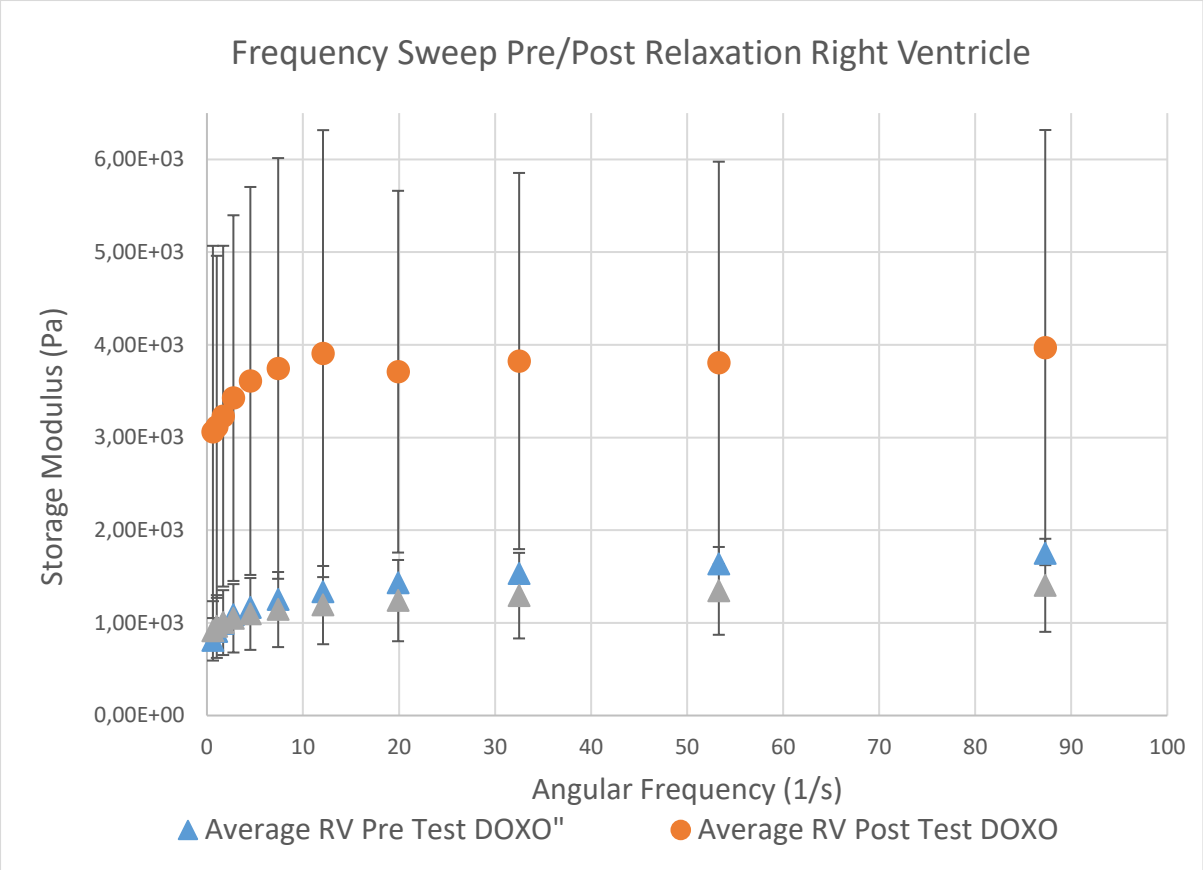

Figure 3.30 Frequency Sweep redone on right ventricle samples post relaxation test

Based on the data in Figure 3.30, the curves followed similar tendencies pre relaxation test with similar average storage modules. Due to performing the untreated samples before the introduction of the post frequency sweep test, we did not calculate the post test results of samples

1 & 2 of the (40-014-UNTREATED) samples. The general storage modulus seems to have benefited the samples after being solicited to a stress-relaxation test. The table below also culminate the results obtained in the data but in the form of numerical values. The loss modulus is also provided.

The results obtained for the right ventricle reflect the same conclusion drawn from the posterior and anterior left ventricle samples. The overall properties for the samples increased post relaxation test. It is important to note that due to the inability of performing the post test of the untreated samples, we were unable to draw any conclusions for samples 40-014 though it would have probably comported the same way as sample 96 - DOXO.

3.4 **Mechanical Testing Discussion**

To summarize the results obtained during the mechanical testing, the strain sweep results of γ =1.6% allowed us to perform the frequency sweep where we noticed varying results between DOXO and untreated samples. We noticed an overall increase in the storage and loss modulus in both the left and right ventricles but a drop in the septum samples. When it comes to similar effects in all compartments of the heart, our results contradict our original hypothesis in that we assumed a homogeneous heart when in fact, the septum obtained varying results for the storage, loss and shear modulus. If the theory of a homogeneous heart was true, the septum and left/right ventricle would have exhibited similar tendencies in terms of overall increase/decrease of the moduli. However, in the stress relaxation tests, the results obtained showed an overall depletion in the DOXO samples' mechanical properties for the shear stress (G). Finally, the frequency sweep pre

and post stress relaxation test showed varying results, however, the graph tendencies remained the same and thus, the overall impact was considered to be negligible for all sectors of the heart studied.

After observing the results obtained on our various samples, we can make a clear affirmation that the composition of doxorubicin has an effect on the overall degradation of the heart's mechanical properties even though it is less evident in the left ventricle samples. These results obtained allow to validate our hypothesis on the 3 zones of the heart.

Although tests were performed for the right ventricle, a detailed analysis was foregone due to the insufficient amount of samples retrieved. However, based on the 2 sample comparison, the right ventricle showed similar tendencies than the left ventricle.

In order to obtain more accurate results, the addition of the butcher samples could have been used since their change factor was seen to be approximately 1.4 when comparing each other's overall frequency sweep. However, given that the untreated samples were injected in a saline solution and were frozen over the course of two years at -80°c, we decided to not use the butcher samples when studying the right ventricle due to these add on differences which can alter overall results.

A previous study by *Zuidema et al*. highlights a protocol for hydrogel tissues with a similar outline than ours worth mentioning. He proceeded with a chronological protocol debuting with the time sweep test (not relevant to our experimentation since were dealing with solid tissues) followed

by a strain sweep test. Once completed, a frequency sweep would follow there after followed by a secondary time sweep test (Zuidema et al., 2014). The second time sweep was conducted in order to obtain the hydrogel equilibrium modulus.

The testing made use of a 20mm diameter plate housed on a TA Instruments AR-G2 rheometer (Zuidema et al., 2014). The main difference was that he disposed each hydrogel sample so that it be used only for one test. Given the limited sample we were able to extract from the parts and the fact that we wanted to highlight potential correlations among test, we proceeded with using the same samples for all three of our tests post strain sweep.

3.4.1 **Strain Sweep**

The strain sweep was the gateway to all the additional tests needed to define the main mechanical properties of the miniature swine samples. The actual samples used during the experimentation did not undergo a strain sweep test but rather the samples used were ones purchased at a local butcher. In a previous study conducted by *Sommer et al.,* a strain sweep test to study the relationship between the shear stress versus the strain percentage on human hearts was covered (Sommer at al., 2015). The study found that in the shear stress versus shear amount preconditioning curve, when the shear amount increased, the second loading cycle of the new stress–strain curve repeated the same preconditioning loading curve of the cycle that preceded it. This reflects the same test we conducted at the CrCHUM and validates our protocol. The samples studied were in the shape of a cube with an edge equal to 25mm. The study conducted by Sommer puts a big emphasis on the structure and composition of the human myocardium since, according to his study, this influences the passive mechanical properties of the tissue. Components such as

the myocytes and the extracellular matrix are primarily responsible for the mechanical behavior. By using the shape of a cube, Sommer was able to work considering an equal homogenous repartition of the muscular fiber all oriented in the same direction (Sommer et al., 2015). Given the limitation of our rheometer, the ideal shape candidate to place in the shape of a spindle was of a circular disc. This approach was also used in the previous study conducted by Dr. Périe-Curnier so maintaining this consistency would have been important for our testing results (Périe-Curnier et al., 2013). In addition, the preparation of Sommer's samples concluded that shear testing exists in biaxially-tested myocardium but are very small when compared to normal stressed in the mean fiber direction (MFD). We concluded consequently that sample cuts ignoring fiber orientation would have negligible impact on the sample's shear properties.

The average deformation value used for Sommer's experimentation was of $\gamma = 0.5$ that cover the different shear levels (0.2, 0.3, 0.4, 0.5). Our testing to find the optimal deformation value began as of $\gamma = 0.8$ since no data points were being recorded below it. Based on our linear regression test, we obtained an optimal deformation value at $\gamma = 1.6\%$. Given the difference between our value and the one used for Sommer's human heart samples, we made the assumption that the difference in deformation was due to the different shapes used as well as the difference in myocardium tissue used given that his touched upon the human heart.

The overall perspectives drawn from Sommer's tests cannot be compared to the testing conducted from this study since his myocardium samples were under quasi-static and dynamic multiaxial loading. The study also did not focus so much on comparing diseased tissues versus healthy tissues. He noticed a nonlinear, viscoelastic and orthotropic feature to the human heart.

In another study presented by *Zuidema et al*., hydrogels were used such as collagen, agarose and fibrin to define rheological testing for general tissue engineering. Specifically, the strain sweep was conducted to establish the viscoelastic region of the hydrogel in respect to strain (Zuidema et al., 2014). Hydrogels are good candidates for rheological testing because of its beneficial characteristics in representing both in-vivo and in-vitro tissue engineering cases as well as its ability to be fine-tuned for chemical and physical alterations to best mimic the properties of specific tissues being studied. The study mentions that in order not to tear or modify the composition of the hydrogels, strains and stresses had to be kept low while performing the rheological tests (Zuidema et al., 2014). The strain sweep was studied on a domain of 0.1 to 100% at a frequency of 1 Hz for a fully formed hydrogel whereas our tests studied the deformation simple from 0.01% to 2% with a frequency varying from 1-100Hz. The reason for this is described in the protocol in detail.

The Frequency Sweep test in section 3.4.2 was studied under constant strain which correlates with Zuidema et al.'s study where strain was also held constant for this part of the experimentation. The article concludes stating the necessity of following a rigorous protocol like the study conducted in order to create an increased robustness in tissue engineering research (Zuidema et al., 2014).

3.4.2 **Frequency Sweep Discussion**

The Frequency Sweep test is helpful to characterize the dynamic moduli (G' and G") in order to determine pertinent information of a tissue's structure and mechanical behavior in the linear-viscoelastic region (Zuidema et al., 2016). With that, the frequency allowed us to observe an increase in storage and loss modulus for the left and right ventricle but a diminishment for the septum compartment.

It is important to note that sample code 009 sample #2 posterior left ventricle DOXO had the highest average storage modulus while also exhibiting one of the thinnest sample thickness among all the other samples (2.1mm). This validates the theory presented in the literature review that as the sample thickness decreases, the shear rate remains more constant throughout the thickness of the sample. Since the shear rate is directly proportional to the storage modulus, shear rate increases when the storage modulus increases as well.

In a study lead by *Tabet et al*., an experimentation compared healthy brain tissues with tissues exhibiting a tumor based illness (Tabet et al., 2019). They also studied the similarity of the brain tissue to that of hydrogel materials since they are both neuro-mimetic materials (Tabet et al., 2013). In order to study synthetic materials such as the hydrogel sample used, biomimicry of tissues must include biomechanical properties as per a study conducted by *Owens et al*. (Inal et al., 2017). The study showed an overall increase in the storage modulus for the "ill tissue" with an overall average output of 536 Pa whereas the healthy tissue achieved an average of 189 Pa (Tabet et al., 2013). The studies continued over the span of a day where tumor tissues dropped in overall storage moduli by

half whereas the healthy tissue dropped threefold (Tabet et al., 2013). All tests were performed at ambient temperatures (23°C). This correlated to our left and right ventricles where the "ill" samples exhibited a higher than average ability to absorb energy when compared to their "healthy" counterpart. More explanation requires to understand why the septum samples did not exhibit the same results during the frequency sweep testing.

In a study conducted in 2016 by *Packard et al*., doxorubicin was induced in fish samples to investigate the effects it has on the cardiovascular disease (Packard et al., 2016). The experiment conducted by the researchers presume an overall remodeling of the ventricles due to the doxorubicin samples also known as "ventricular dialostic dysfunction (Packard et al., 2016)." This includes alterations to the chamber systolic function and can ultimately lead to heart failure. This remodeling lead to what they believed was a worsening of the global cardiac function found on the doxorubicin samples. The samples were injected with four rounds of this chemotherapeutic agent on day 1, 3, 30 and 60 (Packard et al., 2016). The underlying theme relating both Packard et al.'s study and this paper is the overall degradation effect doxorubicin has on tissue samples.

In another study performed by *Pianowski et al*. where the goal of the experiment was to introduce a light-induced technique to encapsulate the DNA of cancer cells and the doxorubicin agent, rheological testing that covered frequency sweep showed a general improvement in sample's storage and loss modulus with the increase content of NaCL (Pianowski et al., 2016). It was studied that the salt concentration has an effect on doxorubicin's ability to bind to a cancer cell's DNA (Zunino et al., 1980). Indeed, in our experimentation, the untreated samples needed to be injected by a saline solution to make it more comparable of a study to doxorubicin induced samples to better compare the effects of the agent.

The frequency sweep allowed us to conclude that the doxorubicin agent has varying consequences on the properties of the miniature swine samples tested. Even though not all heart compartments exhibited the same results in overall storage/loss modulus properties, we can say that at least the doxorubicin had an overall impact on the storage and loss modulus meaning it has an impact on the material's ability to store and dissipate energy. The septum portion of the heart was the notable highlight as it showed higher mechanical impact than the left and right ventricle.

3.4.3 **Relaxation Test**

All three compartments of the heart displayed compromising results when containing the doxorubicin agent and this is greatly noticed looking at the stress-relaxation test results. A major observation was how quickly the tests were to obtain 100 data points for the samples induced with doxorubicin. Experimentation for each sample without the agent took approximately 35-43 minutes whereas the induced samples took approximately 20-25 minutes. This could mean two things: 1- The doxorubicin samples let go earlier while a shear stress was being applied because of diminished mechanical properties or 2- the resistance of the material to the general shear stress depleted with the added agent.

In *Iatridis et al.*'s study, the goal of the experimentation was to determine nucleus pulposus's visco-elastic shear properties using a mechanical spectrometer by performing torsional shear testing including a stress-relaxation test (Iatridis et al., 2005). The curves during this test showed high initial peak values for the shear stress response followed by a drastic drop of at least 50% of the initial value within one second. As time (t) increased, a gradual decline in the stress-relaxation was observed during the experimentation and finally reached the x-intercept after 600

seconds (Iatridis et al., 2005). This test was similar in time to our stress-relaxation test length for our DOXO based samples but not our untreated samples. It is important to note that in Latridis's study, the study focused on the degradation of samples with age and suggests that the greater the degeneration and age of the sample, the greater this contributes to the overall energy dissipation exhibited in the viscoelastic samples (Iatridis et al., 2005). The main takeaway from this study was ultimately the similar drop in shear stress results within seconds of the stress-relaxation test.

In Sommer's article, a Cauchy Stress test dependent on time in order to study the relaxation test performed in order to better understand the viscoelastic properties of the tissue. The most drastic relaxation was observed within the first five minutes but the test performed on the specimens continued up until 30 minutes where they continued their relaxation tendency. This abundant collection of data points collected due to the plateaued curve was comparable to the observations found for our experimentation. Another observation from his study was that, after five minutes of collecting data points, the shear stress was found to be greater than 50%. This tendency was observed for all specimens studied. Specifically, for our results, there was an average drop of stress at 50% 320 seconds into our test if you were to include both treated and untreated samples. For DOXO samples, the average 50% marker was at 265 seconds whereas the untreated samples were approximately 400 seconds. The overall corresponding relaxation behavior were comparable in both studies.

The last observation with Sommer's study is that he underwent three sinusoïdal preconditioning cycles. He studied shear modes varying from 0.1% to 0.5% at a deformation γ = 0.5 incrementing by 0.1% every time. For our particular study, we pre-conditioned the samples to 10 cycles of 0.1% at 1 Hz. After the preconditioning, the level of deformation established by the

strain sweep test remained at $\gamma = 1.6$. We studied three shear modes: 0.2%, 0.5% and 1% as opposed to Sommer who studied four varying from 0.1% to 0.5% at a deformation $\gamma = 0.5$ incrementing by 0.1% every time. Even though our protocol slightly varied from that of Sommer's protocol, we repeated our preconditioning step three times to ensure test robustness.

3.4.4 **Retest Frequency Sweep**

The goal of the frequency sweep post relaxation test was to determine if the samples would still exhibit less, similar or greater mechanical property comportment than when the frequency sweep test were originally conducted. We can observe from the experimentation that the left ventricle zone, posterior or anterior, doted with doxorubicin possessed varying results pre and post relaxation test. However, for the same corresponding zone in control samples, the frequency test results pre and post relaxation showed negligible variation in the storage modulus. Based on the results, the general tendencies showed an increase in overall storage and loss modulus for the samples tested. There were mixed results when looking at the septum results but we can conclude that there was a global increase in the storage, loss and shear modulus. This could mean two things: First, the sample exhibited a high viscoelastic strain during stress/relaxation test which caused the sample to be more firm and compact. Additionally, given the prolonged period of time for which the samples are being tested during the stress/relaxation test, ~30-40 minutes, the samples dried up due to the loss of moisture causing the sample to harden. Though the samples were still supple when removed from rheological testing, it was quite noticeable that the samples hardened since the time they were taken out of the tyrode solution. In Addition, the value of the storage modulus on

both the doxorubicin induced and the untreated models show a slight variation after the relaxation test. It increases minimally but as mentioned earlier, more the G' increases, the more the material will withstand resistance. The sample specifically used for our purposes underwent a force by pressure method which explains the augmentation of the overall storage modulus. Having a sample with decreased thickness, meaning increased compactness, allows for less deformation during the tests and, thus, an increased storage modulus. In addition, the thicker the specimen, the more it allows for a decreased shear rate and, thus, a greater resistance for the sample to deform. As sample thickness increases, this also means that shear distribution is non-homogenous throughout the thickness of these samples, and thus, the results obtained would have be under-estimated, meaning less accurate percentage from reality. This is why we maintained as very thin sample thickness for each sample studied taking into consideration the possibility of fractures. This ideal thickness hovered around 2 mm.

At the end of all three experimentations, we removed the samples from the spindle and noticed a shrinkage of roughly 5-10% of the original sample's radius. This shrinkage was consistent with the literature.

3.4.5 **Limitations with Mechanical Testing**

There were a few limitations with our study that prevented us to draw definitive conclusions from our test. The first limitation was the lack of DOXO right ventricle samples. Like the experimentation presented by *Sommer et al*., most of our right ventricle samples were either too thin or did not meet the radial specification of our study. This did not prevent us from generating

the graphs but rather the lack of data drew us to generalize results based on one or two samples for each given heart compartment and using those as a basis for are drawn conclusions. The second limitation with our experimentation was a lack of untreated samples compared to the DOXO samples. This proved some difficulty when determining the average sample's standard deviation and not knowing what the average upper and lower limit were. Ultimately, the more samples retrieved, the more data collected and, thus, a lesser variation in the average storage modulus, loss modulus and relaxation modulus. Thirdly, there was a limitation with the reproducibility of samples within the same animal code. The results obtained should have been nearly identical one sample from another if coming from the same part. However, the results ultimately outputted a tolerable variance between each of these samples and can be considered as reproducible. In addition, some samples due to their storage in a freezer at -80°C for approximately two years caused fractures as seen in figure 3.31 along with figure 3.27. We still proceed in testing some of these samples since the data point difference compared to other samples within the same band were negligible.

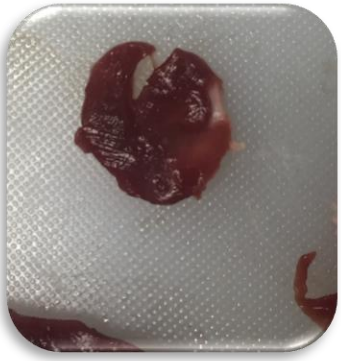

Figure 3.31 Example of Samples with Fracture contributing to testing limitation

Another limitation involved the criteria of a full drop in the shear stress during the stress/ relaxation test which did not meet for a couple untreated samples. This forced us to terminate the

test by applying a manual stop after ~ 42 minutes of testing the untreated sample, equivalent to 200 data samples collected.

Originally, the intention was to extract and prepare samples with 25mm diameter. The planned diameter established in the protocol phase proved difficult in achieving given the remainder pieces that were left at our disposal that were smaller than expected. This left us working with 20mm in diameter samples being sheared with a 25mm diameter. This leads to another limitation in our mechanical test results where applying shear on a smaller surface area may have over-estimated our results obtained. Luckily, given the potential shifts in all our graphic results, we were consistent in the 20mm diameter and set a priority on similitude in sample thickness and diameter. Unfortunately, there was no 20mm spindle diameter at our disposal at the time our tests were conducted.

Lastly, it is difficult for us to neglect the pieces of myocardium having been placed in the freezer for approximately 2 years and it not playing a role in the sample's mechanical properties. In an ideal world, the rheological test would have been conducted on the samples a few weeks after the administration of the doxorubicin agent on the subjects. It is practically impossible to avoid the natural physiological properties that may have been altered during the freezing and thawing process. A common phenomenon tied to this is the thaw-rigor process which can cause contractions in the fibriller structure (B.J Luvet). The rate at which the sample are left frozen can be a variable taken into consideration as well both in the freezing and thawing phases. There still isn't a clear preference between low temperature liquid nitrogen freezing or standard -80°C freezing as it is still being debated (Stenman et al., 2013).

3.5 Conclusion Myocardium Mechanical Test

The perspectives drawn from the Mechanical Testing show key differences between the untreated samples and doxorubicin induced samples derived from the myocardium sample. These differences include a general increase in DOXO sample's storage modulus, loss modulus during the frequency sweep test but a clear decrease in shear resistance during the relaxation test. The septum samples generated slightly different results where there was not only a decrease in the frequency sweep results but a diminishment in samples' shear modulus properties.

CHAPTER 4 RAMAN SPECTROMETRY

Raman Spectrometry was conducted in a previous study using the same samples as for the mechanical tests to further understand the impact doxorubicin has at a molecular level. Raman spectrometry allows through means of an optical probe placed in contact with the tissue to obtain pertinent information on the nature of the molecules present and the changes associated with the diseased tissues (Short et al., 2006).

The goal is to combine both the spectrometry results with the results obtained in the mechanical testing in order to formulate direct correlations between the left ventricle, right ventricle and septum data.

4.1 Method

The tissues conserved in the solution during the period of a year were rinsed and then placed in a saline solution during the course of the experimentation. The tests were conducted in total darkness in order to minimize the interference of external lighting.

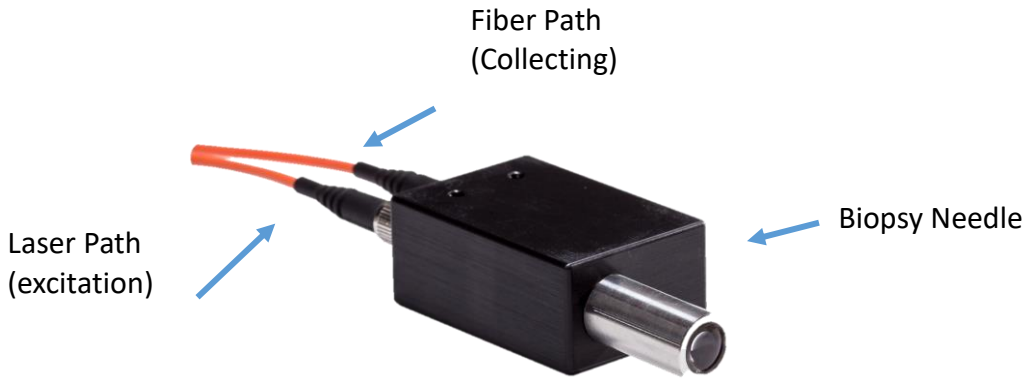

Figure 4.1 Standard Raman Probe used Spectrometry experimentation (modified from from https://w2innovations.com/?page_id=52)

The Raman probe contains a biopsy needle that is placed on the surface of the samples being studied. Once applied, the information of the tissue is gathered and sent to an attached black box where it is then mixed with a laser path signal, also known as an excitation signal. The laser path sends an excitation signal through a band pass and dichroic filter where it is then mixed with the information gathered from the biopsy needle. Once the two signals are collected, this combined signal is converted into wavelength and then directed towards the fiber path also known as the collecting path. This outputs curves such as Figure 4.2.

The Raman Probe testing was conducted at the CrCHUM. The laser attached to the probe was connected to the facilitie's computer with a LabView interface. The spectrum covered a domain ranging from 381 to 1653cm $^{-1}$ with a spectral resolution varying between 1.2 and 2.1cm. laser and the im- aging spectrometer were connected to a PC computer with a LabVIEW interface. All the data retrieved was processed using the MatLab interface (MathWorks Inc.)

To begin, we had to place the samples in a saline solution in order to properly position them in the Raman probe's aluminum blade. Once placed, five measurements were conducted for each sample. We disposed of six left ventricle samples, two right ventricle samples and three septum (four of which were dotted with doxorubicin and seven being left untreated). In total, the results culminated a combined 450 measurements. We required the use of software programs made available at the CrCHUM, which allowed treating the measurements for each sample by generating a cartography found below:

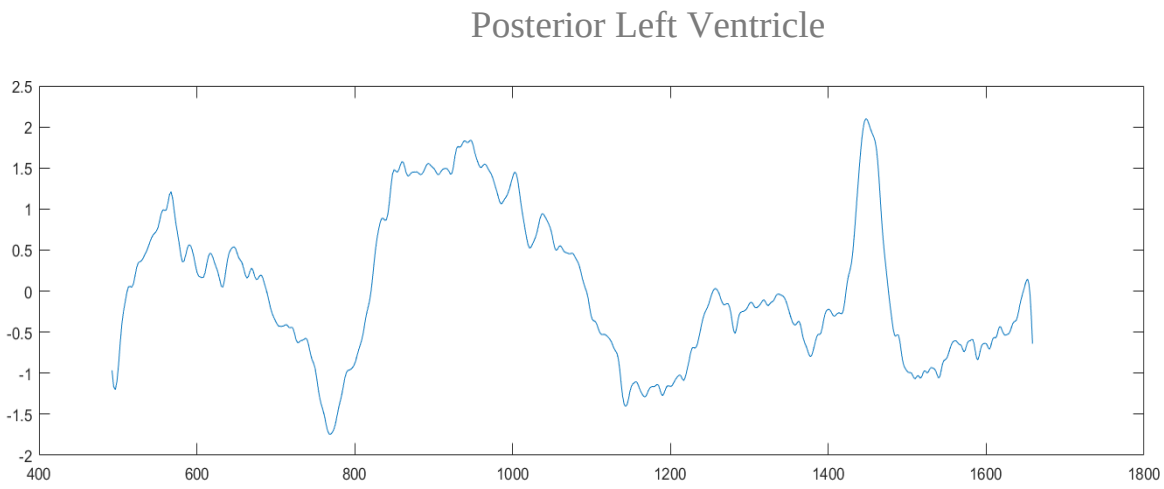

Figure 4.2 Raman Curve Posterior Left Ventricle DOXO

Generating Figure 4.2 allowed to effectuate the averages and standard deviations for each of the ventricle and septum samples using Matlab. We then applied a superposition of both curves (untreated and DOXO) allowing to better detect and measure the peaks. The program allowed us to generate the superposed graph in Figure 4.3 to help with the overall statistical analysis.

The generated graph allows the experimenter to determine the peak height of an untreated sample versus a treated sample induced with doxorubicin going on a downward phase. This specific section is an area of interest because it shows the sign of a Raman shift. In Figure 4.3, this peak is statistically the most present over the domain. Here, one can observe a downshift phase of the DOXO curve (red curve) well below the untreated sample (green curve). This highlights the presence of a Raman shift.

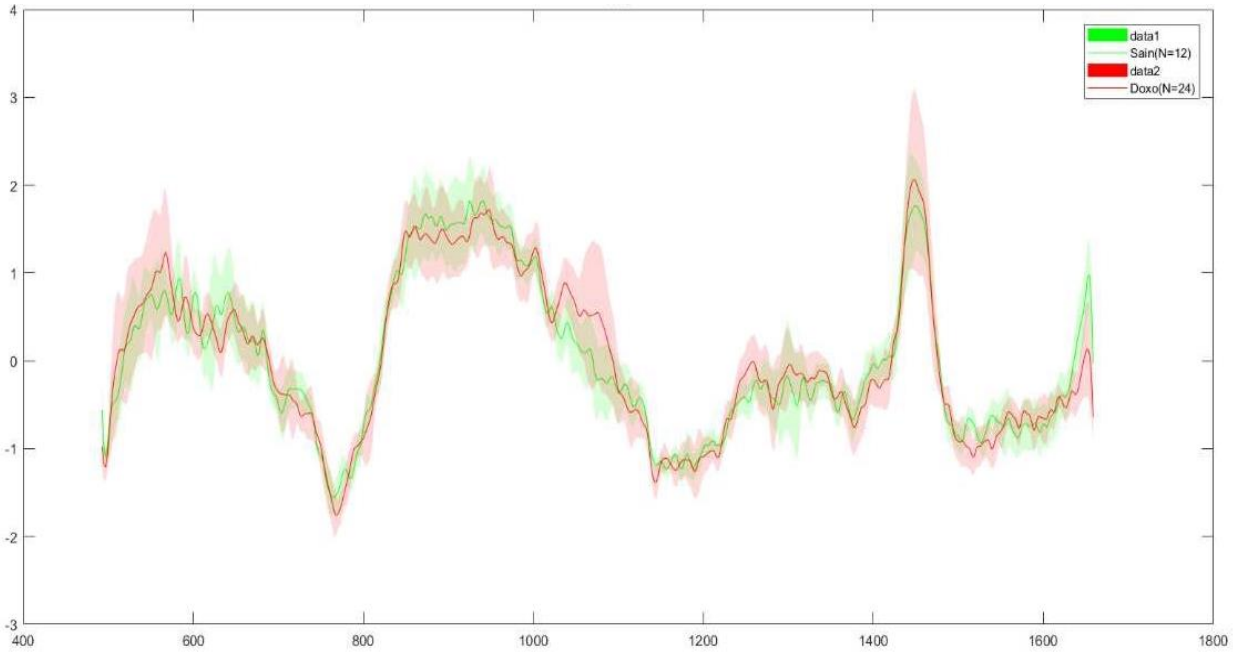

Figure 4.3 Raman Spectrometry data superposing both DOXO and untreated samples

Specifically, there is a Raman shift taking place at x= 602.3cm^{-1} which explains the presence of a molecule in the heart sample being experimented (Figure 4.4). The highest peak corresponds to the type of molecule which in this case is an untreated sample. Though we cannot conclude that

the molecule is completely absent from the sample induced with doxorubicin, we can say that it is present in a lot less quantity.

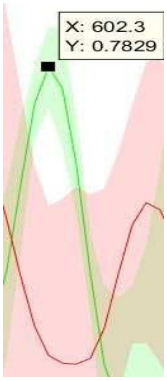

Figure 4.4 Difference in Raman shift peak

Following this, the program evaluated the importance of every peak, generating an important list which consisting of providing the Raman shift relative to the P-value. The P-value is a measure of how likely the Raman spectrum of a test sample is matched to a reference spectrum (Kalyanamaran et al., 2012). This means the lower the P-value, the most likely the molecule is to be present in the studied sample. This was conducted for each section of the heart evaluated and then were regrouped in order to verify the peaks that appeared more regularly amongst the three studied heart compartments. This operation was done given our hypothesis of homogeneity of the cardiac tissue.

After this evaluation, the peaks were classified into four categories in order to evaluate their importance relative to one another. The 1st category were P-values that scored < 0.001 [***], the 2nd were the P-values that were inferior to 0.01[**], the 3rd included P-values scored under 0.05 [*] and finally the 4th category combined the remainder values which are considered to be insignificant.

Table 4.1 Raman table for Raman Shift equal to 602cm^{-1}

Raman Shift	P-Value	Level	Molecule	Type
602.273167	4.51E-12	***	CHOLESTEROL(608)/phosphatidylinositol(596)	UNTREATED

Table 4.1 shows the P-value as well as the associated type of group the cholesterol molecule is associated to. This is based on which curve is at the highest peak relative to the other superposed curve at the Raman shift taking place at x=602cm^{-1}. Based on Figure 4.3, the highest curve when superposed is the untreated curve and this is why the molecule type is untreated at x=602cm^{-1}. This theory is based on the Taylor & Francis' Raman's spectroscopy of biological tissues [19]. We take into consideration a tolerance of +/- 4 cm^{-1} when possible. This is the last step of the experimentation which helps determine the molecule in doxorubicin which has the highest overall impact on the cardiac muscle.

The Raman Spectrometry allows for two particular aspects which includes having the same molecules at different Raman shifts throughout the test as well as multiple molecules at the same Raman shift. The first aspect mentioned helps validate the presence of a particular molecule in the tissue.

The last stage to the experimentation consisted of assigning the most significant peaks to a molecule using MATLAB in order to determine what was the importance of doxorubicin on the heart. In order to effectuate this part, we relied on an article grouping the molecules with their corresponding Raman shift and the second was a table provided by the CrCHUM.

4.2 Results

The results using the same samples tested during rheology derived Table 4.2. In this table, the associated molecule was retrieved from the article, “Raman Spectroscopy of Biological Tissues”, which covers all the Raman Shifts and its associated reference (Talari et al., 2015). The order is based on the chronology of the Raman Shift and encompassed the shifts found for all three compartment studied during this experimentation: the left ventricle, right ventricle and septum. For each individual compartment, an additional table, which encapsulates the values of Table 4.2, was generated to identify the specific Raman Shifts for that specific sector of the heart.

In table 4.2, the p-value column expresses the strength of each peak detected for each Raman Shift along with its strength level $p < 0.001$ [***], $p < 0.01$[**] and $p < 0.05$ [*]. The wavelength is based on the table that covers all possible Raman Shift molecules (Talari et al., 2015). Lastly, the type of molecule is based again on the curve found on top of the other superposed curve at a given significant Raman Shift.

Table 4.2 Table identifying the various molecules found given the Raman shift

Raman Shift	P-Value	Level	Type	Associated Molecule	Wavelength (nm)
513.382	1.14E-02	*	Doxo	S-S disulfide & colagen	509
565.252	1.32E-02	*	Doxo	tryptophnan /guanine,cytoine	573
567.316	4.80E-03	**	Doxo	tryptophnan /phosphatidylinositol	576
581.740	2.75E-07	***	Untreated	out of plane bending	(583-586)
592.017	1.64E-02	*	Doxo	glycerol/phosphatidylinositol	589/?
602.273	4.51E-12	***	Untreated	glycerol/cholesterol	607/608
616.597	8.05E-04	***	Doxo	cholesterol ester	614
628.841	1.68E-06	***	Untreated	glycerol	630
641.055	2.01E-02	*	Untreated	Protein tyrosine/phenylalanine	640/645
695.643	2.11E-02	*	Doxo	cholesterol ester	702
727.703	1.44E-07	***	Untreated	acide nucleiqu/A(ring breathing ade of ADN/DNA base)/C-S proteine(cytosine uracilee)/, CH2 roking adenine	724/725/726
779.340	6.77E-05	***	Untreated	phosphatidylinositol/Uracil/DNA 110, 122 Thymine, cytosine, uracil 122 RNA	776/780/782
840.163	1.71E-03	**	Untreated	α Anomeres glucose sacharide band, schacharide α	840
849.898	1.81E-03	**	Doxo	Monosaccharide (α-glucose), (C-O-C)Discchacarose(maltose))	847
873.175	7.67E-03	**	Untreated	Lipide/collagen	868-870/874
875.109	2.63E-02	*	Untreated	choline groupe $N^{+}(CH_3)_3$	875
880.907	2.14E-04	***	Untreated	Trypptophan	880
892.480	2.69E-02	*	Untreated	Saccharide band	891
927.016	1.33E-04	***	Untreated	Proline ring/ glucose/ acide lactique	921
940.374	3.34E-02	*	Untreated	Skeletal model(polysaccharide, Amylose), Skeletal model(polysaccharide, amylopectin)	96.2
963.176	5.62E-03	**	Untreated	phosphate d'hydroxyapatite de calcium hydroxyapatite	962/966
972.641	2.07E-04	***	Untreated	γ(C-C) wagging / lipid	971/972
1021.522	9.67E-05	***	Untreated	Ribose	1022/1017
1036.447	1.82E-09	***	Doxo	Phenylalanine/collagen	1034/1035
1066.137	4.66E-02	*	Doxo	Acide gras palmitique/proline	1065/1066
1073.526	1.30E-05	***	Doxo	Acide gras (tryglycerine)	1073
1080.901	4.01E-04	***	Doxo	Acide nucleique/collagen	1078
1091.938	6.39E-02	*	Doxo	Phosphate / Lipid	1090:1095
1108.438	5.53E-04	***	Untreated	phenylalamine(proteine)	1104
1126.691	8.83E-04	***	Untreated	phospholipid (proteine)	1125-32
1157.528	2.00E-04	***	Doxo	glycogene	1155
1173.756	7.87E-03	**	Doxo	CYOSINE GUANINE TYROSINE	1173
1202.435	1.06E-05	***	Untreated	Colagene/Acide nucleique & phosphates	1204/1200
1211.354	1.52E-04	***	Untreated	Tyrosine & Phenylalanine	1210
1213.135	6.08E-04	***	Untreated	amide III	1212-16
1248.581	1.38E-07	***	Doxo	amide III/ Guanine Cytosine (Nh2)	1248/1247-48
1257.390	4.51E-10	***	Doxo	Amide III proteine	1257
1262.665	7.57E-02	*	Doxo	Lipide	1263-65
1299.380	4.12E-02	*	Doxo	Acide gras palmatique / Lipid	1298/1300
1301.119	3.10E-03	**	Doxo	Lipid	1300-1301
1334.001	4.66E-02	*	Doxo	GUANINE	1333
1339.165	2.09E-03	**	Doxo	Acide nucleique	1340
1361.455	1.67E-02	*	Doxo	Guanine	1361
1398.854	2.20E-02	*	Untreated	CH2 Deformation	1398
1400.544	3.13E-02	*	Untreated	Deformation plan NH	1400
1410.668	8.69E-05	***	Untreated	vs COO (assymstric carboxylate)	1409
1511.874	7.39E-09	***	Untreated	A(ring breathing DNA base)	1510
1542.758	1.35E-06	***	Untreated	Single Human RBC(Red Blood Cell)/ Amide II	1542
1558.890	2.11E-02	*	Doxo	Tryptophan	1558
1578.139	7.27E-05	***	Doxo	guanine adenine	1578
1579.737	1.43E-03	**	Doxo	Acide nucleique	1579
1608.367	1.42E-02	*	Doxo	Cytosine	1608

i) Raman Shift for the Septum

Based on the highest Raman shift levels in Table 4.3, molecules found for the septum were collagen (DOXO sample) and carotenoid (untreated sample). These peaks were the most prominent peaks on the Raman Shift domain and, thus, can be considered the standout molecules that represent a good percentage of the overall sample.

Table 4.26 Raman Shift and P-values for the Septum

Raman Shift	P-Value	Level	Type	Associated Molecule	Wavelength
1036.447	4.31E-04	***	Doxo	Phenylalanine/collagen	1034/1035
1511.874	7.54E-04	***	Untreated	A(ring breathing DNA base)	1510
1073.526	1.20E-03	**	Doxo	Acide gras (tryglycerine)	1073
1248.581	1.29E-03	**	Doxo	amide III/ Guanine Cytosine (Nh2)	1248/1247-48
1257.390	2.05E-03	**	Doxo	Amide III proteine	1257
602.273	3.23E-03	**	Untreated	glycerol/cholesterol	607/608
727.703	4.74E-03	**	Untreated	acide nucleiqu/A(ring breathing ade of ADN/DNA base)/C-S proteine(cytosine uracilee)/, CH2 roking adenine	724/725/726
927.016	6.90E-03	**	Untreated	Proline ring/ glucose/ acide lactique	921
972.641	6.90E-03	**	Untreated	γ(C-C) wagging / lipid	971/972
1578.139	6.90E-03	**	Doxo	guanine adenine	1578
1080.901	8.05E-03	**	Doxo	Acide nucleique/collagen	1078
581.740	9.70E-03	**	Untreated	out of plane bending	(583-586)
963.176	9.70E-03	**	Untreated	phosphate d'hydroxyapatite de calcium hydroxyapatite	962/966
1173.756	1.35E-02	*	Doxo	CYOSINE GUANINE TYROSINE	1173
1202.435	1.35E-02	*	Untreated	Colagene/Acide nucleique & phosphates	1204/1200
1579.737	1.35E-02	*	Doxo	Acide nucleique	1579
616.597	1.76E-02	*	Doxo	cholesterol ester	614
1021.522	1.82E-02	*	Untreated	Ribose	1022/1017
1653.919	1.82E-02	*	Doxo	Carbonyl stretch (C O), amide I	1652
1339.165	2.10E-02	*	Doxo	Acide nucleique	1340
628.841	2.45E-02	*	Untreated	glycerol	630
940.374	2.45E-02	*	Untreated	Skeletal model(polysaccharide, Amylose), Skeletal model(polysaccharide, amylopectin)	96.2
1542.758	2.45E-02	*	Untreated	Single Human RBC(Red Blood Cell)/ Amide II	1542
1066.137	2.83E-02	*	Doxo	Acide gras palmitique/proline	1065/1066
880.907	3.20E-02	*	Untreated	Trypptophan	880
1410.668	3.38E-02	*	Untreated	vs COO (assymstric carboxylate)	1409
873.175	4.15E-02	*	Untreated	Lipide/collagen	868-870/874

ii) Raman Shift for the Right Ventricle

Table 4.45 Raman Shift and P-Value for the Right Ventricle

Raman Shift	P-Value	Level	Type	Associated Molecule	Wavelength (nm)
1513.507	4.56E-05	***	Untreated	Cytosine	1513
602.273	5.26E-05	***	Untreated	glycerol/cholesterol	607/608
1653.919	6.99E-05	***	Doxo	Carbonyl stretch (C O), amide I	1653
1539.521	9.25E-05	***	Untreated	Amide carbonyl group vibrations and aromatic hydrogens	1539
583.797	3.09E-04	***	Untreated	out of plane bending	(583-586)
1038.309	3.52E-04	***	Doxo	Phenylalanine/collagen	1034/1035
1166.552	1.35E-03	**	Doxo	glycogene	1155
1075.371	3.07E-03	**	Doxo	Acide gras (tryglycerine)	1073
1248.581	4.57E-03	**	Doxo	amide III/ Guanine Cytosine (Nh2)	1248/1247-48
628.841	7.63E-03	**	Untreated	glycerol	630
1578.139	8.43E-03	**	Doxo	guanine adenine	1578
779.340	1.03E-02	*	Untreated	phosphatidylinositol/Uracil/DNA 110, 122 Thymine, cytosine, uracil 122 RNA	776/780/782
1259.149	1.24E-02	*	Doxo	Amide III proteine	1257
1058.735	1.36E-02	*	Doxo	Acide gras palmitique/proline	1065/1066
592.017	1.64E-02	*	Doxo	glycerol/phosphatidylinositol	589/?
925.105	1.80E-02	*	Untreated	Proline ring/ glucose/ acide lactique	921
1108.438	2.15E-02	*	Untreated	phenylalamine(proteine)	1104
1633.586	2.15E-02	*	Doxo	Amide I	1632
1021.522	2.35E-02	*	Doxo	Phenylalanine/collagen	1034/1035
1211.354	2.56E-02	*	Untreated	Tyrosine & Phenylalanine	1210
616.597	2.79E-02	*	Doxo	cholesterol ester	614
1400.544	3.60E-02	*	Untreated	Deformation plan NH	1400
1340.885	4.23E-02	*	Doxo	Acide nucleique	1340
804.945	4.59E-02	*	untreated	Uracil-based ring breathing mode	803
1412.352	4.59E-02	*	Untreated	vs COO (assymstric carboxylate)	1409
1558.890	4.59E-02	*	Doxo	Tryptophan	1558

The Raman Shifts with the greatest peak also represents the samples with the smallest p-value. The main molecules detected on our right ventricle samples were carotenoids, cholesterol, prolines, phosphatidylinositol which are all derived from untreated samples and finally collagen which is a molecule typically found with samples induced with doxorubicin based on Table 4.2.

iii) Raman Shift for the Left Ventricle

Table 4.5 Raman Shift and P-value for the left ventricle samples

Raman Shift	P-Value	Level	Type	Associated Molecule	Wavelength (nm)
602.273	3.36E-06	***	Untreated	glycerol/cholesterol	**607/608**
1257.390	1.39E-05	***	Doxo	Amide III proteine	**1257**
583.797	2.38E-04	***	Untreated	out of plane bending	**(583-586)**
1541.140	3.52E-04	***	Untreated	Single Human RBC(Red Blood Cell)/ Amide II	**1542**
925.105	4.54E-04	***	Untreated	Proline ring/ glucose/ acide lactique	**921**
1248.581	2.67E-03	**	Doxo	amide III/ Guanine Cytosine (Nh2)	**1248/1247-48**
1038.309	2.98E-03	**	Doxo	Phenylalanine/collagen	**1034/1035**
1617.849	3.32E-03	**	Doxo	phenylalanine, tyrosine	1617
1168.354	6.90E-03	**	Doxo	CYOSINE GUANINE TYROSINE	**1173**
904.022	7.63E-03	**	Untreated	skeletal stretching	904
1040.170	7.63E-03	**	Doxo	Phenylalanine/collagen	**1034/1035**
1513.507	7.63E-03	**	Untreated	Cytosine	**1510**
779.340	1.50E-02	*	Untreated	phosphatidylinositol/Uracil/DNA 110, 122 Thymine, cytosine, uracil 122 RNA	**776/780/782**
1155.721	1.80E-02	*	Doxo	glycogene	**1155**
1652.360	1.97E-02	*	Doxo	Lipid	1652
840.163	2.15E-02	*	Untreated	α Anomeres glucose sacharide band, schacharide α	**840**
849.898	2.15E-02	*	Doxo	Monosaccharide (α-glucose), (C-O-C)Discchacarose(maltose))	**847**
880.907	2.56E-02	*	Untreated	Trypptophan	**880**
1417.400	3.26E-02	*	Untreated	vs COO (assymstric carboxylate)	**1409**
639.021	3.31E-02	*	Untreated	Protein tyrosine/phenylalanine	**640/645**
1023.390	3.31E-02	*	Untreated	Ribose	**1022/1017**
1108.438	3.31E-02	*	Untreated	phenylalamine(proteine)	**1104**
1302.857	3.90E-02	*	Doxo	Lipid	**1300-1301**
1211.354	4.23E-02	*	Untreated	Tyrosine & Phenylalanine	**1210**
567.316	4.59E-02	*	Doxo	tryptophnan /phosphatidylinositol	**576**

The primary molecules found for the left ventricle are similar to the right ventricle samples. This includes glycerol/cholesterol, red blood cell/amide II, glucose, which were all prominent peaks with the untreated curve having strengthened peaks over the DOXO curve. The molecule found in the left ventricle DOXO sample was triglyceride.

4.3 Discussion Raman Spectrometry

Raman spectrometry is a promising cancer detection technique for surgical guidance applications (Santos et al., 2017). It can help provide quantifiable tissue properties associated to the structural, metabolic, immunological and genetic biochemical composition such as the tissues' amino acids, lipids, proteins and nucleic acid (DNA) (Santos et al., 2017).

4.3.1 Collagen Deposition

The average septum samples when compared to the left and right ventricle exhibited many less category 1 peaks (p value < 0.001). In the actual experimentation for mechanical testing, we noticed a decrease in the overall structural integrity of the septum samples meaning they were less rigid. Indeed, looking at Table 4.3, there was a lack of molecule consisting of collagen which is an important protein that contribute to the overall rigidity of a tissue. These two theorem correlate to one another and explain the lack of collagen in the septum samples and consequently, a diminishment in the overall mechanical properties. The opposite is true for the left and right ventricle, which displayed an increased presence of overall collagen based on the results obtained. Again, these results were in line with our Frequency Sweep test where we noticed an increase in the sample's storage and loss modulus.

Cardiac Fibrosis up until now has been linked to the overproduction of collagen whereas the lack of collagen has been linked to dilation in a given myocardium sample (Asbun et al, 2006). The results obtained suggest a dilation in our septum samples, a fixed wall, given the drop in the lack of the collagen molecule found in the Raman test . However, given the abundance of collagen molecules and increase in storage and loss modulus, Asbun et al. leaves us to believe the presence

of fibrosis in our left and right ventricles, the mobile walls. This point is validated through histological studies that show that tissue is remodeled after being induced with Mitoxantrone (DHAQ) (Perkins et al., 1984). This last agent had comparable myocardial effects than that of doxorubicin. This caused a decrease in the left ventricle volume but also a decrease in its collagen content when induced with Mitoxantrone (Perkins et al., 1984). These previous histological studies including that of Asbun et al. indicate differences in collagen based molecule concentrations in the heart's fixed wall versus when compared to its mobile wall.

In another study propose by Herman et al., presented in the literature review, where dosages of doxorubicin were injection using the dog as the subject, studies concluded showing a general loss of myofibril protein in the doxorubicin treated subjects (Herman et al., 1983). This study among the many studies found share common results where the lack of protein molecules is noticed

4.3.2 **Lipid Deposition**

In the memoire of *Clemence et al.*, the myocardial T1 mapping suggested a higher lipid content when compared to the DOXO samples (Moon et al., 2013 & Balosetti et al, 2016). This can explain why the miniature swine exhibited a weight loss throughout the treatment (Moon et al., 2013 & Balosetti et al, 2016). This can also explain why the lipid-based molecules are found more recurringly in our untreated samples than in our DOXO samples. For example, Raman Shift 972cm^{-1} and 873cm^{-1} had the untreated peak higher than that of the DOXO peaks. A longer longitudinal relaxation time T1, is generally associated to the deposition of lipids or iron (Moon et al., 2013). In addition, the mapping of the T1 parameter can be used in the detection of cardiac fibrosis (Giri et al., 2009). Not only did we notice a decrease in the presence of fat on the surface of the DOXO samples compared to untreated samples when preparing the samples, Table 4.3, 4.4, 4.5 showed a lack of the presence of lipids in the DOXO samples as well. A direct correlation between a diminishment of lipids and the increase of cardiac fibrosis remains to be studied.

A limitation incurred was the possibility of having the same molecule present at different Raman shift. For example, tryglyceride (acidic saturated fat) was found both at x= 1073cm^{-1} and x= 1264cm^{-1} for the DOXO samples. In the end, this was not a limitation but rather a confirmation that a presence of fat on most samples was important because it well represented the composition of the outer layer of the heart.

4.4 Conclusion Myocardium Raman Spectrometry Test

The perspectives drawn from the Raman Spectrometry Testing suggests a dilation in our septum samples, serving as the heart's fixed wall, due to a drop in the collagen concentration with the help of the Raman test. In our right and left ventricle samples however, the increased presence of collagen suggests the presence of fibrosis in the heart's mobile walls. The binding of the doxorubicin agent along the DNA stride of the cancer cells seems to cause an overall general diminishment in the collagen and lipid molecules found in the DOXO myocardium sample. The perspectives derived from the Raman tests, being the primary form of physiological tissue composition, allow us to validate and strengthen our theories presented in the mechanical testing, as there appears to be a common denominator relating both tests.

CHAPTER 5 GENERAL DISCUSSION

The perspectives drawn from chapter 3 and chapter 4 help determine the effects doxorubicin has on the myocardium sample and, thus, on the human heart. These effects include diminished mechanical properties in the septum but increased properties such as the storage modulus and loss modulus in both the right and left ventricles. During the stress-relaxation test, the inability for the untreated samples to decrease in shear modulus with respect to time shows that DOXO samples have a more viscoelastic behaviour with increased angular frequency. In parallel, Raman Spectrometry studies showed a tendency for an overall diminishment of lipid and protein in the DOXO sample's molecular composition. Collagen is a major determinant of the mechanical properties of an infarcted myocardium so the absence of it when studying the samples will determine if it has weakened properties (Fomovsky et al., 2010). The lack of rigidity in the sample's structure can lead to some form of cardiac dilation.

In a previous study using the same myocardium samples, the count of white blood cells and platelet was found decreased in the DOXO group while remaining stable in the control group (Balosetti et al., 2016). This makes sense since chemotherapy decreases the overall immune system. With that, one can assume that due to the decrease in the immunological defence function, weight loss occurred and this can explain why the structural rigidity of the samples suffered in consequence. In this previous study done by cardiac MRI, due to a decrease of T2, both groups did not present infarcted region (Giri et al., 2009). T2 study was also used to detect other troubles including changes to the myocardial water content (Abdel-Aty et al., 2005). The slight decrease of T2 in the doxorubicin group could be associated to the drop in water level content compared to the

untreated group. T2 can also be associated to the accumulation of collagen in the cardiac tissue. This means that with the decrease of T2, there was a decrease in the amount of protein detected in the DOXO family which again correlates to our study where we observed similar results in all three sectors of the heart.

There are a few correlations that can be drawn between the two experiments which will help explore objective #3 of this study which was the ability to draw a comparison between the mechanical testing results and the results found in the Raman Spectrometry study.

5.1 Correlations between Rheometry and Raman Spectrometry Study

Table 5.1 summarizes the results obtained in both studies and underlines the common denominators between both experiments.

Table 5.1 Overview of results found in Mechanical and Raman Spectrometry Tests

	Mechanical Testing Results	Raman Spectrometry Results	Conclusions
Septum	Diminishment in overall structural integrity	Lack of Collagen in significant category	Drop in overall structural integrity
	Depletion in its shear modulus (relaxation)	Drop in lipid content in significant category	Dilation linked to this overall degradation
Left & Right Ventricle	Increase in storage and loss modulus	Increased presence of Collagen in significant category	Increase in overall structural integrity
	Depletion in its shear modulus (relaxation)	Drop in lipid content in significant category	Formulation of cardiac fibrosis linked to this overall degradation in DOXO samples

The septum as opposed to the left and right ventricle exhibited many less category 1 peaks (p value < 0.001). In the experimentation for mechanical testing, we noticed a decrease in the overall structural integrity of the septum samples meaning they were less rigid. Indeed, looking at Table 4.3, there was a lack of molecule consisting of collagen, which is an important protein that helps with the overall rigidity of a tissue. This can be correlated to the mechanical testing observed where we noticed a depletion in the septum sample's ability to absorb energy.

The left and right ventricle during the mechanical testing exhibited an overall increase in sample's storage and loss modulus. These two features which points to myocardium sample's viscoelasticity show an overall increase in structural rigidity. Since collagen has a primordial role in structural rigidity, it should be present in category I for the p-value. Indeed, Raman Spectrometry results point to similar conclusions where the DOXO samples contained an increase in protein deposition for the left and right ventricles.

Another notice related to collagen was that samples with a higher drop time in the shear modulus during the relaxation test, such as it appears in the untreated samples seen in the results in chapter 3, appears to be associated to the reduction of the systolic function or it can also represent an increase in the deposition of protein [37]. This can maybe why that in our mechanical results in chapter 3, doxorubicin induced samples saw a sudden drop during the stress-relaxation test. This was due to the drop in collagen count, which suggests a higher count of protein content in the untreated samples.

The last correlation observed during the study is that all DOXO samples showed depletion in its shear modulus (relaxation modulus) during the stress-relaxation test. The Raman spectrometry also concluded an overall drop in lipid content for the doxorubicin injected samples.

In Balosetti et al.'s review, a weaker immune system combating the treatments of doxorubicin causes weight loss and a drop in lipid content (Balosetti et al., 2016). We are still uncertain after this experimentation that the near immediate drop in relaxation modulus for the DOXO based samples is directly linked to the diminishment in lipid content or if collagen played a bigger role. Clemence et al.'s paper leads us to believe that through a relaxation test, the formulation of cardiac fibrosis is linked to this overall degradation of the DOXO samples while combating the doxorubicin treatment (Balosetti et al., 2016).

CHAPTER 6 CONCLUSION

In the framework of this experimentation, we explored Raman Spectrometry in order to study the physiological composition of each given sample. In parallel, a mechanical based experimentation through the science of rheology allowed us to study the mechanical characteristics of each sample. The mechanical properties are a primordial indicator of the myocardium's viability of the cardiac tissue as well as heart failure rate. In order to quantify a specimen's mechanical properties, we made use of a rheometer, which allowed us to measure important properties such as the heart's storage modulus, shear modulus, loss modulus and viscoelasticity. The results obtained showed a general diminishment in the miniature swine's heart's mechanical properties which can be correlated to the human heart. Quantifying that exact diminishment remains difficult but it is based on the compilation of the results obtained for both the *Frequency Sweep* and *Stress – Relaxation test*. Our original hypothesis that touches upon this anthracycline agent having a negative overall impact on the mechanical properties was not refuted though future advancements will only help validate even further the framework put in place for this study. In addition, the molecular composition points towards a decrease in fatty based lipids for doxorubicin induced samples for all heart compartments based on the Raman Shifts found when superposing both the untreated and DOXO curves. The increased presence of collagen in the left and right ventricle during the Raman spectrometry test points towards why we saw an increase in these samples' storage and loss modulus. For the septum, the decrease in collagen content explains why there was a decrease in its sample's storage and loss modulus.

Like the mechanical testing, further modalities related to the Raman Imaging study can be used to further push the validation of our results obtained such as autofluorescence imaging or a diffuse reflectance system. These other form of imaging modalities could help acquire image in real time and the Raman Spectrometry can be activated when needed to further analyze the samples at hand. Knowledge of the mechanical and microstructural properties for both DOXO and untreated samples is important for comparative studies where side effects on the myocardial infarctions take place.

The characterization of soft tissues can be studied through many mediums and can vary in application from tissue engineering to diagnosing various diseases. It is recommended as a future study to explore samples' tissue properties by means of Magnetic Resonance Elastography. This study permits the experimenter to map out soft tissue's elastic properties using medical imaging (Li et al., 2019). Given that tissues are multiple-layer composed structures, elastography, specifically guided wave elastography, has the unique feature of elastic waves being smaller than a standard wavelength (Li et al., 2019) which would allow users to further characterize the mechanical properties of biological soft tissues. The data would then get analyzed using FEA (Finite Element Analysis) to quantify properties such as soft tissues' stiffness.

A general limitation with biological tissues is that the jump from freshly euthanized animals to living function hearts with reliable measures of the mechanical properties remains difficult because of the vascularity of the tissue that changes drastically immediately after death. This is why all of our testing represent estimates of what the mechanical properties were when the myocardium was still alive.

As of today, anthracycline's doxorubicin remains to be the most effective way to locally target and kill cancer cells. Another medium used to help reduce doxorubicin's toxicity is that of the add-on platform that uses naturally engineered membrane vesicle exosomes for an even greater targeted therapy. Through the use of exosomes, an endogenous nano-sized membrane, one can help deliver chemotherapeutic agents such as doxorubicin in a more targeted way by the engineered creation of a membrane protein. For example, in a study conducted by Tian et al., they made use of a nude mouse. To reduce doxorubicin's toxicity in this case, mouse immature dendritic cells, also known as imDCs were used for exosome production. By engineering the imDCs containing doxorubicin, they were able to load via electroporation into a targeted region with an encapsulation efficiency close to 20% (Tian et al., 2014). Increased targeted exosomes combined with doxorubicin by means of an intravenous injection has led to the hindering of tumor growth with a decrease in toxicity. The study concludes stating that doxorubicin remains the agent of choice when targeting cancer cells during treatment and that finding parallel techniques, such as engineered membrane vesicle, that includes the already successful formula of doxorubicin should add great value to clinical applications.

The data compiled from this study and others coming can be used to help characterize biomarkers to help build computational models of the heart. This will allow to better understand pathological changes due to biomechanical factors and will help improve research such as clinical diagnostics, medical devices and material design for tissue engineering or even drug development. All this to ultimately improve the health care delivery to one day reduce the cardiotoxic effects doxorubicin has on the heart. Finally, the combination between this experimentation and future advancements will help characterize biomarkers for the doxorubicin agent, which can ultimately lead to finding solutions on how to reduce its manifestation on the central cardiac cavity.

REFERENCES

H. Abdel-Aty, P. Boyé, P. Bock, A. Kumar, and M. G. Friedrich, "Stenotic mitral valve prosthesis with left atrial thrombus," Journal of Cardiovascular Magnetic Resonance, vol. 7, pp. 421-423, 2005.

C. F. Aissiou M., Curnier D., Hafyane T., Friedrich M., Laverdière C., Andelfinger G, Krajinovic M., Sinett D., Périé D. , "Early detection of doxorubicin-induced cardiotoxicity using myocardial T1 (pre- and post-gadolinium) and T2 relaxation times: a PETALE study," The International Journal of Cardiovascular Imaging, 2016.

J. Asbun, F. Villarreal "The Pathogenesis of Myocardial Fibrosis in the Setting of Diabetic Cardiomyopathy," Journal of the American College of Cardiology, pp 693-700, Feb 2006. DOI: 10.1016/j.jacc.2005.09.050

Clémence Balosetti, "Détection Précoce De La Cardiotoxicité Due À La Doxorubicine Chez Le Miniporc Par Imagerie Par Résonance Magnétique," PolyPublie Génie Biomédical, August, 2016.

C. R. Butler, R. Thompson, M. Haykowsky, M. Toma, and I. Paterson, "Cardiovascular magnetic resonance in the diagnosis of acute heart transplant rejection: a review," Journal of Cardiovascular Magnetic Resonance, vol. 11, pp. 7, 2009.

S. C. Cassidy, D. P. Chan, D. G. Rowland, and H. D. Allen, "Effects of Doxorubicin on Diastolic Function, Contractile Reserve, and Ventricular–Vascular Coupling in Piglets," 1998.

Marco Cespi , Giulia Bonacucina, Monica Misici-Falzi, Roberto Golzi, Luigi Boltri, Giovanni F. Palmieri, “Stress relaxation test for the characterization of the viscoelasticity of pellets,” European Journal of Pharmaceutics and Biopharmaceutics, vol. 67 p. 476–484, 2007.

A. Chandra, S. Talari, Z. Movasaghi, S. Rehman, and I. Rehman “Raman Spectroscopy of Biological Tissues” Applied Spectroscopy Reviews, vol. 50, pp. 46–111, 2015.

Chen, Terri, Hesse, Nathan, “Rheology Theory and Applications” TA Instruments, pdf 2019.

Van Dalen EC, Caron HN, Dickinson HO, Kremer LC. Cardioprotective interventions for cancer patients receiving anthracyclines. Cochrane Database Syst Rev. 2005.

G.M. Fomovsky, S. Thomopoulos, J.W. Holmes, “Contribution of extracellular matrix to the mechanical properties of the heart,” J. Mol. Cell. Cardiol., 48 pp. 490-496, 2010. 10.1016/j.yjmcc.2009.08.003

Geisberg, C. A., & Sawyer, D. B. “Mechanisms of anthracycline cardiotoxicity and strategies to decrease cardiac damage”, *Current hypertension reports*, *12*(6), pp. 404–410. 2010. doi:10.1007/s11906-010-0146-y

S. Giri, Y.-C. Chung, A. Merchant, G. Mihai, S. Rajagopalan, S. V. Raman, *et al.*, "T2 quantification for improved detection of myocardial edema," *Journal of cardiovascular magnetic resonance*, vol. 11, p. 56, 2009.

E. H. Herman and V. J. Ferrans, "Influence of vitamin E and ICRF-187 on chronic doxorubicin cardiotoxicity in miniature swine," Laboratory investigation; a journal of technical methods and pathology, vol. 49, pp. 69-77, July. 1983.

J. Iatridis, L. Setton, M. Weidenbaum, V. Mow, “Alterations in the mechanical behavior of the human lumbar nucleus pulposus with degeneration and aging,” Journal of Orthopedic Research, pp. 318-322, 2005. https://doi.org/10.1002/jor.1100150224

S. Inal, A. Hama, M. Ferro, C. Pitsalidis, J. Oziat, D. Iandolo, A. Pappa, M. Hadida, M. Huerta, D. Marchat, P. Mailley, R. Owens, “Conducting Polymer Scaffolds for Monitoring 3D Cell Culture” Advanced Biosystems. 2017. doi: 10.1002/adbi.201700052

VG. Kaklamani, WJ. Gradishar, “Epirubicin versus Doxorubicin: Which is the anthracycline of choice for the treatment of breast cancer?” Rev, Abstract, April, 2003

R. Kalyanamaran, M. Ribick, G. Dobler, B-M Squibb, “Portable Raman Spectrometry for Pharmaceutical Counterfeit Identification,” European Pharmaceutical Review, Vol. 15. Issue 5. 2012.

S H Kim, “A feasibility work on the applications of MRE to automotive components” IOP Conference Series, 2018. doi:10.1088/1757-899X/333/1/01201

F. Köhn, "History and Development of Miniature, Micro- and Minipigs," in The Minipig in Biomedical Research, C. Press, Ed., ed: Taylor & Francis Group, LLC, Ch. 1, 2011.

G. A. Krombach, C. Hahn, M. Tomars, A. Buecker, A. Grawe, R. W. Günther, *et al.*, "Cardiac amyloidosis: MR imaging findings and T1 quantification, comparison with control subjects," *Journal of Magnetic Resonance Imaging*, vol. 25, pp. 1283-1287, 2007.

Y. Kumamoto, K. Fujita, “Basic of Raman Scattering,” *Nanophoton Corporation* Chapter 1, Lesson 1. February 2003.

GY. Li, Y. Zheng, YX Jiang, Z. Zhang, Y Cao, “Guide Wave Elastography of Layered Soft Tissues,” *Acta Biomater* pp. 293-304, January 2019. doi: 10.1016/j.actbio.2018.12.002.

B.J Luvet, “Effect of Freezing on Muscle Tissue,” *American Foundation for Biological Research*, pp.210-219. 1964.

RA, Manno, A. Grassetti, G Oberto, A Nyska, Y. Ramot, “The Minipig as a New Model For The Evaluation of Doxorubicin-Induced Chronic Toxicity,” Journal of Applied Toxicology, DOI 10.1002/jat.3266 , 2015.

F. Mettler, D. Young, and J. Ward, "Adriamycin-induced cardiotoxicity (cardiomyopathy and congestive heart failure) in rats," Cancer Research, vol. 37, pp. 2705- 2713, 1977.

A. Mohamed, D. Périe, F. Cheriet, N. Dahdah, C. Laverdiere, D. Curnier, “Imaging of early modification in cardiomyopathy: the doxorubicin-induced model,” Int J Cardiovasc Imaging 29: pp. 1459-1476, 2013. DOI 10.1007/s10554-013-0248-0.

J. C. Moon, D. R. Messroghli, P. Kellman, S. K. Piechnik, M. D. Robson, M. Ugander, et al., "Myocardial T1 mapping and extracellular volume quantification: a Society for Cardiovascular Magnetic Resonance (SCMR) and CMR Working Group of the European Society of Cardiology consensus statement," J Cardiovascular Magnetic Resonance, vol. 15, p. 92, 2013.

R. Moudgil “Molecular Mechanisms of Anthracycline-Induced Cardiotoxicity” *Cardio Oncology*, September, 2017.

S. Nicolle, J-F Palierne, “Dehydration effect on the Mechanical Behabior of Biological Tissues: Observations on Kidney Tissues,” Journal of the Mechanical Behavior of Biomedical Materials, Vol. 3, pp. 630-635, 2010

R. R. Packard “Advanced Imaging and Bioengineering Approaches to Cardiovascular Disease.” *UCLA*. 2016.

M. Pecoraro, R. Sorrentino, S. Franceschelli, M. Del Pizzo, M. Pinto, A. Popolo, Doxorubicin-Mediated Cardiotoxicity: Role of Mitochondrial Connexin 43. *Cardiovasc. Toxicol.* vol. *15*, pp. 366–376. 2015.

M. Pecoraro; A. Rodríguez-Sinovas, S. Marzocco, M. Ciccarelli, M. Iaccarino, G. Pinto, A. Popolo, A. Cardiotoxic Effects of Short-Term Doxorubicin Administration: Involvement of Connexin 43 in Calcium Impairment. *Int. J. Mol. Sci.* vol. 18, 2017.

D. Perie-Curnier, N. Dahdah, A. Foudis and D. Curnier, “Multi-parametric MRI as an indirect evaluation tool of the mechanical properties of in-vitro cardiac tissues,” March, 2013. https://doi.org/10.1186/1471-2261-13-24

W. Perkins, RL. Schroeder, RA Carrano, AR Imondi, “Myocardial effects of mitoxantrone and doxorubicin in the mouse and guinea pig,” Cancer Treatment Reports, 841-847, 1984.

A. Phaniendra, DB. Jestadi, L. Periyasamy, Free radicals: properties, sources, targets, and their implication in various diseases. *Indian J Clin Biochem*. Pp.11-26, 2015. doi:10.1007/s12291-014-0446-0

Z. Pianowski, J. Karcher, K. Schneider, "Photoresponsive self-healing supramolecular hydrogels for light-induced release of DNA and doxorubicin," Royal Society of Chemistry, 2016. DOI: 10.1039/c5cc09633b

CJ. Pipe, T. Majmudar; G. McKinley, "High Shear-Rate Viscometry". *Rheologica Acta*. 47 (5–6): pp. 621–642 2008.

Y. Qiao, Q. Duong, B. Li, S. Obaid, C. Miccile, R. Yin, T. Talapatra, Z. Lin, S. Li, Z. Li, "Multiparametric slice culture platform for the investigation of humancardiac tissue physiology," Science Direct, pp. 139-150, 2019.

J. Robert, "Preclinical assessment of anthracycline cardiotoxicity in laboratory animals: predictiveness and pitfalls," Cell Biol Toxicol, vol. 23, pp. 27-37, Jan 2007.

I. Santos, E. Barroso, T. Bakker-Schut, "Raman spectroscopy for cancer detection and cancer surgery guidance: translation to the clinics," Analyst, Issue 17, 2017.

J. H. Schellens, H. L. McLeod, and D. R. Newell, *Cancer clinical pharmacology*: Oxford University Press, 2005.

L. Seymour, V. Bramwell, and L. Moran, "Use of dexrazoxane as a cardioprotectant in patients receiving doxorubicin or epirubicin chemotherapy for the treatment of cancer. The Provincial

Systemic Treatment Disease Site Group," *Cancer prevention & control: CPC= Prevention & controle en cancerologie: PCC,* vol. 3, pp. 145-159, 1999.

M.A. Short, L. McLean, D. Zeng, H. Alajlan, and X. Chen, "Changes in nuclei and peritumoral collagen within nodular basal cell carcinomas via confocal micro-Raman spectroscopy". *J. Biomed. Optic.*, 11 (3): 34003–34013. Feb 2006.

G. Sommer, A. Schriefl, M. Andrä, M. Sacherer, C. Viertler, H. Wolinski, G. Holzapfel, "Biomechanical properties and microstructure of human ventricular myocardium," *Science Direct,* p.172-192, 2015.

Mazin S. Sirry, J. Ryan Butler, Sourav S. Patnaik, Bryn Brazile, Robbin Bertucci, Andrew Claude, Ron McLaughlin, Neil H. Davies, Jun Liao, Thomas Franz, "Characterisation of the mechanical properties of infarcted myocardium in the rat under biaxial tension and uniaxial compression," *Science Direct,* p.252-264, 2016.

St-Arnaud, K. "Développement D'une Sonde Portable D'imagerie Raman Pour Guider L'exérèse De Tumeur," PolyPublie Génie Biomédical, June, 2017

A.Stenman, N. Kiss, C.C. Juhlin, A. Hoog, "Long-Term Storage of Endocrine Tissues at -80 °C Does Not Adversely Affect RNA Quality or Overall Histomorphology," Biopreservation and Biobanking, pp.366-370, December 2013.

M. M. Swindle, A. Makin, A. J. Herron, F. J. Clubb, Jr., and K. S. Frazier, "Swine as models in biomedical research and toxicology testing," Vet Pathol, vol. 49, pp. 344-56, Mar 2012.

A. Tabet, S. Mommer, J. Vigil, C. Hallou, H. Bulstrode, O. Scherman, “Mechanical Characterization of Human Brain Tissue and Soft Dynamic Gels Exhibiting Electromechanical Neuro-Mimicry,” Advance Science News, January, 2019.

https://doi.org/10.1002/adhm.201900068

A.Talari, Z. Movasaghi, S. Rehman, and I. Rehman, “Raman Spectroscopy Of Biological Tissues,” Applied Spectroscopy Reviews, vol. 50, pp. 46–111, 2015.

Y. Tian, L. Suping, J. Song, T. Ji, M. Zhu, G. Anderson, J. Wei, G. Nie, “A Doxorubicin Delivery Platform Using Engineering Natural Membrane Vesicle Exosomes For Targeted Tumor Therapy,” vol. 35, pp. 2383-2390, February 2014.

H. M. Vargas, A. S. Bass, J. Koerner, S. Matis-Mitchell, M. K. Pugsley, M. Skinner, et al., "Evaluation of drug-induced QT interval prolongation in animal and human studies: a literature review of concordance," Br J Pharmacol, vol. 172, pp. 4002-11, Aug 2015.

E. Widmaier, H. Raff, K. Strang, “Human Physiology The Mechanisms of Body Function,” McGraw Hill Publishing, 9th edition, pp. 381-384. 2014.

Zhang, Y.; Chen, Y.; Zhang, M.; Tang, Y.; Xie, Y.; Huang, X.; Li, Y. Doxorubicin induces sarcoplasmic reticulum calcium regulation dysfunction via the decrease of SERCA2 and phospholamban expressions in rats. *Cell Biochem. Biophys. 70*, pp. 1791–1798. 2014.

JM Zuidema, CJ Rivet, RJ Gilbert, FA Morisson, “A Protocol for Rheological Characterization of Hydrogels for Tissue Engineering Strategies,” J. Biomed Mater Res Part, pp. 1063-1072, 2014.

F. Zunino, A. Di Marco, A Zaccara, A. Gambetta, “The Interaction of Daunorubicin and Doxorubicin with DNA and Chromatin,” pp. 206-214, 1980. Https://Doi.Org/10.1016/0005-2787(80)90073-8

APPENDIX A – GRAPH GENERATION SAMPLE CODES

Below are additional graphs that cover the frequency sweep and stress-relaxation test but would have weighed down the body of the results.

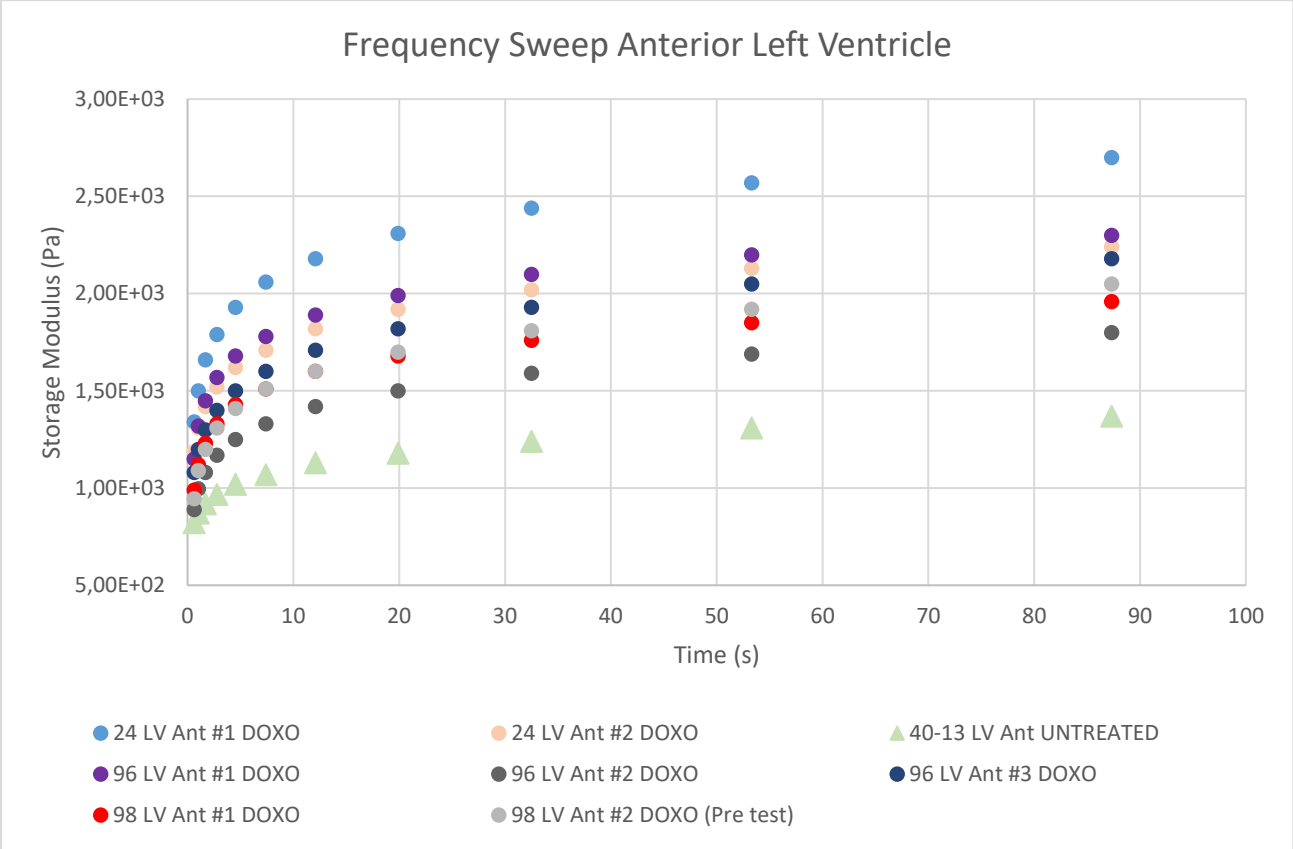

Figure A1: Average Storage Modulus by sample code Anterior Left Ventricle

Figure A1 shows the data collected for each sample before we computed the overall average storage modulus for each type of molecule studied (DOXO and untreated). The graph tendencies was the same for each sample studied.

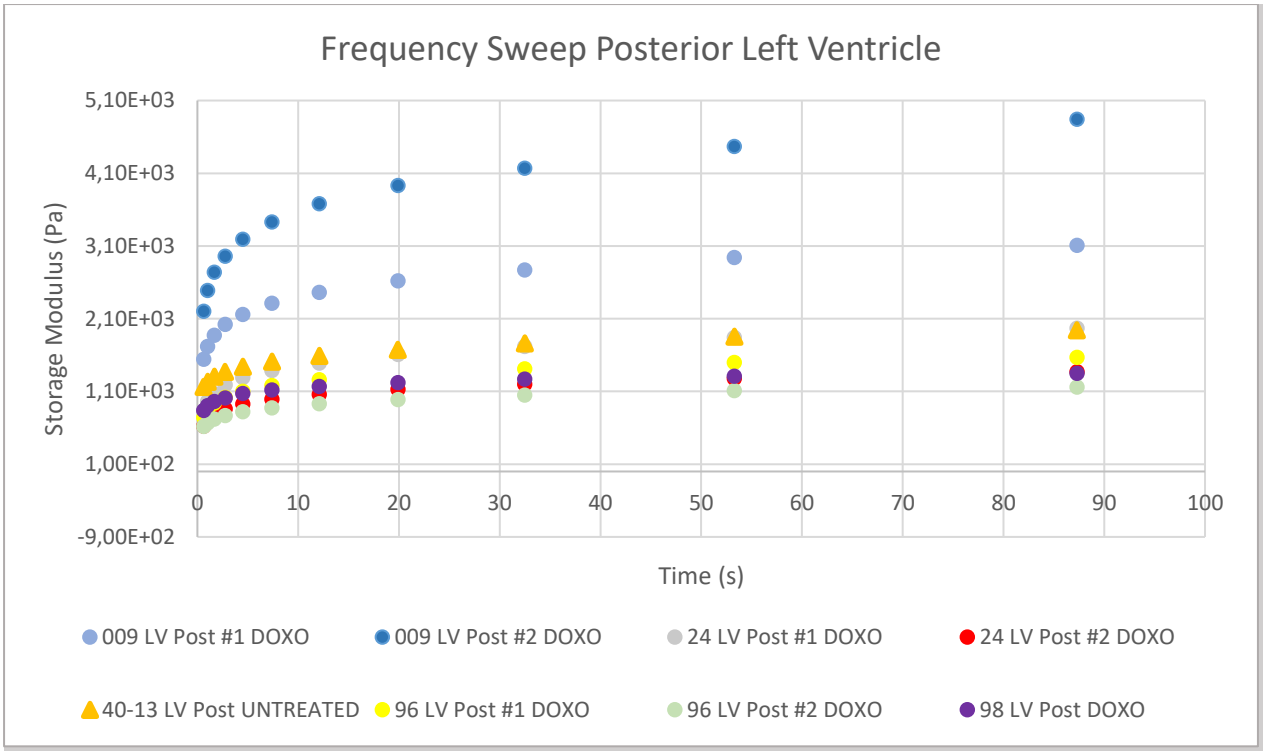

Figure A2: Average Storage Modulus by sample code Posterior Left Ventricle

Figure A2 shows the data collected for each sample before we computed the overall average storage modulus for each type of molecule studied (DOXO and untreated). The graph tendencies was the same for each sample studied.

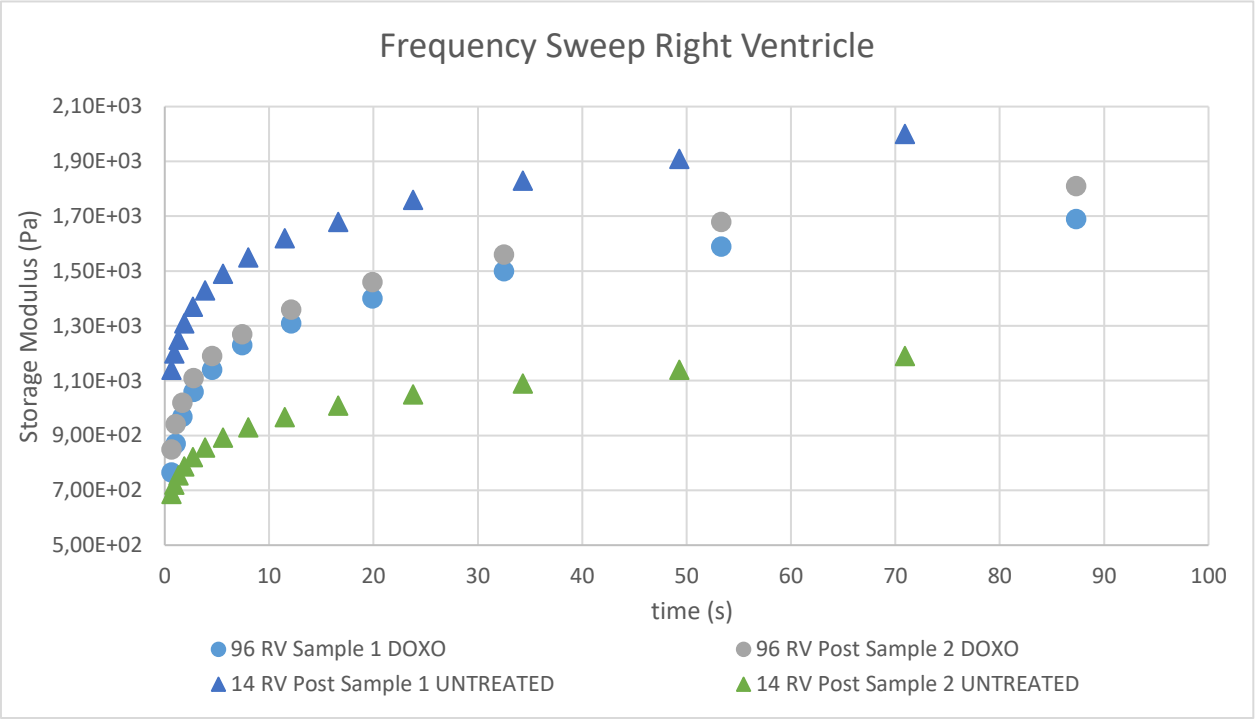

Figure A3: Average Storage Modulus by sample code Right Ventricle

Figure A3 shows the data collected for each sample before we computed the overall average storage modulus for each type of molecule studied (DOXO and untreated). The graph tendencies was the same for each sample studied.

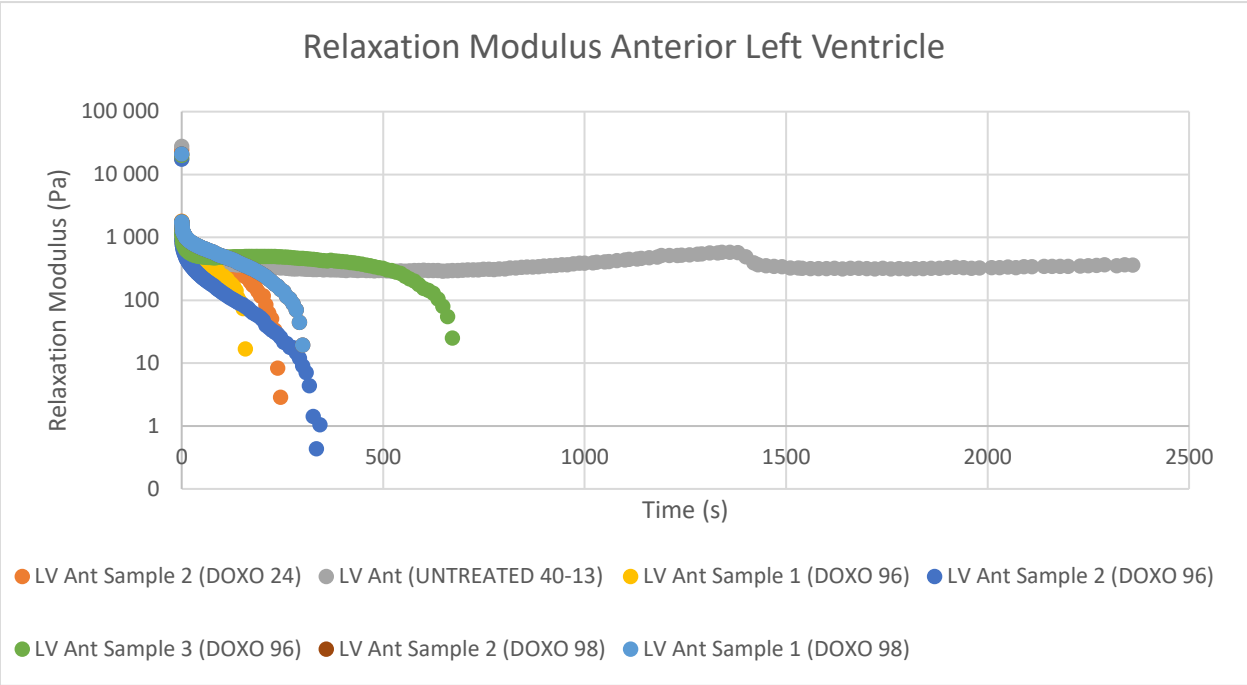

Figure A4: Average Relaxation Modulus by sample code Left Ventricle

Figure A4 shows the data collected for each sample before we computed the overall average relaxation modulus for each type of molecule studied (DOXO and untreated).

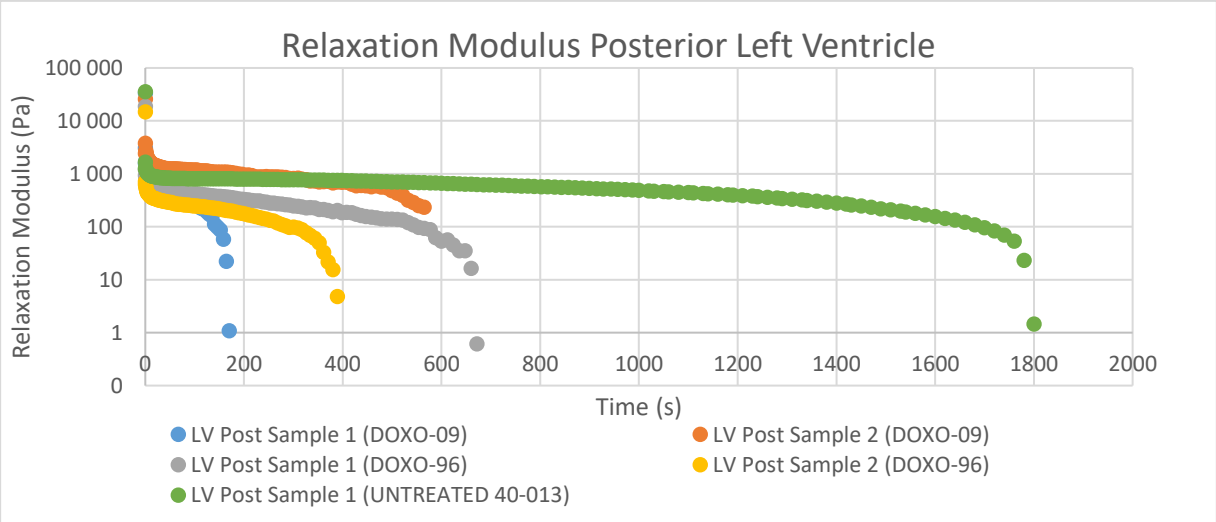

Figure A5: Average Relaxation Modulus by sample code Left Ventricle

Figure A5 shows the data collected for each sample before we computed the overall average relaxation modulus for each type of molecule studied (DOXO and untreated).

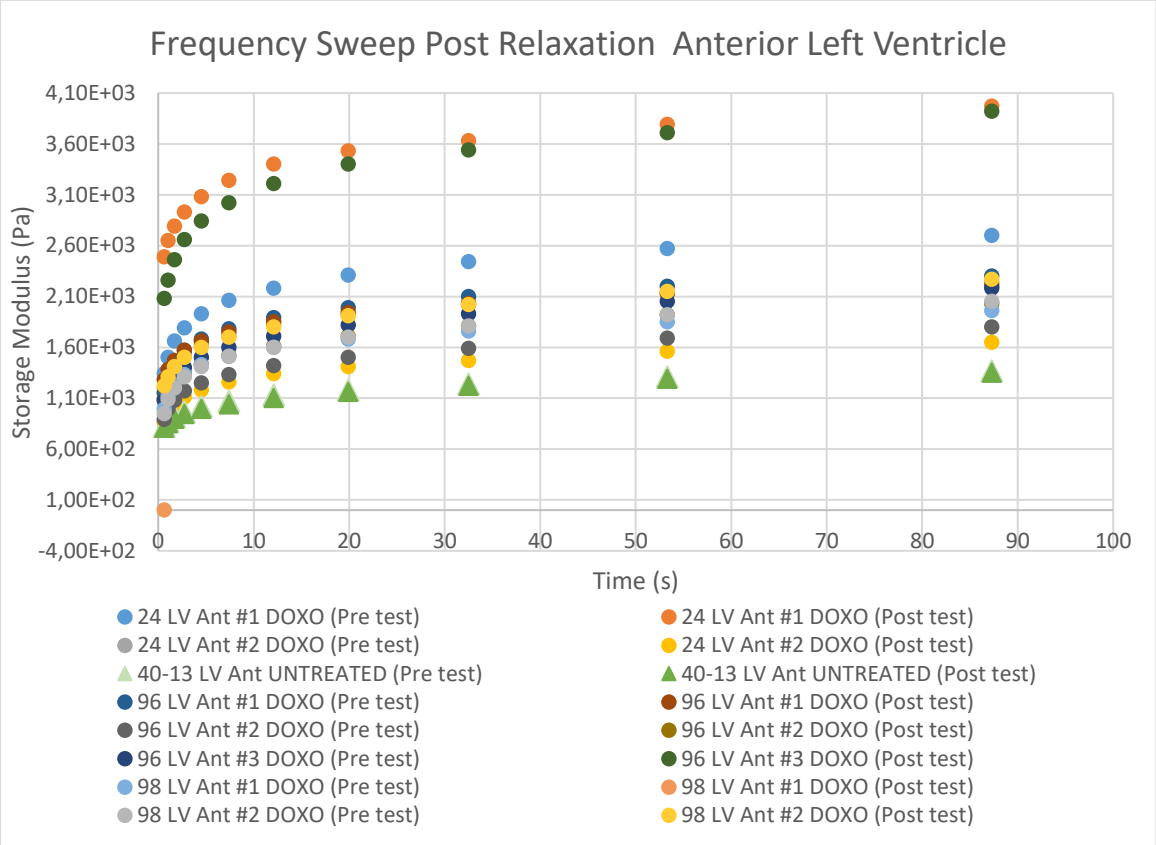

Figure A6: Average Storage Modulus by sample code Anterior Left Ventricle

Figure A6 shows the data collected for each sample before we computed the overall average relaxation modulus for each type of molecule studied (DOXO and untreated).

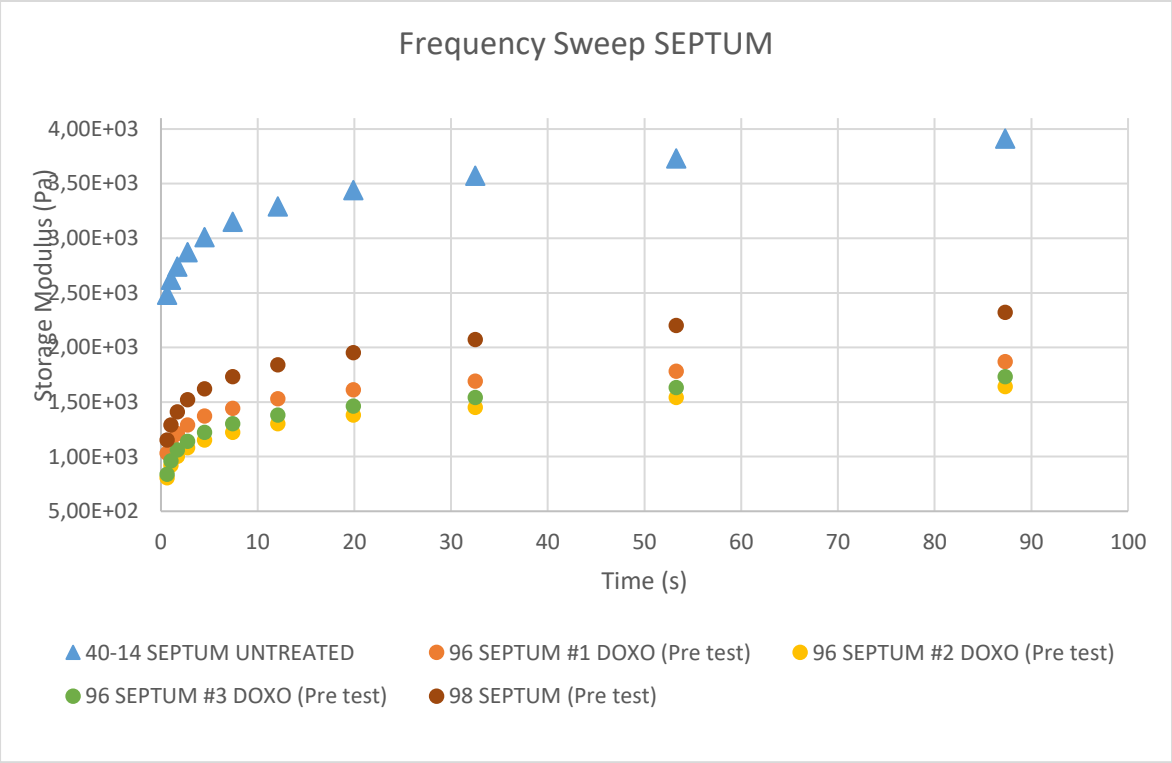

Figure A8: Average Storage Modulus by sample code Septum

Figure A8 shows the data collected for each sample before we computed the overall average storage modulus for each type of molecule studied (DOXO and untreated). The graph tendencies were the same for each sample studied.

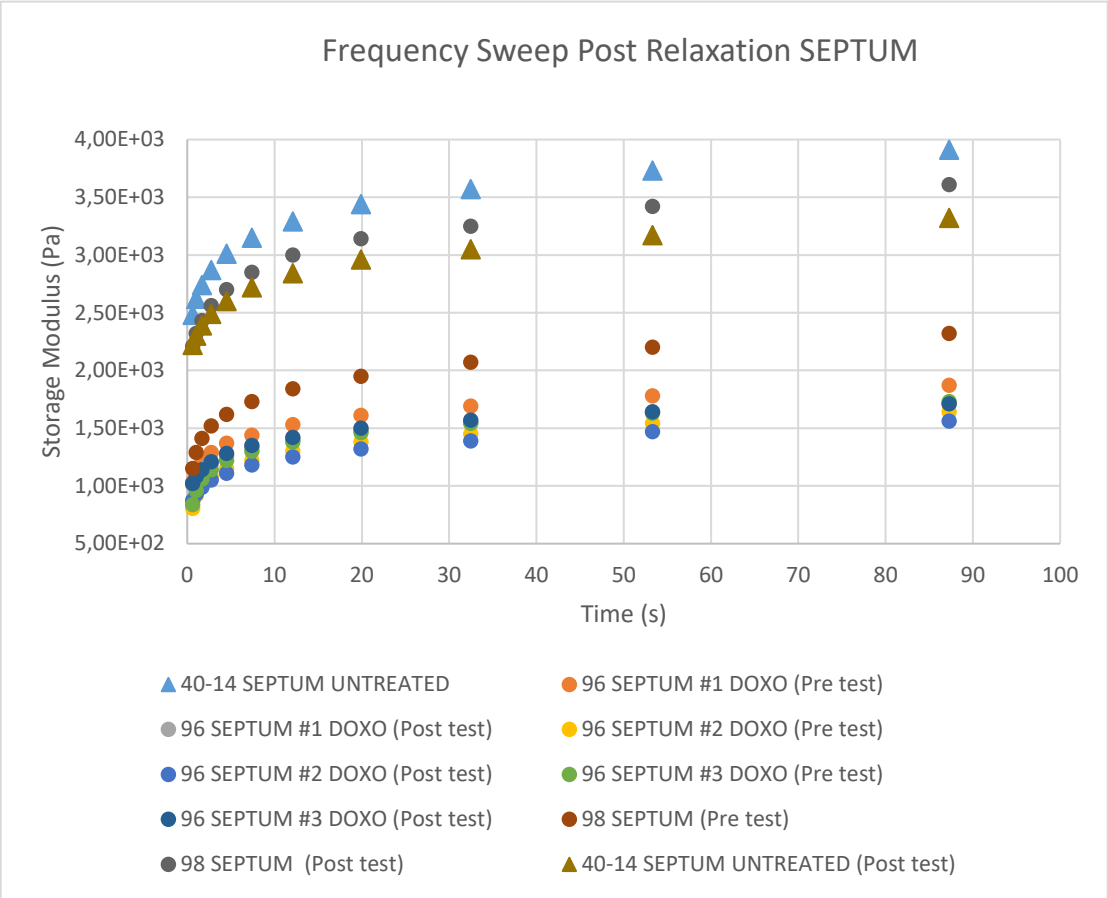

Figure A9: Average Storage Modulus by sample code Septum

Figure A9 shows the data collected for each sample before we computed the overall average relaxation modulus for each type of molecule studied (DOXO and untreated). The graph tendencies were the same for each sample studied.

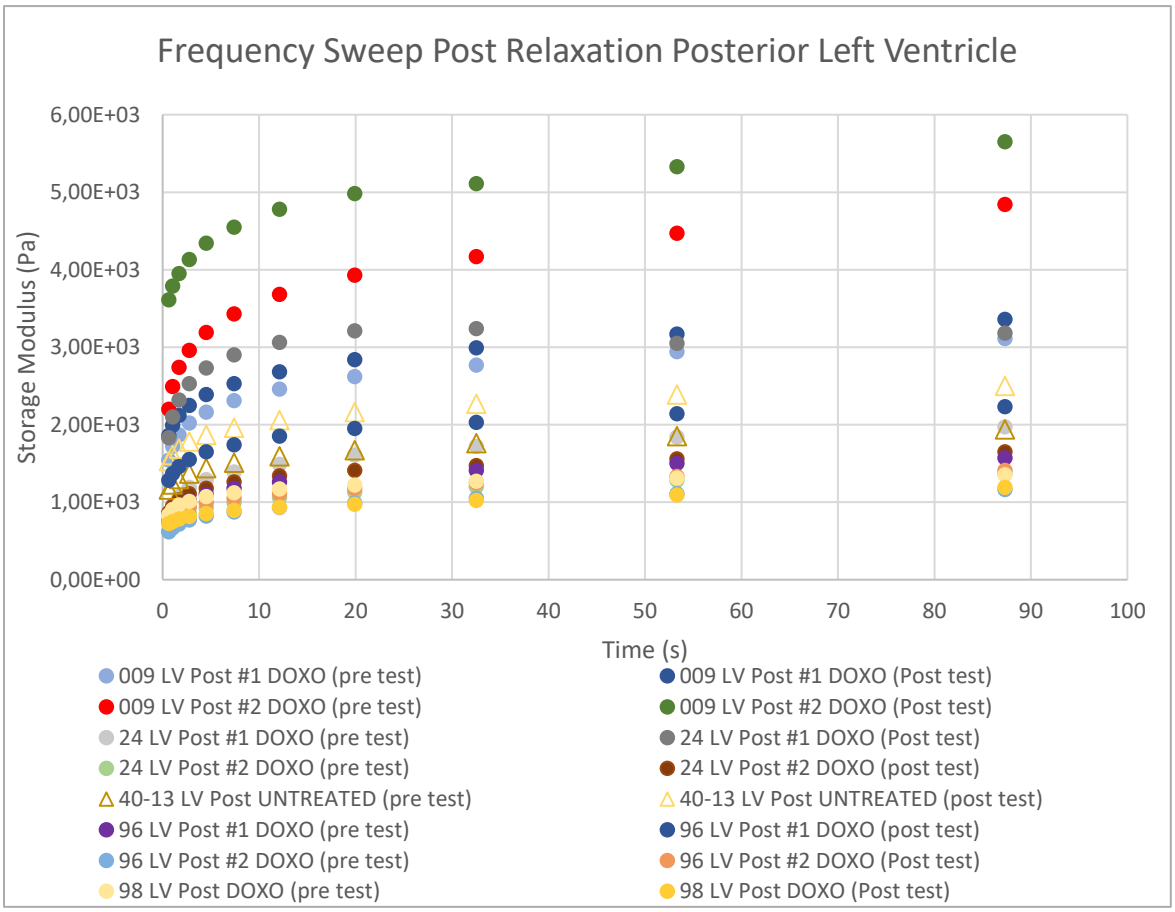

Figure A10: Average Storage Modulus Posterior Left Ventricle Post Relaxation Test

Figure A10 shows the data collected for each sample before we computed the overall average storage modulus for each type of molecule studied (DOXO and untreated). The graph tendencies were the same for each sample studied.

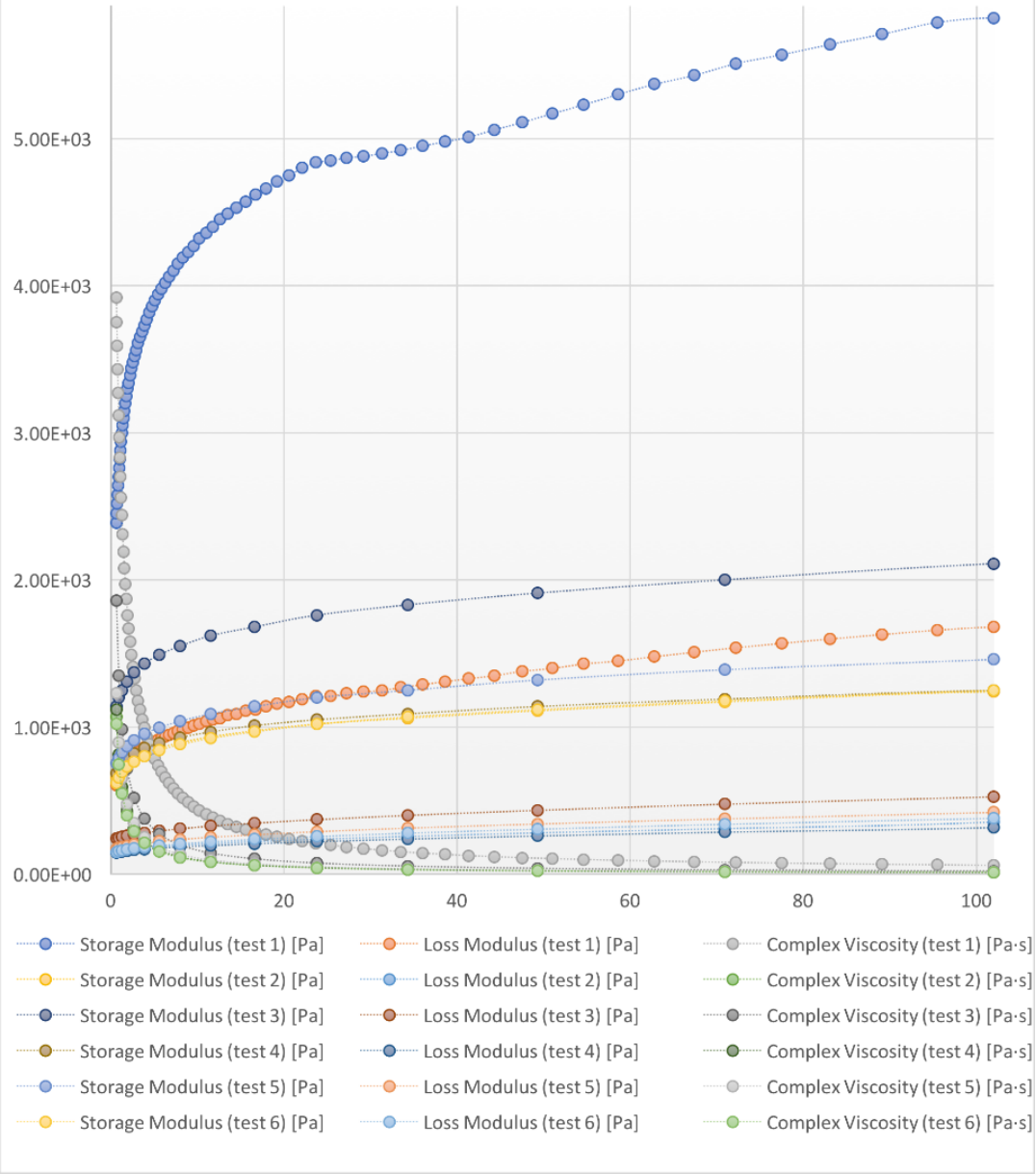

Figure A11: Overview Frequency Sweep 1.6% for Storage & Loss Modulus & Complex Viscosity

Above presents the results obtained for 6 tests for each of the parameters of interest during the frequency sweep G, G'& G'' up until 100 Hz. Test #1 to determine the storage modulus is the reason why we chose a range of 0.1Hz to 100Hz for the frequency sweep.

APPENDIX B – TABLE GENERATION FREQUENCY SWEEP FOR EACH SAMPLE CODE

Table B1: Average Storage Modulus & Loss Pre/Post Frequency Sweep Left Ventricle

	Average Storage Modulus	STD Dev Storage Modulus	Average Loss Modulus	STD Dev Loss Modulus
98 LV Pre Test	1.29E+03	7.47E+02	1.30E+03	3.05E+03
98 LV Post Test	1.86E+03	2.76E+03	9.84E+02	2.34E+03
24 LV Pre Test #1	1.57E+03	4.33E+02	9.05E+02	1.50E+03
24 LV Post Test #1	3.01E+03	6.77E+02	1.22E+03	1.47E+03
24 LV Pre Test #2	1.36E+03	1.04E+03	1.36E+03	2.08E+03
24 LV Post Test #2	1.70E+03	1.21E+03	1.04E+03	2.08E+03
96 LV Pre Test	1.27E+03	2.98E+02	9.25E+02	1.86E+03
96 LV Post Test	1.71E+03	4.80E+02	1.02E+03	1.73E+03
96 LV Pre Test #2	1.11E+03	8.30E+02	1.21E+03	2.84E+03
96 LV Post Test #2	1.47E+03	1.21E+03	1.19E+03	2.69E+03
009 LV Pre Test	2.37E+03	5.92E+02	1.64E+03	2.73E+03
009 LV Post Test	2.76E+03	5.92E+02	1.64E+03	2.66E+03
009 LV Pre Test	4.86E+03	2.50E+03	2.27E+03	2.71E+03
009 LV Post Test	5.74E+03	2.15E+03	2.63E+03	2.60E+03
40-013 LV Pre Test	1.81E+03	8.60E+02	1.44E+03	3.25E+03
40-013 LV Post Test	2.29E+03	8.78E+02	1.49E+03	3.08E+03

Table B1 summarizes the average and standard deviations achieved for two important moduli studied during the frequency sweep for the left ventricle. It covers these measurements for each given sample code both pre relaxation test and post relaxation test. The black outlined box represents the untreated sample.

Table B2: Average Storage Modulus & Loss Pre/Post Frequency Sweep Septum

	Average Storage Modulus	STD Dev Storage Modulus	Average Loss Modulus	STD Dev Loss Modulus
96 Sept Pre Test	1.65E+03	5.25E+02	1.04E+03	2.07E+03
96 Sept Post Test	1.44E+03	3.28E+02	1.04E+03	2.14E+03
96 Sept Pre Test #2	3.17E+03	5.68E+02	1.32E+03	1.56E+03
96 Sept Post Test #2	1.68E+03	1.29E+03	1.04E+03	2.13E+03
96 Sept Pre Test #3	1.61E+03	8.15E+02	1.23E+03	2.70E+03
96 Sept Post Test #3	1.67E+03	9.65E+02	1.25E+03	2.73E+03
98 Sept Pre Test	2.18E+03	1.12E+03	1.23E+03	2.35E+03
98 Sept Post Test	3.36E+03	1.21E+03	1.67E+03	2.45E+03
40-014 Sept Pre Test	3.46E+03	6.59E+02	1.51E+03	2.40E+03
40-014 Sept Post Test	2.87E+03	4.06E+02	1.41E+03	2.40E+03

Table B2 summarizes the average and standard deviations achieved for two important modulus' studied during the frequency sweep for the septum parts. It covers these measurements for each given sample code both pre relaxation test and post relaxation test. The black outlined box represents the untreated sample (40-014).

Table B3: Average Storage Modulus & Loss Pre/Post Frequency Sweep Right Ventricle

	Average Storage Modulus	STD Dev Storage Modulus	Average Loss Modulus	STD Dev Loss Modulus
96 RV Pre Test	1.35E+03	3.41E+02	9.78E+02	1.84E+03
96 RV Post Test	4.83E+03	1.29E+03	1.82E+03	1.70E+03
96 RV Pre Test #2	1.84E+03	9.81E+02	9.74E+02	1.55E+03
96 RV Post Test #2	2.48E+03	6.93E+02	1.15E+03	1.52E+03
40-014 Sept Pre Test	1.94E+03	8.92E+02	7.87E+02	1.23E+03
40-014 Sept Pre Test #2	1.25E+03	8.50E+02	7.30E+02	1.53E+03

Table B3 summarizes the average and standard deviations achieved for two important moduli studied during the frequency sweep for the right ventricle samples. It covers these measurements for each given sample code both pre relaxation test and post relaxation test.